Investigating the dynamics of hydrogen peroxide metabolism in the peroxiredoxin system of *Saccharomyces cerevisiae*

by

Melinda Badenhorst

Thesis presented in partial fulfilment of the requirements for the degree of Master of Science (Biochemistry) in the Faculty of Science at Stellenbosch University

Supervisor: Prof. J.M. Rohwer

Co-supervisor: Dr. C.S. Pillay University of KwaZulu-Natal

March 2020

Stellenbosch University https://scholar.sun.ac.za

Declaration

By submitting this thesis electronically, I declare that the entirety of the work contained therein is my own, original work, that I am the sole author thereof (save to the extent explicitly otherwise stated), that reproduction and publication thereof by Stellenbosch University will not infringe any third party rights and that I have not previously in its entirety or in part submitted it for obtaining any qualification.

Date: .....March 2020.....

Copyright © 2020 Stellenbosch University
All rights reserved.

Stellenbosch University https://scholar.sun.ac.za

Abstract

Reactive oxygen species (ROS) are derivations of molecular oxygen that can have detrimental effects in cells. ROS can readily react with DNA, proteins and lipids often resulting in the loss of structure integrity of these essential cellular components. Living cells are exposed to a normal level of ROS produced by metabolic processes such as aerobic respiration or immune responses. During oxidative stress, however, the level of ROS increases to such an extent that the mechanisms to neutralize them become exhausted. Hydrogen peroxide (H_2O_2), being a ROS itself, has been associated with cancer, age-related diseases, human immunodeficiency virus infection and cardiovascular diseases. Despite these undesired effects of H_2O_2, it has also been recognized as a signaling molecule that functions in important cellular processes such as cell proliferation and differentiation, immune response and apoptosis. Fortunately, the cell is equipped with an antioxidant system that can neutralize H_2O_2, while maintaining its levels for important signaling functions: the peroxiredoxin system. Peroxiredoxins belong to a family of redox proteins that are ubiquitously expressed across all kingdoms of life. They form part of a larger redox network that accepts reducing energy upstream from the thioredoxin system (thioredoxin, thioredoxin reductase and NADPH) to reduce H_2O_2 to H_2O. The dynamics of the peroxiredoxin system remain poorly understood. The aim of this study was to further our understanding of the kinetic behaviour of this system and how it metabolizes H_2O_2 by constructing a kinetic model for the peroxiredoxin system of *Saccharomyces cerevisiae*. A kinetic model could enable us to determine exactly how this system is able to homeostatically maintain levels of H_2O_2 for signaling function and antioxidant defense. First, the proteins of the peroxiredoxin system were purified using recombinant protein expression techniques. The proteins were then used in spectrophotometric assays to obtain experimental data that were used to estimate the required model pa-

Stellenbosch University https://scholar.sun.ac.za

rameters. Once the model was constructed and evaluated, a stress condition was simulated by subjecting the system to a pulse-like H_2O_2 input of varying concentrations. The response of the system with regard to its capacity to efficiently neutralize H_2O_2 under these conditions were then determined. The peroxiredoxin system proteins were successfully expressed to a high degree of homogeneity. The spectrophotometric assays and parameter estimations resulted in usable values for parameters to construct a simple kinetic model that could describe the system. Model simulations could further explain some discrepancies found in the experimental data for the H_2O_2 reduction reaction of the system. Additionally, the pulse-like simulation results demonstrated that when a certain H_2O_2 concentration threshold is reached, the capacity of the system to efficiently neutralize H_2O_2 becomes limited.

Stellenbosch University https://scholar.sun.ac.za

Opsomming

Reaktiewe suurstofspesies (RSS) is reaktiewe molekules afgelei van molekulêre suurstof wat nadelige gevolge in selle kan hê. RSS reageer maklik met DNA, proteïene en lipiede wat kan lei tot die verlies van struktuurintegriteit van sulke noodsaaklike sellulêre komponente. Lewende selle word oor die algemeen blootgestel aan 'n normale vlak van RSS deur middel van metaboliese prosesse soos aërobiese respirasie of gedurende 'n immuunrespons. Tydens oksidatiewe stres neem die vlakke van RSS egter tot so 'n mate toe, dat die meganismes om RSS te neutraliseer uitgeput raak. Waterstofperoksied (H_2O_2) is 'n RSS tipe wat met kanker, ouderdomsverwante siektes, menslike immuniteitsgebrekvirus-infeksie en kardiovaskulêre siektes geassosieer word. Ten spyte van hierdie ongewenste gevolge van H_2O_2, word dit ook erken as 'n seinmolekule wat funksioneer in belangrike sellulêre prosesse soos selproliferasie en differensiasie, immuunrespons en apoptose. Die sel is egter toegerus met 'n antioksidantsisteem wat H_2O_2 effektief kan neutraliseer, terwyl die vlakke vir belangrike seinfunksies gehandhaaf word: die peroksiredoksiensisteem. Peroksiredoksiene behoort aan 'n familie van redoksproteïene wat in al die koninkryke van lewe voorkom. Hulle vorm deel van 'n groter redoksnetwerk wat reduserende energie ontvang van die tioredoksiensisteem (tioredoksien, tioredoksien reduktase en NADPH) om H_2O_2 na H_2O om te skakel. Die dinamika van die peroksiredoksiensisteem word egter nie goed verstaan nie. Die doel van hierdie studie is om ons begrip van die kinetiese gedrag van hierdie sisteem en hoe dit H_2O_2 metaboliseer beter te verstaan deur die bou van 'n kinetiese model vir die peroksiredoksiensisteem van *Saccharomyces cerevisiae*. 'n Kinetiese model kan ons in staat stel om presies te bepaal hoe hierdie sisteem dit regkry om H_2O_2-vlak homeostase te handhaaf vir seinfunksie en beskerming teen oksidante. Eerstens was die proteïene wat aan die peroksiredoksiensisteem behoort gesuiwer met behulp van rekombinante proteïenuitdrukkingstegnieke. Die proteïene was daarna in

Stellenbosch University https://scholar.sun.ac.za

spektrofotometriese eksperimente gebruik om eksperimentele data te win wat gebruik is om die vereiste modelparameters te skat. Sodra die model gebou en geëvalueer is, was 'n strestoestand gesimuleer deur die sisteem aan 'n pulsagtige H_2O_2 inset van wisselende konsentrasies te onderwerp. Die reaksie van die sisteem ten opsigte van sy kapasiteit om H_2O_2 effektief te neutraliseer onder hierdie toestande was daarna bepaal. Die proteïene van die peroksiredoksiensisteem is suksesvol tot 'n hoë mate van homogeniteit uitgedruk. Die spektrofometriese eksperimente en parameterberamings het gelei tot bruikbare waardes vir parameters om 'n eenvoudige kinetiese model te bou wat die sisteem kon beskryf. Modelsimulasies kon verder enkele teenstrydighede teenwoordig in die eksperimentele data vir die H_2O_2 reduksie-reaksie verklaar. Daarbenewens het die resultate van die puls-simulasie getoon dat wanneer 'n sekere H_2O_2 konsentrasiedrempel bereik word, die vermoë van die sisteem om H_2O_2 effektief te neutraliseer beperkend raak.

Stellenbosch University https://scholar.sun.ac.za

Acknowledgements

I would like to express my sincere gratitude to the following people and organisations:

To my supervisor, Professor Johann Rohwer, for all the guidance and support he provided during this project. He allowed me to work independently, but was always available and willing to go the extra mile whenever I needed help.

To my co-supervisor, Dr. Ché Pillay, for all his support and input towards this project.

To our laboratory manager, Arrie Arends, for making the environment in the laboratory safe, easy and comfortable. I would like to express gratitude for all his support.

To my friends in the Biochemistry Department, for all the motivation and many coffee breaks in the Neelsie.

I would like to express sincere gratitude especially to my parents and sister, without their love and support this thesis would not have been possible.

The financial assistance of the National Research Foundation (NRF) towards this research is hereby acknowledged. Opinions expressed and conclusions arrived at, are those of the author and are not necessarily to be attributed to the NRF.

Stellenbosch University https://scholar.sun.ac.za

Contents

Stellenbosch University https://scholar.sun.ac.za

Stellenbosch University https://scholar.sun.ac.za

Stellenbosch University https://scholar.sun.ac.za

Stellenbosch University https://scholar.sun.ac.za

List of Figures

Stellenbosch University https://scholar.sun.ac.za

Stellenbosch University https://scholar.sun.ac.za

Stellenbosch University https://scholar.sun.ac.za

Stellenbosch University https://scholar.sun.ac.za

Stellenbosch University https://scholar.sun.ac.za

Stellenbosch University https://scholar.sun.ac.za

Stellenbosch University https://scholar.sun.ac.za

List of Tables

Stellenbosch University https://scholar.sun.ac.za

Nomenclature

List of abbreviations

BSA	Bovine serum albumin
DTNB	5,5'-dithio-bis (2-nitrobenzoic acid) or Ellman's reagent
DTT	Dithiothreitol
EDTA	Ethylenediaminetetraacetic acid
IMAC	Immobilized metal affinity chromatography
IPTG	Isopropyl β-D-1-thiogalactopyranoside
LB	Luria Bertani
mqH_2O	Milli-Q® ultrapure water
OD_{600}	Optical density at 600 nm
PEG	Poly(ethylene glycol)
ROS	Reactive oxygen species
rpm	Revolutions per minute
SDS	Sodium dodecyl sulfate
TCE	2,2,2-trichloroethanol
TEMED	N,N,N',N'-tetramethylethylenediamine
TrxR	Thioredoxin reductase
Trx	Thioredoxin
Trx_{SH}	Reduced Trx
Trx_{SS}	Oxidized Trx
TSA	Thiol-specific antioxidant protein

Stellenbosch University https://scholar.sun.ac.za

TSA_{SH}	Oxidized TSA
TSA_{SS}	Oxidized TSA

Parameters

$k_{insulin}$ second order rate constant for mass action reaction between Trx and insulin

k_2 second order rate constant for mass action reaction between Trx and TSA

k_3 second order rate constant for mass action reaction between TSA and H_2O_2

k_{cat} catalytic rate constant for TrxR

K_{NADPH} binding constant of NADPH to TrxR

$K_{Trx_{SS}}$ binding constant of oxidized Trx to TrxR

Stellenbosch University https://scholar.sun.ac.za

Chapter 1

Introduction

1.1 Background information and research motivation

Living organisms come into contact with reactive oxygen species (ROS), including hydrogen peroxide (H_2O_2), on a daily basis originating from both internal and external sources[1]. Oxidative stress is a cellular state in which ROS are elevated to such an extent that the antioxidant mechanisms of the cell become exhausted[2]. This state can have severe cellular consequences since ROS can readily react with biomolecules such as DNA, proteins and lipids. Peroxiredoxins, ubiquitously found in all kingdoms of life, are redox proteins that form part of a larger network with dual functionality to maintain H_2O_2 below levels of severe oxidative stress while keeping it high enough for important signaling functions[3].

H_2O_2 plays important roles in conditions related to aging, cancer, cardiovascular diseases and human immunodeficiency virus infection[4–7]. Despite the negative effects associated with H_2O_2, it also acts as an important signaling molecule for metabolic processes essential for survival[8]. How exactly does the cell manage to balance the levels of H_2O_2 to prevent severe oxidative stress while maintaining the right concentration to allow for important signaling function? The peroxiredoxin system could provide some insight into this question. The dynamics of this system is, however, still poorly understood. Additionally, to the best of our knowledge, a kinetic model for the peroxiredoxin system of

Stellenbosch University https://scholar.sun.ac.za

Saccharomyces cerevisiae does not yet exist. Development of such a model could improve our understanding of eukaryotic H_2O_2 metabolism and will allow for comparison to prokaryotic systems which could in turn lead to the identification of potential drug targets. Investigating the dynamics of H_2O_2 metabolism and the peroxiredoxin system of *S. cerevisiae* could enable us to make accurate inferences about how exactly this system functions to homeostatically maintain levels of H_2O_2 below oxidative stress levels and above levels required for normal signaling events.

Using a combination of both experimental and computational techniques while applying the principles of systems biology can allow us to investigate this complex system.

1.2 Aims and thesis outline

The main goal of this study was to investigate the dynamics of the peroxiredoxin system and how H_2O_2 gets metabolized in *S. cerevisiae*. To achieve this, the project was divided into three main aims:

1. **To purify three *S. cerevisiae* proteins that form part of the peroxiredoxin system: TrxR, Trx and TSA.** This was achieved by inducing overexpression of recombinant proteins in a host organism (*Escherichia coli* BL21 DE3) cloned with His-tagged TrxR, Trx and TSA from *S. cerevisiae*. Proteins were extracted and the His-tagged proteins purified with immobilized metal affinity chromatography.

2. **To construct a simple model of the peroxiredoxin system in *S. cerevisiae* by determination of the required model parameters from experimental data.** Published spectrophotometric assays for each protein were optimized and established in the laboratory of our research group for the first time. Initial rates for varying substrate concentrations were obtained and the processed experimental data were used to fit a particular model parameter. The assays consisted of both high throughput microtiter plate assays as well as single sample assays using a cuvette. Parameter fitting was done computationally using a non-linear least-squares minimization and curve-fitting method based on the

Stellenbosch University https://scholar.sun.ac.za

Levenberg-Marquardt algorithm to fit corresponding kinetic equations to experimental data.

3. **Simulation of the constructed *S. cerevisiae* peroxiredoxin system model.** All model simulations were performed in a Python programming language environment using PySCeS, a software previously developed in our research group specifically for simulation of cellular system models. First, the parameterized model was evaluated to test the reproducibility of experimental conditions. Second, a time simulation experiment was designed in which the model was subjected to a pulse-like input of H_2O_2 to investigate how the system responds towards this type of stress input.

This thesis is divided into five chapters, including this introductory chapter. Chapter 2 is an extensive review with specific focus on the role of H_2O_2 in oxidative stress, the most important features of the peroxiredoxin system and how it functions as both a defense mechanism against H_2O_2 and a regulator of signaling function. The review also discusses the value of using computational systems biology as a tool for studying complex cellular systems such as the peroxiredoxin network. Chapter 3 provides a detailed description of all materials and methodologies that were utilized in this study to achieve the above-mentioned aims. Chapter 4 is a comprehensive report on all the results obtained in this study. Chapter 5 gives a thorough discussion of the results obtained, how they implicate the original research questions, states the limitations of this project and provides recommendations for future studies as well as suggestions to overcome some of the limitations mentioned.

Stellenbosch University https://scholar.sun.ac.za

Chapter 2

Hydrogen peroxide and the peroxiredoxin system

2.1 Cellular oxidants and their consequences

2.1.1 Reactive oxygen species: where do they come from and what do they do?

Reactive oxygen species (ROS) are chemically reactive molecules derived from molecular oxygen[1;9;10]. The reactivity arises due to an unpaired electron in the outermost shell of the oxygen atom present, which enables ROS to readily react with essential biological components such as DNA, proteins and lipids. Oxidation of DNA bases, guanine in particular, can lead to mutations, strand breakage and cross-linkage with proteins, which in turn leads to the inhibition of important processes such as DNA replication and transcription[11]. Repair mechanisms for proteins that have been subjected to oxidation are further limited and ultimately they get marked for degradation[12]. Moreover, lipid peroxidation, mediated by ROS, has been shown to result in the loss of structure integrity, function, fluidity and permeability of lipid bilayers[13]. Hydrogen peroxide (H_2O_2), superoxide, singlet oxygen, hypochlorous acid and the hydroxyl radical are some examples of ROS, with varying degrees of reactivity, that are present in the cellular environment[1;10]. This reactivity is governed by the preference of the specific ROS towards one- or two-electron reactions, the former being more highly reactive[14].

Stellenbosch University https://scholar.sun.ac.za

Living cells are constantly exposed to ROS throughout the course of their life span, whether from environmental sources or as by-products produced by metabolic processes[15]. Environmental sources that lead to the build up of ROS include ultraviolet radiation emitted by the sun, ionizing radiation and cigarette smoke[15–18]. ROS are also generated by normal metabolic processes (Figure 2.1). Aerobic respiration, for example, inevitably leads to the incomplete electron reduction of some oxygen molecules to form superoxide, which is then rapidly dismutated to form H_2O_2[10]. Furthermore, H_2O_2 takes part in Fenton chemistry to form the hydroxyl radical, which is a highly reactive type of ROS, in a reaction catalyzed by transition metals[19]. Despite its negative implications, ROS also serve important physiological functions, especially during the immune response. Upon activation of phagocytic cells by ingestion of a pathogen, the NADPH oxidase complex localized within the membranes of these cells reacts to produce superoxide and H_2O_2 which then results in phagocytic killing of these organisms[20]. Furthermore, in a reaction catalyzed by myeloperoxidase in neutrophils, H_2O_2 forms hypochlorous acid, which is highly reactive and toxic to ingested microbes[20].

Stellenbosch University https://scholar.sun.ac.za

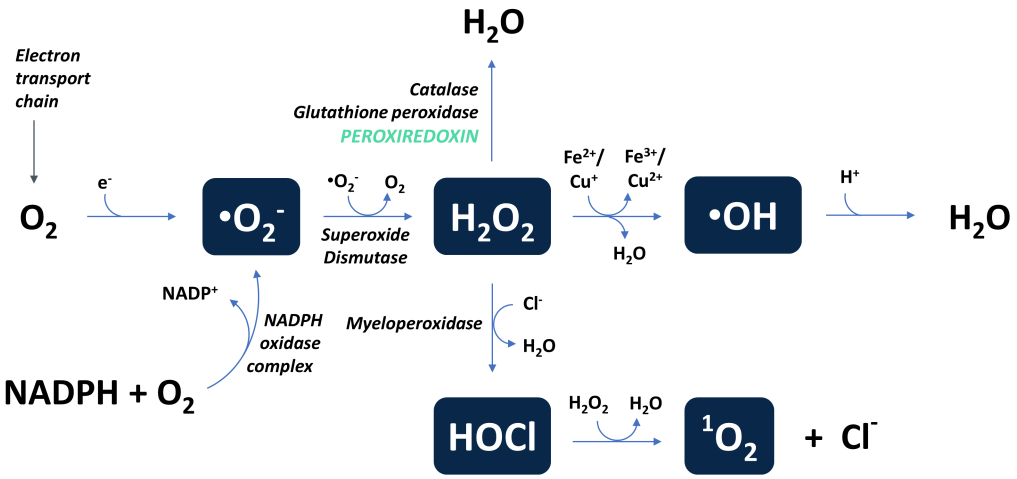

Figure 2.1: Internal sources of ROS. Normal metabolic processes can lead to ROS formation. Aerobic respiration can ultimately lead to the formation of superoxide. Superoxide is further dismutated to H_2O_2 by superoxide dismutase. H_2O_2 can then take part in more reactions to form other types of ROS such as the hydroxyl radical, hypochlorous acid and singlet oxygen. During an immune response, the NADPH oxidase complex also contributes to the formation of superoxide. Figure adapted from: Nordberg, J. and Arnér, E. S.: Reactive oxygen species, antioxidants, and the mammalian thioredoxin system. *Free Radical Biology and Medicine*, vol. 31, no. 11, pp. 1287-1312, 2001.

2.1.2 Physiological relevance of oxidative stress

The cell is in a state of oxidative stress when the levels of ROS increase to such an extent that the mechanisms to remove them become exhausted[2;21;22]. Oxidative stress is considered an undesired state as chronic exposure to ROS can have detrimental cellular effects such as those mentioned above[23]. Being a type of ROS itself, H_2O_2 plays a central role in the generation of other types of ROS (Figure 2.1) and as such, is an important contributor to oxidative stress. Fortunately, the cell is equipped with various antioxidant mechanisms to efficiently neutralize H_2O_2, such as catalases, glutathione and peroxiredoxins[24–26] which will be discussed in more detail in Section 2.2. In addition to oxidative stress, ROS and H_2O_2 in particular, have become increasingly recognized as important signaling molecules essential in the regulation of normal physiological processes[3;27–29].

A strong correlation exists between oxidative stress and human disease[30].

Stellenbosch University https://scholar.sun.ac.za

For example, DNA damage due to elevated ROS levels is one of the leading causes for the development of cancer[23;31]. Moreover, the production and secretion of H_2O_2 by cancer cells leads to increased oxidative stress in associated fibroblasts[4]. As a consequence, processes such as inflammation, glycolysis and autophagy occur which provide cancer cells with nutrients and thereby promote metastasis[5]. H_2O_2 further causes increased entry of Ca^{2+} into cardiomyocytes which has been implicated in heart dysfunction and the development of atherosclerosis and hypertension[6;32]. A study conducted by Sandstrom *et al.* further demonstrated that H_2O_2, at levels considered non-cytotoxic, is a causative factor for the decrease of human immunodeficiency virus-infected CD4 T cells[7]. Furthermore, significant evidence supports the contribution of oxidative stress to neurodegenerative disease progression specifically in Alzheimer's, Parkinson's and Huntington's diseases[33–36]. It is clear that generation of excessive cellular H_2O_2 and the subsequent state of oxidative stress can be detrimental to human health.

2.1.3 The bifunctionality of H_2O_2

H_2O_2 is a strong oxidant with a high reduction potential, however, many reactions with it are slow due to the high activation energy[29]. Some biomolecular targets for oxidation by H_2O_2 include transition metals within metalloproteins, cysteine and methionine residues with second-order rate constants of varying magnitudes[19;37;38]. Other low molecular weight thiol targets of H_2O_2 have rate constants that are relatively low and decrease with increasing thiol pK_a[39]. The thiolate anion (R-S$^-$) is exclusively targeted by H_2O_2 for oxidation explaining the increased susceptibility of thiol proteins with low pK_a-values[14;40]. Although the direct biomolecular targets of H_2O_2 are fewer compared to those for other types of ROS such as the hydroxyl radical or superoxide, it has the potential to cause serious biological damage. Notably, H_2O_2 functions as a precursor of types of ROS with higher reactivity and plays a role in oxidative stress through complex and indirect metabolic processes. H_2O_2, although not as reactive as other types of ROS, can cause serious damage due to it being a small molecule that can easily diffuse from its site of generation to other cellular compartments where it can be converted to a more harmful type of ROS[1].

Stellenbosch University https://scholar.sun.ac.za

Despite the negative connotations to H_2O_2, mounting evidence suggests that it has essential secondary messenger and signaling functions[8;27;41–43]. H_2O_2 is an ideal candidate for a signaling molecule as it is small, can easily diffuse across biological membranes and is generated by most cell types[44]. Some studies have suggested that H_2O_2 signaling has a protective role within the cell by stimulating repair mechanisms when the cell enters a state of severe oxidative stress[43;45].

Secondary messenger function of H_2O_2 has been reported in a study by Bae *et al.* in which the production of H_2O_2 upon stimulation of human epidermoid carcinoma cells to epidermal growth factor was demonstrated[46]. The messenger function of H_2O_2 is further conveyed to downstream signaling pathways or gene expression, which upregulates key metabolic processes such as cell proliferation and differentiation, immune response and apoptosis[8;47]. H_2O_2, in fact, plays an important role in the activation of the mitogen-activated protein kinase (MAPK) signaling cascade, one of the most important signaling pathways responsible for regulation of essential metabolic processes[47]. More specifically, H_2O_2 acts as a potent activation stimulus for members of the MAPK family, namely extracellular signal-regulated kinases 1 and 2. This specific signaling pathway has important physiological downstream effects such as cell survival and proliferation, especially following injury caused by oxidative stress[48]. Often, due to the severe cellular damage caused by excessive oxidative stress, it is necessary for cells to undergo programmed cell death, or apoptosis. H_2O_2 is a strong activator of another MAPK cascade member called apoptosis signal-regulating kinase 1 (ASK1)[47]. Stress-induced activation of ASK1 subsequently leads to activation of the JNK and p38 MAPK signaling pathways which are the primary initiators of apoptosis[49].

The role of H_2O_2 metabolism in both normal and diseased states has sparked interest into its further investigation. More specifically, investigating the mechanisms employed by the cell to balance H_2O_2 for normal signaling events in the presence of various antioxidants while homeostatically maintaining its concentration below oxidative stress levels, may have important therapeutic implications. Therefore, considering its contribution to oxidative stress conditions, H_2O_2 metabolism is a subject worthy of further investigation.

Stellenbosch University https://scholar.sun.ac.za

2.2 Peroxiredoxins as antioxidant defense

The cell is equipped with many defense mechanisms to combat oxidative stress which act as sinks for ROS. Some well-known protein-based oxidant scavengers include catalase, glutathione peroxidase and peroxiredoxin. Vitamins A, C and E, β-carotene and glutathione are some low molecular weight compounds that also contribute to the antioxidant pool[15]. Together, all of these antioxidants provide the cell with adequate defense against normal physiological oxidant levels. However, during disease pathogenesis and severe oxidative stress conditions the balance between oxidants and antioxidants becomes disrupted and the available defense systems become overwhelmed[30]. In this section, one of these oxidant scavengers will be described in more detail: peroxiredoxins. The primary focus of this work lies with a eukaryotic peroxiredoxin from *S. cerevisiae* and will be referred to as thiol-specific antioxidant protein (TSA).

2.2.1 An introduction to peroxiredoxins

Peroxiredoxins can briefly be described as heme- and selenium-free, thiol-dependent, redox active proteins which function to reduce peroxides such as H_2O_2[50]. They are ubiquitously expressed proteins and have been identified in living organisms across all kingdoms of life[51]. Since their discovery in the late 1960s, or rather the discovery of a decameric protein of which the subunit is now commonly known as erythrocyte peroxiredoxin II, significant variation has emerged regarding the nomenclature and terminology used to describe peroxiredoxins[52]. Different names, including TSA, antioxidant protein, protector protein, thioredoxin peroxidase, alkyl hydroperoxide reductase, to name only a few, have been assigned to proteins sharing function and sequence homology[52–56]. As a matter of fact, numerous different peroxiredoxin subfamilies and isoforms expressed in both prokaryotes and eukaryotes have also since been identified[50;56;57]. Due to the vast diversity of these proteins, it was decided by Chae *et al.*[56] in 1994 to classify all of these redox active proteins sharing sequence homology as belonging to a protein superfamily called the peroxiredoxins[54].

All peroxiredoxins, despite the great diversity across species, contain a well conserved redox active cysteine (Cys) residue found within the N-terminal domain[58]. This Cys-residue, termed the peroxidatic Cys (C_P), plays a critical

Stellenbosch University https://scholar.sun.ac.za

role during the catalytic cycle. Another Cys-residue is found in the catalytic site of the two-cysteine peroxiredoxins and is termed the resolving Cys (C_R). Peroxiredoxins are classified into three subfamilies based on the catalytic mechanism: typical-two-cysteine, atypical-two-cysteine and one-cysteine peroxiredoxins[59]. The name of each subfamily essentially describes the functional dependency on the number of Cys-residues that take part in substrate (hydroperoxide) reduction[60]. For one-cysteine peroxiredoxins a single C_P takes part in the catalytic reaction. A detailed description of the catalytic mechanism is given in Section 2.2.2 below. Different classes further exist within each subfamily. Great diversity exists within the members of this group of proteins with some being targeted to different cellular compartments and/or expressed at varying levels[61].

Prokaryotic peroxiredoxins, such as typical-two-cysteine alkylhydroperoxidase (AhpC) and atypical-two-cysteine thiol peroxidase (Tpx), play vital roles in the survival of bacteria by assisting mainly with defense against peroxides[62]. It is speculated that higher eukaryotic organisms, such as yeast, plants and mammals, have evolved a more advanced peroxiredoxin system to fulfill a regulatory function, by using H_2O_2 as a secondary messenger in addition to the system's role in antioxidant defense[41;57;59]. This theory is supported by the increased number of peroxiredoxin classes found in eukaryotes compared to prokaryotes. Six different classes of peroxiredoxins have been discovered to date: Prx I - Prx IV, typical-two-cysteine type; Prx V, an atypical-two-cysteine type; and Prx VI, a one-cysteine type peroxiredoxin[60].

2.2.2 Catalytic cycle of peroxiredoxins

As mentioned above, despite the diversity found in this superfamily of proteins, the C_P residue is present in the catalytic active site of all peroxiredoxins, regardless of the type[58]. In addition, all peroxiredoxins are characterized by a universal three-reaction catalytic cycle and a single conformational change[58]. The first reaction of the catalytic cycle is a nucleophilic attack on the terminal oxygen of a hydroperoxide substrate, such as H_2O_2, to its corresponding alcohol (H_2O if the substrate is H_2O_2) by the C_P. At this stage, the substrate binding pocket of the peroxiredoxin is in a fully folded and protected conformation. The reactivity of the C_P towards hydroperoxide substrates is attributed to

Stellenbosch University https://scholar.sun.ac.za

its low pK_a[63]. The C_P thus exists as a thiolate anion (C_PS^-) at neutral pH, which can readily react with hydroperoxides, compared to its protonated form[63]. During this reaction, the C_P is oxidized to a sulfenic acid (C_PSOH). The next substrate for the C_PSOH is a thiol group from another Cys-residue known as C_R, either found on the same or a different peroxiredoxin subunit[63]. A conformational change is required at this point to allow the larger substrate to get access to the binding pocket by conforming to a more unfolded state from the original fully folded state[63]. The reaction that follows is referred to as a resolution reaction wherein the C_PSOH is resolved into a disulfide by reaction with the free thiol while one H_2O molecule is released[63]. The cycle is completed when the C_P (and C_R in the case of the two-cysteine peroxiredoxins) are recycled by a reduction reaction involving a thiol-containing reductant such as thioredoxin (Trx)[63;64].

The basic catalytic mechanism described above is identical for all three peroxiredoxin sub-families. However, the difference amongst the three is attributed to the number of Cys residues that take part in the catalytic cycle as well as the species responsible for supplying the reducing equivalents during the recycling step[50]. Typical-two-cysteine peroxiredoxins are obligate homodimeric proteins with a single catalytic active site formed across the two subunits[64] (Figure 2.2). A peroxiredoxin of this type, therefore, consists of two identical catalytic active sites and is thus able to reduce up to two H_2O_2 molecules at a time[64]. The peroxidation reaction involves the N-terminal C_P of the first subunit in which a H_2O_2 molecule is reduced to H_2O by nucleophilic attack[64]. The resulting C_PSOH is then attacked by the C-terminal C_R of the second subunit to form a head-to-tail intersubunit disulfide bond releasing a second H_2O[59]. For atypical-two-cysteine peroxiredoxins, both the C_P and C_R residues are located on a single subunit which ultimately results in an intramolecular disulfide bond[59]. In the case of one-cysteine peroxiredoxins, the C_R is not present at all and its C_P is recycled back to the reduced form by glutathione[65].

2.2.3 The role of peroxiredoxin hyperoxidation in cell signaling

Another feature of the catalytic cycle of some peroxiredoxins, is further oxidation of C_PSOH to sulfinic (C_PSO_2H) and sulfonic (C_PSO_3H) acids[66] (Fig-

Stellenbosch University https://scholar.sun.ac.za

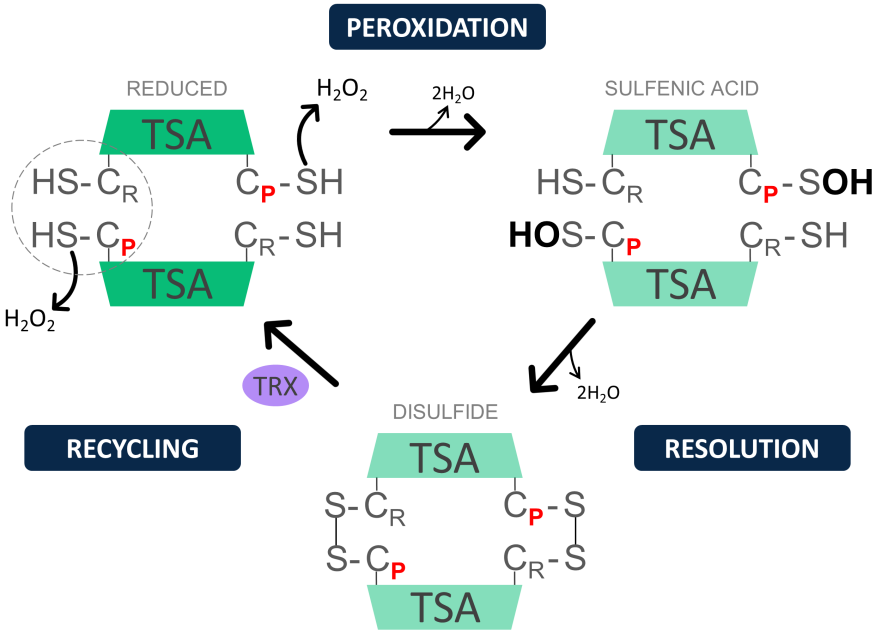

Figure 2.2: The catalytic cycle of TSA, a typical-two-cysteine peroxiredoxin from *S. cerevisiae*. This figure illustrates the universal three-reaction catalytic cycle of typical-two-cysteine peroxiredoxins. The first reaction, peroxidation, is the nucleophilic attack on the terminal oxygen of H_2O_2 to form H_2O which also transforms TSA to a sulfenic acid. The sulfenic acid then gets resolved into a disulfide during resolution. The disulfide form of TSA, exclusively, can then be recycled back to its original reduced state by Trx. Note that in this case C represents the cysteine residue of the protein; C_P = peroxidatic cysteine, C_R = resolving cysteine. Figure adapted from: Karplus, P.A. and Hall, A.: Structural Survey of the Peroxiredoxins. In: Flohé, L. and Harris, J.R. (eds.), *Peroxiredoxin Systems*, chap. 3, pp. 41-60. Springer, 2007.

ure 2.3). During conditions of oxidative stress, and thus an elevated H_2O_2 concentration, the resolution reaction of the catalytic cycle competes with a hyperoxidation reaction. When more H_2O_2 is present, the sulfenic acid form of the peroxiredoxin can be oxidized further to form a sulfinic acid. An additional enzyme, sulfiredoxin, is required to return peroxiredoxin to the sulfenic acid form[67]. With reducing equivalents supplied by another reductant such as Trx or glutathione, sulfiredoxin reduces hyperoxidized peroxiredoxin in a reaction coupled to ATP hydrolysis and in the presence of magnesium[68]. This reaction is slow (k_{cat} = 0.18 min^{-1}) compared to the other reactions in the system which supports the role for H_2O_2 as a signaling molecule[68].

Stellenbosch University https://scholar.sun.ac.za

Hyperoxidation is a property of eukaryotic typical-two-cysteine peroxiredoxins and it is speculated that this additional feature has evolved to mediate signaling function in higher organisms[3;69]. More specifically, hyperoxidized peroxiredoxin is catalytically inactive and it has been proposed that this inactivation is what facilitates the secondary messenger function of H_2O_2[3;50;70].

A study done by Yang *et al.* reported that the concentration of hyperoxidized peroxiredoxin was increased considerably at H_2O_2 concentrations ranging between 0.1 - 1 mM[66]. Interestingly, the same study also found that inactive hyperoxidized peroxiredoxins could still be identified in cells that were grown in the absence of H_2O_2, although to a lesser extent compared to the presence of increased H_2O_2 levels[66]. These results suggest that the peroxiredoxin system is not only functional in cellular oxidative stress conditions, but is also important under normal physiological conditions.

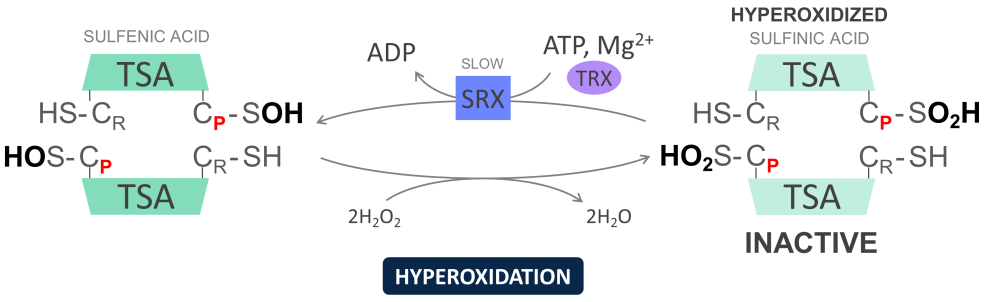

Figure 2.3: Hyperoxidation of a peroxiredoxin. The peroxiredoxin in the sulfenic acid form can be further oxidized by H_2O_2 during oxidative stress conditions when the concentration of ROS is elevated. Hyperoxidized peroxiredoxin is inactive and can be reduced back to the sulfenic acid form in a slow ATP-dependent reaction catalyzed by another enzyme known as sulfiredoxin (Srx). C_P = peroxidatic cysteine, C_R = resolving cysteine.

2.2.4 The thioredoxin system as an extension of the peroxiredoxin system

The reactivity of peroxiredoxins is sustained by shuttling of reducing equivalents through the highly conserved and ubiquitous Trx system[10;70]. The Trx system consists of the following: another thiol-containing, redox-active protein, Trx; a selenium-containing flavoenzyme, Trx reductase (TrxR); and the

Stellenbosch University https://scholar.sun.ac.za

primary supplier of reducing equivalents, NADPH (Figure 2.4)[71]. The active site disulfide in the oxidized form of Trx is reduced by TrxR in an enzymatic reaction with reducing equivalent supplied by NADPH[71]. The Trx system mainly functions to reduce protein disulfides, making it an important role player in redox homeostasis and redox signaling[72]. While the extracellular environment is generally more oxidative, the reducing capacity of Trx aids in keeping the environment inside the cell primarily reduced by reducing other protein disulfides.

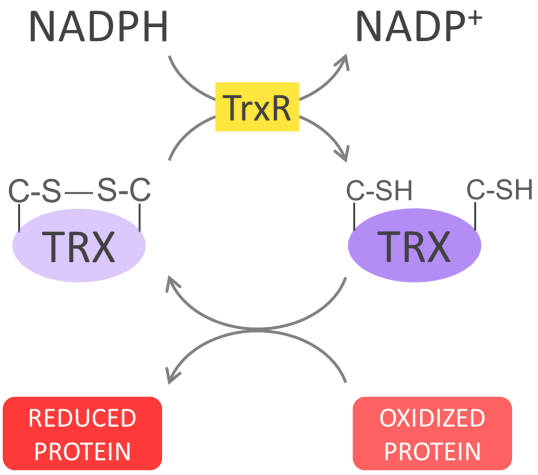

Figure 2.4: The thioredoxin system. The Trx system is comprised of Trx, TrxR and NADPH. Trx is reduced in an enzymatic reaction catalyzed by TrxR with reducing equivalents supplied by NADPH. The reduced form of Trx is important for cellular redox homeostasis as it reduces protein disulfides, including the disulfide form of peroxiredoxins. Note that *C* represents the cysteine residue of Trx.

The Trx system is associated with a vast array of physiological functions ranging from simple to more specialized depending on the organism[73]. For example, in *E. coli* cells, it has been shown that Trx is an important contributor to the process of filamentous phage assembly[74]. More specialized functions of Trx include acting as a hydrogen donor for methionine sulfoxide reductase, 3'-phosphoadenylsulfate reductase and ribonucleotide reductase during important metabolic processes such as protein repair, sulfur assimilation and DNA synthesis, respectively[75–77]. Additionally, Trx can act as a regulatory switch for the activation of the MAPK cascade member, ASK1, by forming a complex

Stellenbosch University https://scholar.sun.ac.za

with this kinase[72]. In the reduced form, Trx is associated with ASK1 which is reflective of an inactive kinase. Upon stress-induced oxidation of Trx, ASK1 dissociates and becomes activated to initiate apoptosis[72].

Trx plays a significant role in many physiological processes. A dysregulated Trx system, by implication, can contribute to various pathophysiological diseases often associated with oxidative stress and apoptosis[78;79]. A strong correlation between apoptotic HIV-infected cells and a down-regulated Trx system has been demonstrated by Masutani *et al.*[80]. Moreover, the ability of the Trx system to maintain redox homeostasis determines whether the cell death mode shifts from apoptosis to necrosis during oxidative stress conditions[81]. Taken together, these studies demonstrate the importance of a well-regulated Trx system. Some of these effects may well be due to associated downstream peroxiredoxin functionality.

The Trx system can be considered as an extension to the peroxiredoxin system since it is the provider of reducing equivalents for the regeneration of reduced peroxiredoxin[63]. Interestingly, it has been proposed that hyperoxidation of peroxiredoxin maintains the pool of reduced Trx and thereby directs its activity to processes critical for survival during high levels of oxidative stress[82]. Taken together, the peroxiredoxin and the Trx system (by extension) make ideal candidates that could be used to identify drug targets as these systems contribute to redox homeostasis and other metabolic processes necessary for cellular survival. In fact, antioxidative properties of peroxiredoxins and Trx system members in *Mycobacterium tuberculosis* have been correlated with resistance against the host's immune responses[83]. With this fact in mind, peroxiredoxins and H_2O_2 metabolism in pathogenic organisms show great potential for the identification of drug targets and development of therapeutic strategies.

2.3 Modeling the peroxiredoxin system

2.3.1 Taking a computational systems biology approach

Systems biology is a multidisciplinary field of study that applies principles of biology, computer science, mathematics, chemistry and physics to study cellular networks[84]. Although stoichiometric characterization is important when

Stellenbosch University https://scholar.sun.ac.za

studying metabolic systems, it is crucial to also determine the dynamic behaviour and interaction between the system components in order to deduce functional properties[84;85]. Systems biology aims to further our understanding of the function that arises from dynamically interacting molecules[84]. This is achieved by developing realistic computational models that not only describe system stoichiometry, but also detailed kinetic information[86]. Moreover, emergent system properties would likely go undiscovered if the system components were studied in isolation using the traditional *reductionist* approach[84].

The peroxiredoxin and Trx systems are not the exclusive sensors and regulators of the cellular redox state. Transcription factors, protein kinases, chaperones and low molecular weight compounds like ascorbate and glutathione all contribute to maintaning the intracellular redox environment[87–90]. Together, these sensors form a large integrated redox network responsible for neutralizing ROS and mediating redox signaling. How do we start the investigation into these complex, intricate and connected systems? Taking a computational systems biology approach has the potential to provide a quantitative framework to elucidate dynamic behaviours within these metabolic systems that could be challenging using only standard biochemical techniques in the laboratory[91;92]. The complexity of such a network of interacting macromolecules will be best studied using a combination of computational and experimental approaches[92].

2.3.2 Top-down and bottom-up computational modeling

Two distinct modeling approaches that exist within the field of systems biology are top-down and bottom-up[84]. The top-down approach begins with large experimental systemic data sets, often generated from high throughput "-omics" methods, and uses these to fit model parameters in an iterative process to identify new system components or the underlying kinetic mechanisms[84]. Models constructed using the top-down approach are considered phenomenological as prior knowledge of the specific mechanistic interactions is not required[84]. In constrast, the bottom-up approach entails disentangling the complete system into smaller parts and assigning a mathematical rate equation to each part based on a previously determined mechanism[84]. These smaller parts are then studied individually and later combined into a larger integrated model that can simulate the behaviour of the complete system[91]. Bottom-up modeling is

Stellenbosch University https://scholar.sun.ac.za

mechanism-based and relies on detailed and accurate kinetic descriptions of system constituents[84].

While both of these approaches have successfully been used to model cellular processes[93–97], some limitations can be addressed. Top-down modeling is advantageous in the sense that the result output is representative of the complete system. However, the correlations found between system components are essentially inferences of the true underlying mechanisms[84]. Another limitation is the uncertainty in the data generated by high throughput "-omics" methods which could implicate any downstream data analyses[98]. While the bottom-up approach can provide insights into the mechanism and organization of a metabolic system, it relies heavily on a highly accurate and complete parameter set[99]. It is not always possible to obtain kinetic parameters for certain reactions using direct experimental techniques or from curated online databases such as BRENDA (https://www.brenda-enzymes.org)[100]. It becomes necessary, thus, to fit unknown parameters using other available data which can lead to another complication such as parameter unidentifiability[101]. In addition to parameter uncertainty, further uncertainty in the kinetic descriptions of individual system reactions can lead to inaccurate models[102]. In principle, the most accurate models can be constructed using a combination of the top-down and bottom-up modeling approaches since the limitations of the one can be overcome by the strengths of the other[103].

2.3.3 Discrepancies in kinetic descriptions of redoxins

As mentioned above, the quality and predictive potential of a model constructed using the bottom-up approach is dependent on accurate kinetic descriptions of the constituent parts. Reactions involving peroxiredoxin, Trx and glutaredoxin (collectively called redoxins) have previously been given inconsistent kinetic descriptions[102]. While some have described redoxins as redox couples with redox potentials, other studies have characterized them as enzymes with Michaelis-Menten or ping-pong kinetics[104–108]. These discrepancies have impeded the development of accurate models for peroxiredoxin systems until recently when our research group was able to clarify these inconsistencies[102].

A feature of all redoxins is redox cycling. During redox cycling the reduced redoxin, for example Trx, reduces an oxidized protein, for example insulin.

Stellenbosch University https://scholar.sun.ac.za

Following reduction of insulin, unlike conventional enzymes, Trx becomes inactive[102]. Reducing energy provided by the other parts of the Trx system is required to reduce and activate Trx once again. Peroxiredoxins also undergo redox cycling and use Trx as reductant[64]. Pillay *et al.* were able to show that apparent Michaelis-Menten and ping-pong kinetics exhibited by Trx and peroxiredoxin reactions were in fact inherent kinetic properties of these systems[102]. For the analysis, they constructed a simple model with a generic one-cycle redoxin system modeled with mass action kinetics, while reduction of the redoxin itself was modeled with irreversible Michaelis-Menten kinetics[102]. They were able to show that the apparent enzymatic substrate saturation from an *in vitro* data set for insulin reduction by Trx[106] is attributed to the redistribution of reduced Trx to oxidized Trx at high substrate concentrations[102]. Additionally, using a similar approach with a two-cycle redoxin model they were able to show that the apparent ping-pong kinetics exhibited by peroxiredoxins from a study by Akerman *et al.*[108] could also be described sufficiently with mass action kinetics for the redoxin reactions[102]. Two important outcomes from this study can be highlighted: First, the inconsistencies found within literature can now be explained and redoxins should be modeled with mass action kinetics. Second, this discovery stresses the importance of systems biology by studying metabolic systems as a whole and not as isolated parts.

2.3.4 Existing computational peroxiredoxin system models

A computational model for *E. coli*, developed in our research group, investigated the connectedness of the individual Trx reactions[109]. An interesting discovery from this study was that the coupling of the peroxiredoxin redox cycle to the Trx system resulted in abrupt increases of reduced Trx concurrent with increases in TrxR[109]. Moreover, the model predicted a similar ultrasensitive decrease in the fluxes of other Trx-dependent reactions when increasing the concentration of H_2O_2 compared to the fluxes through the peroxiredoxin and TrxR reactions, which remained steady[109]. This ultrasensitivity observed in the peroxiredoxin system is a typical feature of signaling[110]. The computational analyses using this model led to intriguing results suggestive of complex modes of regulation within this redox network[109;110]. Moreover, these find-

Stellenbosch University https://scholar.sun.ac.za

ings are a step towards gaining an improved understanding of the underlying mechanisms in H_2O_2 metabolism.

Other recently published computational models for eukaryotic peroxiredoxin systems and H_2O_2 metabolism also aim to improve our understanding of the complexity of this network[96;97;111]. Tomalin *et al.* developed a model for *Schizosaccharomyces pombe* that could sufficiently predict the response of peroxiredoxin hyperoxidation *in vivo*[96]. They found that the intracellular H_2O_2 concentration reaches a threshold dependent on the extracellular H_2O_2 concentration that leads to the increase hyperoxidized peroxiredoxin[96]. Furthermore, a different study investigated the true function of peroxiredoxins in human erythrocytes[111]. This group addressed the fact that peroxiredoxins are one of the proteins present in high abundance in human erythrocytes, and reported rate constants within the 10^7 - 10^8 $M^{-1}s^{-1}$ range[97;112–114] suggest that all H_2O_2 should be consumed instantly, which is an overestimation of the experimentally determined activity of peroxiredoxins in erythrocytes[111]. The model that they developed incorporated a lower activity for H_2O_2 reduction by peroxiredoxins and was able to predict experimental observations[111]. Adimora *et al.* have gone a step further towards elucidating the mechanisms employed in H_2O_2 metabolism[97]. This group constructed a computational model aimed at describing the larger redox network in Jurkat T cells that comprises kinetic contribution by peroxiredoxins, Trxs, glutaredoxins, catalases and glutathione peroxidases[97]. Their model was able to determine redox states and fluxes for all antioxidant branches modeled, that would not have been possible experimentally[97].

Despite the many efforts towards building accurate computational models for the peroxiredoxin system and its role in H_2O_2 metabolism, the dynamics and regulation of the system remain poorly understood. Furthermore, published models such as those mentioned above, are often capable of describing some experimental observations, but these models are rarely used to investigate emergent properties of these systems[96;97;111]. In addition to gaining a comprehensive understanding of the dynamics and regulation of peroxiredoxin systems, being able to draw comparisons between different species could enable us to identify strengths and weaknesses within these systems. This could make the identification of drug targets or novel therapeutic intervention for infec-

Stellenbosch University https://scholar.sun.ac.za

tious diseases realistic prospects. For example, the survival of pathogens such as *M. tuberculosis* and *Plasmodium falciparum* is dependent on functional antioxidant systems[83;115]. Studies dedicated to the study of H_2O_2 metabolism in *M. tuberculosis* have led to extensive information about how these pathogens cope with oxidative stress conditions[83;116–118]. If a predictive computational model for the peroxiredoxin system of *M. tuberculosis* could be developed, it could be used to simulate inhibition of its antioxidative activity. It would be useful if the simulation could be repeated using a counterpart model for the human peroxiredoxin system and see whether the inhibition will have a significant effect on the host's antioxidant defense mechanisms[118].

2.3.5 Modeling the peroxiredoxin system of *S. cerevisiae*

The peroxiredoxin of *S. cerevisiae*, TSA, has been characterized and studied extensively over the last few decades *in vitro*[53;112;119–122]. However, to the best of our knowledge, a computational model for the peroxiredoxin system of *S. cerevisiae* does not yet exist. Developing such a model would be a step towards understanding the kinetic dynamics of eukaryotic H_2O_2 metabolism and being able to compare that to prokaryotic systems. The research goals for peroxiredoxin systems and H_2O_2 metabolism stated above are quite ambitious. Thus, the first attempt to achieve these goals will be to first develop a simple model and to improve and optimize it from there. As a widely used eukaryotic model organism, *S. cerevisiae* was a good choice for developing an initial simple model that can still represent higher organisms[123]. Furthermore, *in vitro* experiments are relatively easy to perform since *S. cerevisiae* proteins can easily be purified using bacterial expression hosts[124].

Well-established experimental assays that have previously been used to characterize the individual components of the peroxiredoxin system can be used to obtain experimental kinetic parameters[119;125–128]. Fitting the appropriate rate equation to each reaction in the system will yield a kinetic model that can be populated with these parameters[99]. Model simulation in conjunction with data sets from validation experiments could then be used to test the predictive power of the model constructed[99]. Once the model has passed validation tests, several computational analyses can be performed including steady state

Stellenbosch University https://scholar.sun.ac.za

and metabolic control analysis[129]. Results from these analyses could provide useful information about the distribution of flux through the system at steady state[130]. These analyses can help to identify the reactions that are responsible for regulation and control of flux through the system.

An intriguing recent discovery is the relationship between peroxiredoxins and circadian rhythm in eukaryotes[131–133]. Remarkably, O'Neill *et al.* demonstrated that a circadian rhythm of oxidized peroxiredoxin could be sustained in red blood cells which are anucleate[134]. This is a significant finding since feedback loops of transcription and translation are the basis of most circadian models[134]. Oscillatory behaviour of hyperoxidized peroxiredoxin has established a link between oxidative stress, redox signaling and circadian clocks which could have further implications for regulation H_2O_2 metabolism[133]. Subjecting a peroxiredoxin model with an oscillatory or pulse-like input of H_2O_2 could reveal potential emergent system properties that could improve our understanding of this relationship between peroxiredoxins and circadian rhythm. Using a computational modeling approach for this type of investigation is much more feasible compared to standard biochemical techniques.

2.4 Concluding remarks

Oxidative stress, and H_2O_2 metabolism, play important roles in both normal conditions and in diseased states. The peroxiredoxin system is an efficient neutralizer of H_2O_2, but somehow maintains its levels for essential signaling functions to occur. This system forms part of an intricate and complex redox network. The kinetic dynamics that govern this functionality are still poorly understood. A combination of experimental and computational techniques can enable us to embark on the investigation into this complex network. Computational model simulations could lead to the discovery of emergent properties and inherent system behaviours that would otherwise be challenging using only standard wet laboratory techniques.

Stellenbosch University https://scholar.sun.ac.za

Chapter 3

Materials and methodology

3.1 Research design

Briefly, the study was designed as follows: three peroxiredoxin system proteins from *S. cerevisiae* with a poly-histidine tag were overexpressed in an *E. coli* BL21 (DE3) host organism. The His-tagged proteins were then purified using immobilized metal affinity chromotography (IMAC). Protein overexpression and purity were confirmed on a tricine-SDS-PAGE gel. A range of previously established spectrophotometric assays were then performed to experimentally obtain parameters to populate a simple computational model of the peroxiredoxin system of *S. cerevisiae* using modeling software developed by our research group (PySCeS - discussed in Section 3.4.5.3). This software was then used to perform model simulations. Specifically, the model was subjected to a pulse-like input of H_2O_2 to demonstrate the system behaviour in response to a transient stress input.

3.2 Materials

All general laboratory reagents such as salts and buffer components used in this study were of the highest quality available.

The following items were obtained from Sigma-Aldrich: Glass beads ($\leq$106 µm), kanamycin sulfate, PEG (average Mr 20 000), insulin (human recombinant), acrylamide/bis-acrylamide (30%), hydrogen peroxide (30%), β-mercaptoethanol, imidazole, tricine, ammonium persulfate, isopropyl β-D-1-thiogalactopyranoside

Stellenbosch University https://scholar.sun.ac.za

(IPTG), dithiothreitol (DTT), nicotinamide adenine dinucleotide phosphate (NADPH), bovine serum albumin (BSA), 2,2,2-trichloroethanol (TCE), 5,5'-dithio-bis (2-nitrobenzoic acid) (DTNB), sodium dodecyl sulfate (SDS) and N,N,N',N'-tetramethylethylenediamine (TEMED). LB growth media were obtained from Merck. Protein Molecular Weight Standards (Broad Range) were obtained from Bio-Rad. cOmplete^{TM} EDTA-free protease inhibitor and cOmplete^{TM} His-Tag purification resin were obtained from Roche. SnakeSkin Dialysis Tubing was purchased from Thermo Fisher Scientific.

3.2.1 Common reagents

3.2.1.1 NADPH (5 mM)

All NADPH stock solutions were freshly made up directly before use to avoid degradation. Before use, a stock of 5 mM was made up by weighing out 2.1 mg of NADPH and the volume brought up to 0.5 mL using 0.01 M NaOH as solvent.

3.2.1.2 DTT (0.1 M)

DTT stock solutions were all made up freshly on the day of use. To make up 1 mL of a 0.1 M DTT stock, 15.4 mg of DTT was weighed out and brought to a volume of 1 mL using mqH_2O (Milli-Q® ultrapure water).

3.2.1.3 DTNB (50 mM)

To make up 15 mL of a 50 mM DTNB stock, 0.297 g of DTNB powder was weighed out and brought to a volume of 15 mL using mqH_2O. The container of the solution was then covered in foil and stored in the dark at 4°C as DTNB in solution is light sensitive.

3.2.1.4 Insulin (1.6 µM)

To make up 1 mL of a 1.6 µM insulin stock, 9.3 mg of insulin powder was weighed out and brought to a volume of approximately 200 µL using 50 mM Tris-HCl (pH 7). The pH was then brought down using small volumes of 0.01 M HCl until the insulin solubilized. The pH was subsequently brought back to 7 using small volumes of 0.01 M NaOH. The volume was adjusted to

Stellenbosch University https://scholar.sun.ac.za

1 mL using 50 mM Tris-HCl (pH 7). The insulin stock was then aliquoted and stored at -20°C.

3.2.1.5 H_2O_2 (2 mM)

H_2O_2 stock solutions were made up fresh every time before use. The concentration of the 30% (w/w) stock H_2O_2 was determined spectrophotometrically at 240 nm each time before use using an extinction coefficient of 43.6 $M^{-1}cm^{-1}$[135]. A range of different millimolar stocks were made up using the 30% (w/w) stock H_2O_2 with mqH_2O as solvent. All tubes containing H_2O_2 stocks were covered in foil and kept on ice until use.

3.2.2 Microorganisms

Agar plates with colonies of *E. coli* BL21 (DE3) cells containing pET-28a(+) expression vectors cloned with *S. cerevisiae* Trx, TrxR and TSA gene sequences with an added N-terminal His-tag were kindly supplied by the laboratory of Dr. Ché Pillay (University of KwaZulu-Natal). Subsequently, glycerol freezer stocks were made from these plates and stored at -80°C for future use.

3.2.3 Bacterial growth media

LB medium was used for all bacterial plates, starter and expansion cultures. All media were sterilized by autoclaving and supplemented with kanamycin to a final concentration of 30 µg/mL.

3.2.4 Buffers

All buffers used for IMAC (Sections 3.2.4.2 - 3.2.4.4 below) were prepared according to the manufacturer's instructions for the cOmplete™ His-Tag purification resin (Roche). cOmplete™ EDTA-free protease inhibitor (Roche) was added to the extraction buffer before use (Section 3.2.4.1).

3.2.4.1 Extraction buffer

The extraction buffer used contained Tris-HCl (20 mM), EDTA (1 mM), DTT (5 mM) and NaCl (10 mM). The pH was adjusted to 7.5 and the buffer stored at 4°C. 25 mL aliquots of extraction buffer were stored at -20°C and thawed

Stellenbosch University https://scholar.sun.ac.za

only once before use followed by the addition of a half tablet of cOmplete^{TM} EDTA-free protease inhibitor. After use, the remaining extraction buffer was kept at 4°C. Thawed extraction buffer was disposed of after 14 days if not used.

3.2.4.2 IMAC equilibration buffer

IMAC equilibration buffer was prepared using mqH_2O as solvent and contained NaH_2PO_4 (50 mM) and NaCl (300 mM). The pH was adjusted to 8.0 with NaOH and the buffer stored at 4°C. The equilibration buffer contained no imidazole.

3.2.4.3 IMAC wash buffer

IMAC wash buffer was prepared using mqH_2O as solvent and contained NaH_2PO_4 (50 mM), NaCl (300 mM) and imidazole (15 mM). The pH was adjusted to 8.0 with NaOH and the buffer stored at 4°C.

3.2.4.4 IMAC elution buffer

IMAC elution buffer was prepared using mqH_2O as solvent and contained NaH_2PO_4 (50 mM), NaCl (300 mM) and imidazole (250 mM). The pH was adjusted to 8.0 with NaOH and the buffer stored at 4°C.

3.2.4.5 Tricine-SDS-PAGE 2x sample buffer

A 2x sample buffer for tricine-SDS-PAGE was prepared and contained Tris-HCl (100 mM), SDS (1% m/v), glycerol (24% v/v), Coomassie Brilliant Blue R-250 (0.02% m/v) and β-mercaptoethanol (4% v/v). The pH was adjusted to 6.8 with HCl and the buffer stored at -20°C [136]. A non-reducing tricine-SDS-PAGE 2x sample buffer was prepared with the same components as for the reducing sample buffer above but did not contain β-mercaptoethanol.

3.2.4.6 Tricine-SDS-PAGE Tris-HCl buffer

A Tris-HCl buffer was prepared and used only for the casting of all tricine-SDS-PAGE resolving and stacking gels [136]. To make up 250 mL of a 2.5 M Tris-HCl buffer 75.713 g of Tris-HCl was weighed out and dissolved in mqH_2O. The pH was adjusted to 8.8 with NaOH and 50 mL aliquots were stored at 4°C.

Stellenbosch University https://scholar.sun.ac.za

3.2.4.7 Tricine-SDS-PAGE running buffer

Tricine-SDS-PAGE running buffer was prepared and contained Tris-HCl (25 mM), tricine (25 mM) and SDS (0.05% w/v)[136]. There was no need to adjust the pH of this buffer and was stored at 4°C and at room temperature before use.

3.3 Recombinant protein expression and purification

3.3.1 Culturing of *E. coli* for recombinant expression of Trx, TrxR and TSA

The following methodology for culturing of *E. coli* cells to express all recombinant proteins (Trx, TrxR, TSA) was used. Differences will be indicated where necessary. The optimal concentration of IPTG and time of induction for each protein were determined with expression trials and activity assays (results not shown).

Starter cultures (LB media supplemented with 30 µg/mL kanamycin) were seeded with *E. coli* BL21 (DE3) cells cloned with the recombinant protein sequence of interest from glycerol freezer stocks. These starter cultures were grown overnight (12 hours) in a shaking incubator (150 rpm) at 37°C. The following day, expansion cultures of 12.5× the volume of the starter culture were seeded with the overnight starter culures and grown in a shaking incubator (150 rpm) at 37°C until the optical density at 600 nm (OD_{600}) reached 0.6 (approximately 2 hours). IPTG was then added to a final concentration of 0.1 mM to induce recombinant protein expression. Induced cultures were then grown further in a shaking incubator (150 rpm) at 30°C for 6 hours (Trx and TrxR) and 5 hours (TSA). Cells were harvested by centrifugation of the liquid culture at 10 000 rpm at 4°C for 15 minutes. Harvested cells were concentrated 40×, relative to the original culture volume, by resuspending the pellet with 100 mM Tris-HCl (pH 7). The cell suspension was then aliquoted into 2 mL tubes and centrifuged again at 10 000 rpm at 4°C for 15 minutes. The supernatant was discarded and harvested cell pellets stored at -80°C. If the harvested cells were not stored at -80°C directly after culturing, then the re-

Stellenbosch University https://scholar.sun.ac.za

suspension step would be replaced by resuspension using extraction buffer and extraction of the suspension would follow directly (see Section 3.3.2 below).

3.3.2 Preparation of crude cell lysate

Harvested cell pellets were taken from the -80°C freezer to thaw and kept on ice. Pellets were resuspended in 10 to 15 mL of ice cold extraction buffer (Section 3.2.4.1). The disruption of *E. coli* cells were performed using glass beads (≤106 µm particle size from Sigma). 1 mL of cell suspension was added to 1 g of glass beads in a glass cuvette. The cells were then disrupted by vortexing the cell-glass bead suspension for 60 seconds on high speed followed by 20 seconds on ice. This cycle was repeated seven times. The suspension was subsequently centrifuged at 10 000 rpm at 4°C for 15 minutes. Afterwards, the crude cell lysate (supernatant) was removed very carefully and kept on ice for the next step: incubation of crude lysate onto the IMAC resin. In the case of the preparation of TSA crude lysate, an additional amount of DTT was added to a final concentration of 5 mM to ensure that TSA would be purified in its fully reduced form.

Cell disruption was monitored using a lactate dehydrogenase activity assay. Specifically, the reverse reaction, in which pyruvate gets converted to lactate, was monitored. The oxidation of NADH to NAD^+ was measured spectrophotometrically at 340 nm. The assay consisted of NADH (0.8 mM), pyruvate (2 mM), Tris-HCl (100 mM). The reaction was initiated with the addition of 10 µL of lactate-containing crude cell lysate. An observable decrease in absorbance at 340 nm over time was an indication of lysate activity.

Protein concentration of the crude cell lysate was determined using the bicinchoninic acid (BCA) assay[137].

3.3.3 Protein purification with IMAC

A sepharose-based, Ni^{2+} chelate resin (cOmplete^{TM} His-Tag purification resin) was used for the purification of His-tagged recombinant Trx, TrxR and TSA. Columns (20 mL syringes) were packed to obtain a resin bed volume of 5 mL. Buffers used for the equilibration and elution steps were prepared in accordance with the manufacturer's recommendations. The imidazole concentration in the

Stellenbosch University https://scholar.sun.ac.za

wash buffer had to be optimized to ensure a highly purified elution fraction. An imidazole concentration of 15 mM in the wash buffer resulted in wash fractions with no His-tagged proteins and elution fractions with minimal impurities.

Columns were first equilibrated with 20 column volumes of equilibration buffer (Section 3.2.4.2) before incubation with lysate. Previously prepared crude cell lysate was first filter sterilized by passing it through a 0.22 µm syringe filter. The clear lysate was then added to the column and incubated on a Barnstead Labquake® Rotisserie Shaker at 4°C for 16 hours. The column flow through fraction contained the unbound proteins and were eluted by gravity, collected and the volume noted. The columns were subsequently washed with at least 5 column volumes of wash buffer (Section 3.2.4.3) to elute histidine-rich proteins. Elution buffer was then added to the column and incubated on the rotator for 30 minutes at 4°C. His-tagged recombinant proteins were then eluted with 4 column volumes of elution buffer (Section 3.2.4.4) and kept on ice. Protein concentration of all IMAC fractions were determined using the BCA assay.

The columns were cleaned in accordance with the manufacturer's instructions and stored in 20% ethanol at 4°C until the next purification.

3.3.4 Concentration of purified recombinant proteins by dialysis

IMAC was immediately followed by buffer exchange and protein concentration by dialysis. The complete elution fraction was added to an appropriate amount of SnakeSkin Dialysis Tubing with a molecular weight cut-off of 3.5 kDa. The tubing was placed on dry poly(ethylene glycol) 20 000 powder for 3 hours to remove the majority of water present in the sample. Hereafter, imidazole was removed by dialyzing the sample against the appropriate buffer required for subsequent kinetic assays. For TrxR, the dialysate was composed of 500 mM potassium phosphate and 10 mM EDTA (pH 7). For Trx, the dialysate was composed of 100 mM potassium phosphate and 2 mM EDTA (pH 7). For TSA, the dialysate was composed of 25 mM potassium phosphate, 100 mM ammonium sulphate and 1 mM EDTA.

Stellenbosch University https://scholar.sun.ac.za

3.3.5 Determination of the protein concentration of purified recombinant proteins

Dialysis was followed by determination of the protein concentration of the purified protein sample by measuring the absorbance at 280 nm[138]. The extinction coefficient and molecular weight of each protein was determined using the ExPASy's ProtParam tool (https://web.expasy.org/protparam/). The values for these parameters are indicated in Table 3.1. The extinction coefficient and molecular weight were used to determine the protein concentration in molar and mg/mL respectively.

Table 3.1: Biochemical parameters for recombinant proteins.

Protein	MW (kDa)	ε_{280} (M^{-1} s^{-1})
TrxR	36.061	24410
Trx	12.057	9970
TSA	22.412	24075

3.3.6 Tricine sodium dodecyl sulfate polyacrylamide gel electrophoresis

IMAC fractions were analyzed with SDS-PAGE. The separation of low molecular weight proteins (1-30 kDa) can be challenging using the original Laemmli glycine-SDS-PAGE method due to the requirement of high-percentage or gradient gels[139]. These in turn, are associated with issues such as irreproducibility, difficulty with gel casting and difficulty with low molecular weight protein recovery for quantitative analyses[140]. A tricine-SDS-PAGE system developed by Schägger and Von Jagow[141] in which tricine is used as the trailing ion offers a method to separate low molecular weight proteins successfully resulting in high resolution bands. A modified method based on the tricine-SDS-PAGE system was used in this study by which low molecular weight Trx (12 kDa), TrxR (35 kDa) and TSA (23 kDa) could be resolved using a low-percentage gel making it suitable for further quantitative analyses using UV-detection[136].

Stellenbosch University https://scholar.sun.ac.za

Protein samples were loaded onto gels that consisted of 15% resolving and 4% stacking gels. Gels were prepared as indicated in Table 3.2. Gel solutions contained ready to use 30% (w/v) acrylamide:bis (37.1:5), Tris-HCl (Section 3.2.4.6) and 2,2,2-tricholoroethanol. The latter was added to the resolving gel only to allow for fluorescent visible detection of proteins in samples. Polymerization of both the resolving and stacking gels was initiated by the addition of TEMED and freshly prepared ammomium persulfate. Protein samples were prepared in reducing sample buffer (Section 3.2.4.5) and boiled for 5 minutes at 95°C before loading. In the case of TSA, both reducing and non-reducing sample buffer were used to visualize monomeric and dimeric forms of TSA, respectively. A 1:20 dilution of SDS-PAGE Molecular Weight Standards, Broad Range, was prepared in reducing sample buffer and stored at -20°C until use.

Once the gel was completely polymerized, 7 µL of the molecular standards was added to a single lane. The electrophoresis chamber was filled with an appropriate volume of tricine-SDS-PAGE running buffer (Section 3.2.4.7). A constant voltage of 135 V was applied until the dye front reached the bottom of the gel (approximately 2 hours). After electrophoresis, the gel was removed from the glass plates and visualized by fluorescent visible detection.

Table 3.2: Protocol for the preparation of the 15% resolving and 4% stacking gels for tricine-SDS-PAGE.

Reagents	*15% Resolving gel (mL)*	*4% Stacking gel (mL)*
Tris-HCl (2.5 M) (Section 3.2.4.6)	5.25	0.76
mqH_2O	0.3728	3.425
Acrylamide:bis, 37.5:1 (30% w/v)	6.0	0.66
2,2,2-Tricholoroethanol (100% w/v)	0.090	0
TEMED	0.0072	0.005
Ammonium persulfate (20% m/v)	0.1	0.15

Stellenbosch University https://scholar.sun.ac.za

3.4 Determination of activities for individual peroxiredoxin system components of *S. cerevisiae*

To obtain kinetic parameters for the complete peroxiredoxin system of *S. cerevisiae*, the system components were studied in isolation. This was achieved by performing a range of spectrophotometric kinetic assays to obtain experimental initial rate data for single reactions. The data from these experiments were then used to obtain the parameters required to populate a computational model for the peroxiredoxin system of *S. cerevisiae*. Parameters include reaction rate constants for mass action reactions and catalytic constants (k_{cat}) and Michaelis constants (K_m) for enzymatic reactions. Those parameters that could not be obtained with direct experimental assays were fitted using the available experimental data sets.

3.4.1 DTNB Reduction Assay

The DTNB reduction assay was used to determine rate kinetics of purified TrxR. TrxR catalyses the conversion of DTNB, or Ellman's reagent, to TNB in an NADPH-dependent enzymatic reaction[128]. TNB is bright yellow in colour with an extinction coefficient of 13 600 M^{-1} cm^{-1} at 412 nm[128]. The assay mixture for all DTNB reduction assays contained 0.5 M potassium phosphate, 10 mM EDTA, 0.5 M NaCl, 50 mM KCl and 0.2 mg/mL BSA (pH 7). All assays were performed in a 96-well microtiter plate with a final sample volume of 100 µL at 25°C. The increase in absorbance at 412 nm were measured using a SPECTROstar® *Nano* spectrophotometer. Three experiments were performed using the DTNB assay under these assay conditions. In each experiment a different component of the reaction was varied while keeping the other two at a constant concentration. Each experiment was done in triplicate from the same batch of enzyme. The value of **n** in the Results chapter thus represents three technical repeats.

3.4.1.1 Thioredoxin reductase

The concentration of TrxR was varied from 0 to 5 µM at fixed NADPH and DTNB concentrations of 250 µM and 2.5 mM, respectively. The following

Stellenbosch University https://scholar.sun.ac.za

controls were included: a control containing no TrxR, a control containing no NADPH for each TrxR concentration and a control containing no DTNB for each TrxR concentration.

The concentration of the substrate DTNB was varied from 0 to 7.5 µM at fixed NADPH and TrxR concentrations of 250 µM and 1.5 µM, respectively. The following controls were included: a control containing no DTNB, a control containing no NADPH for each DTNB concentration and a control containing no TrxR for each DTNB concentration.

The concentration of the substrate NADPH was varied from 0 to 500 µM at fixed DTNB and TrxR concentrations of 2.5 mM and 1.5 µM, respectively. The following controls were included: a control containing no NADPH, a control containing no DTNB for each NADPH concentration and a control containing no TrxR for each NADPH concentration.

For each experiment described above, the reaction was initiated by the addition of NADPH to all other assay components to ensure consistency across different experiments.

3.4.2 Insulin Reduction Assay

A turbidimetric assay of insulin reduction developed by Holmgren[125] was used to obtain kinetic parameters for the thioredoxin system consisting of Trx, TrxR and NADPH. In this assay reduced Trx reduces the interchain disulfide bridges present in oxidized insulin. Precipitation of the free B chain of insulin results in an increase in turbidity which can be measured spectrophotometrically at 650 nm[125].

The assay can include two reductants for Trx: DTT or the TrxR-NADPH couple. The DTT-coupled assay was used to set up a calibration curve for reduced insulin[126]. The TrxR-NADPH-coupled assay was used to obtain the kinetic rate constant for the reaction between insulin and Trx and the dissociation constant for oxidized Trx with TrxR. All assays were performed in a 96-well microtiter plate with a final sample volume of 100 µL at 25°C. The increase in turbidity at 650 nm were measured using a BioTek PowerWave™ 340 spectrophotometer.

Stellenbosch University https://scholar.sun.ac.za

3.4.2.1 Reduced insulin calibration curve

The assay mixture contained 0.4 µM Trx, 1 mM DTT, 2 mM EDTA and 100 mM potassium phosphate (pH 6). The concentration of insulin was varied from 0 to 120 µM. The increase in turbidity was then measured at 650 nm for 2.9 hours until the reaction was complete. At this time the absorbances showed a visible plateau over time. Since insulin also precipitates out of solution at higher pH, 0.5 µL of 0.01 M HCl was added to each well to ensure that turbidity was as a result of reduced insulin B chain only. The plate was then placed back in the spectrophotometer and allowed to shake for 30 seconds to homogenize the solution as the precipitation product might have settled to the bottom of the wells which resulted in a higher absorbance reading at 650 nm that did not reflect the true absorbance reading of the reduced insulin solution. An end-point measurement at 650 nm was then taken immediately after mixing the contents of the plate and was used to construct a calibration curve for fully reduced insulin.

3.4.2.2 Thioredoxin

This section describes the TrxR-NADPH-coupled insulin reduction assay that was used to obtain the experimental kinetic data.

For the first experiment, the concentration of insulin was varied from 0 to 250 µM. The concentration of Trx was kept constant at 0.4 µM. Other assay components included 2 µM TrxR, 250 µM NADPH, 2 mM EDTA and 100 mM potassium phosphate (pH 6.5). The following controls were included: a control containing no insulin, a control containing no Trx for each insulin concentration and a control containing no TrxR for each insulin concentration.

The concentration of Trx was varied from 0 to 5 µM for the second experiment. The concentration of insulin was kept constant at 130 µM. Other assay components included 2 µM TrxR, 250 µM NADPH, 2 mM EDTA and 100 mM potassium phosphate (pH 6.5). The following controls were included: a control containing no Trx, a control containing no insulin for each Trx concentration and a control containing no TrxR for each Trx concentration.

For each experiment described above, the reaction was initiated by the addition of Trx to all other assay components to ensure consistency across different

Stellenbosch University https://scholar.sun.ac.za

experiments.

3.4.3 DTT Oxidation Assay

The activity of TSA was determined using the DTT oxidation assay. This assay is based on the increase in absorbance at 310 nm as DTT becomes oxidized (ε_{310} = 110 M^{-1} cm^{-1})[142]. DTT, present in excess, reduces TSA which in turn reduces H_2O_2. As soon as the reaction is initiated by H_2O_2, the TSA cycle becomes active which will cause a steady initial increase in oxidized DTT which can be monitored spectrophotometrically at 310 nm.

Similar assay conditions used by Tairum *et al.*[119] were also used in this study. However, the buffer components used in this study were those successfully used by Nelson *et al.* for measuring the activity of peroxiredoxins[143]. The concentration of TSA was varied from 0 to 35 µM. The assay mixture contained 10 mM DTT, 100 mM ammonium sulfate, 1 mM EDTA and 25 mM potassium phosphate (pH 7). Each individual sample of TSA was incubated in the DTT-containing assay mixture for 20 minutes before the reaction was started. 10 µL of H_2O_2 was placed in a 100 µL Hellma® Analytics quartz cuvette at a final concentration of 1 mM. The reaction was initiated by addition of the assay mixture to the correct final volume and mixed by resuspension. In this case the final volume was 110 µL. The increase in absorbance at 310 nm was monitored using an Agilent Cary 60 UV-Vis spectrophotometer. A control was also included that did not contain TSA. The absorbance change for the TSA-containing samples was corrected for by subtracting the absorbance change for the control.

3.4.4 Complete System Assay

The activity of TSA towards H_2O_2 was also measured with an NADPH-dependent assay representative of physiological conditions developed by Nelson *et al.* in which all system components were present: TSA, TrxR, Trx and NADPH[143]. In this assay, TSA oxidation is coupled to the Trx system (Trx, TrxR and NADPH) which provides the reducing equivalents for TSA activity. TSA activity is indirectly measured by monitoring the decrease in absorbance at 340 nm as NADPH gets oxidized (ε_{340} = 6 220 M^{-1} cm^{-1})[143].

Stellenbosch University https://scholar.sun.ac.za

The following conditions and steps were applied to all experiments. The assay mixture containing all system components except for H_2O_2 was incubated for 10 minutes before the reaction was started. This was done to ensure the system is fully reduced before H_2O_2 was added to initiate oxidation.

In a first set of experiments, the concentration of TSA was varied from 0 to 2 µM. The assay mixture contained 150 µM NADPH, 0.5 µM TrxR, 10 µM Trx, 20 µM H_2O_2, 100 mM ammonium sulfate, 1 mM EDTA and 25 mM potassium phosphate (pH 7). 10 µL of H_2O_2 was placed in a 100 µL Hellma® Analytics quartz cuvette at a final concentration of 20 µM. The reaction was initiated by addition of the assay mixture to the correct final volume and mixed by resuspension. In this case the final volume was 110 µL. The increase in absorbance at 340 nm was monitored using an Agilent Cary 60 UV-Vis spectrophotometer at 25°C. A control was also included that did not contain TSA.

Two separate sets of experiments were then performed in which the concentration of H_2O_2 was varied. In the first experiment, H_2O_2 was varied from 0 to 10 µM and the concentration of TSA in the assay mixture was 0.05 µM. In the second experiment, H_2O_2 was varied from 0 to 50 µM and the concentration of TSA in the assay mixture was 0.5 µM. For both these experiments, the rest of the assay mixture contained 150 µM NADPH, 0.5 µM TrxR, 10 µM Trx, 100 mM ammonium sulfate, 1 mM EDTA and 25 mM potassium phosphate (pH 7). 10 µL of H_2O_2 was placed in a 100 µL Hellma® Analytics quartz cuvette to the appropriate varying final concentration. The reaction was initiated by addition of the assay mixture to the correct final volume and mixed by resuspension. In both cases the final volume was 110 µL. The increase in absorbance at 340 nm was monitored using an Agilent Cary 60 UV-Vis spectrophotometer at 25°C. For both experiments, a control was also included that did not contain TSA.

3.4.5 Kinetic Modeling

3.4.5.1 Computational programs and packages

All numerical computation and data analyses in this study were performed with software written in the Python programming language (http://python.

Stellenbosch University https://scholar.sun.ac.za

org). The Jupyter notebook (https://jupyter.org) was used as an interactive environment in which all data analysis, manipulation, integration and visualization took place. Together, these notebooks essentially served as an *e-labbook* for the *in silico* experiments of this study[144]. Relevant notebooks and model files used in this study are attached as file appendices to this thesis.

Basic Python packages such as NumPy (https://numpy.org), SciPy (https://scipy.org) and Matplotlib (https://matplotlib.org) were used for numerical computation and data visualization. The Pandas package (https://pandas.pydata.org) was used for handling large, structured data sets. A non-linear least-squares minimization and curve-fitting package for Python known as LmFit (https://pypi.org/project/lmfit/) based on the Levenberg-Marquardt algorithm was used to fit equations to experimental data and obtain kinetic parameters.

3.4.5.2 Fitting of model parameters

The initial linear section of the absorbance time-course for each assay experiment was taken. The slope was then converted to a rate with units µM min^{-1} using the extinction coefficient of the light absorbing component in the assay. The insulin calibration curve (Section 3.4.2.1) was used to convert rates in terms of absorbance units to a rate with units µM min^{-1} in the case of the insulin reduction assay. Rates were plotted against the concentration (in µM) of the varying substrate of the experiment. These plots were then used for fitting. Non-linear least-squares minimization and curve-fitting based on the Levenberg-Marquardt algorithm were used to fit to the corresponding equation for that reaction to experimental data and obtain kinetic parameters. This was done using the LmFit package mentioned above.

3.4.5.3 Model simulation of the peroxiredoxin system of *S. cerevisiae*

The Python Simulator for Cellular Systems (PySCeS, pysces.sourceforge.net) software developed by our research group was used for all model simulations and analyses[145]. The peroxiredoxin model for *S. cerevisiae* (see Appendix A.2) populated with the experimentally obtained kinetic parameters was subjected to simulation experiments using PySCeS. These simulations were de-

Stellenbosch University https://scholar.sun.ac.za

signed to specifically investigate the reaction in which H_2O_2 gets reduced by TSA.

First, the model was evaluated to confirm whether it was able to simulate independent experimental assay results (see Appendix C.1). Examples of model independent results were the complete system assay experiments in which H_2O_2 was varied. The methods for these assay experiments are described in Section 3.4.4 above. For the simulation experiment, the metabolite concentrations were set to the values used in the assay experiment. Using PySCeS, the steady state flux was subsequently calculated for the same range of varying substrate concentrations used in the assay. The model simulation and experimental data were then plotted together. If the y-axis values were not comparable for the model simulation *vs.* experimental result, then the plots were positioned adjacent to one another.

Second, a PySCeS parameter scan was performed. The steady state concentration of the oxidized and reduced state of both system moieties, Trx and TSA, were scanned over a range of H_2O_2 concentrations (see Appendices C.2 and C.3).

Third, the *in vitro* PySCeS model was subjected to a pulse-like H_2O_2 input to evaluate the capacity of the system to cope with this type of stress input. This was done computationally by adding an assignment rule to an arbitrary variable, Y, in the model (see Appendix A.3) . The assignment rule was described by a sinusoidal function that could define the number of pulses added as well as the time period of the simulation. A time dependent event was also incorporated into the model which was triggered at each time point that Y reached the maximum of the sinusoidal function. Specifically, the event triggered the addition of a specified amount of H_2O_2 to the initial H_2O_2 concentration. For the simulation experiments the number of pulses to trigger was set to five over a time period of 40 minutes. Five different concentrations for the H_2O_2-pulse were tested: 0.001, 0.5, 2.5, 5 and 10 µM. The change in concentration of the system moieties, Trx and TSA, was then plotted over time together with the H_2O_2 concentration. See Appendix A.3.

The SUNDIALS CVODE integrator was used in PySCeS for simulations of model that contained an event or forcing function.

Stellenbosch University https://scholar.sun.ac.za

Chapter 4

Results

4.1 Recombinant protein expression and purification

E. coli BL21 (DE3) cells cloned with His-tagged TrxR, Trx and TSA from *S. cerevisiae* were cultured and induced for protein overexpression with IPTG as described in Section 3.3. Cytosolic proteins were extracted and the His-tagged proteins were purified with IMAC. Successful induction and protein purity were confirmed by loading lysate and IMAC fraction samples onto a Tris-tricine SDS-PAGE gel. TrxR and Trx samples were prepared in denaturing (reducing) SDS-PAGE sample buffer and TSA was prepared in both dentaturing and non-denaturing (non-reducing) SDS-PAGE sample buffer. All gels were visualized by fluorescent visible detection.

Results shown below include an SDS-PAGE gel to confirm purity and a table to indicate protein yield from a representative culture batch.

4.1.1 Thioredoxin reductase

TrxR was successfully expressed by IPTG induction indicated by the intense dark band in the lane loaded with cell lysate (Figure 4.1). The protein was purified to a high degree of homogeneity indicated by another intense dark band in the lane loaded with elution sample, which is located at the same size as the overexpressed protein sample, and has minimal contamination. The recombinant protein had the expected size of 35 kDa for TrxR.

Stellenbosch University https://scholar.sun.ac.za

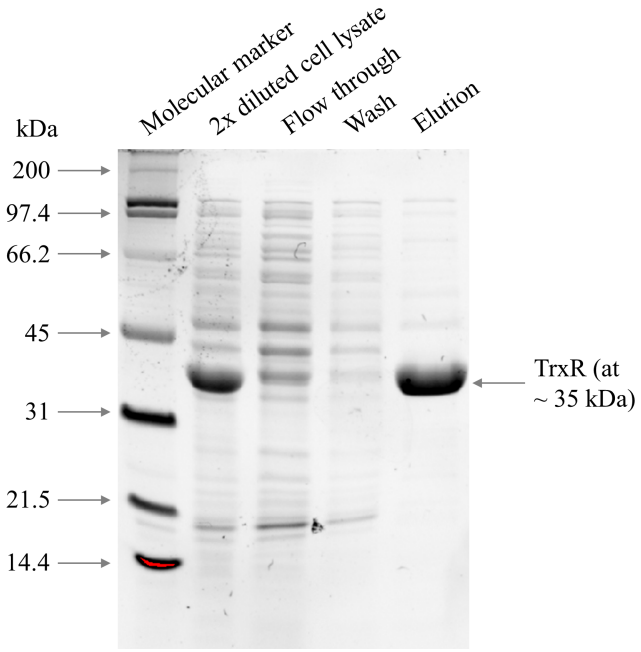

Figure 4.1: SDS-PAGE of TrxR purification by IMAC. *E. coli* BL21 (DE3) cells cloned with *S. cerevisiae* TrxR were induced for protein overexpression with IPTG. An equal volume of protein sample was loaded into each lane. Samples were prepared in denaturing SDS-PAGE sample buffer. The molecular weight marker (7 µL) was loaded in the first lane. The lane loaded with cell lysate shows the overexpressed protein visible as a dark band at approximately 35 kDa. The lanes loaded with IMAC flow through and wash fractions contained no overexpressed TrxR. The last lane shows the IMAC elution fraction with a dark band for TrxR at the expected size of approximately 35 kDa.

4.1.2 Thioredoxin

Trx was successfully expressed by IPTG induction indicated by the intense dark band in the lane loaded with cell lysate (Figure 4.2). The protein was purified to a high degree of homogeneity indicated by dark bands in the lanes loaded with elution fraction samples, which is located at the same size as the overexpressed protein sample, and has minimal contamination. The recombinant protein had the expected size of 12 kDa for Trx.

Stellenbosch University https://scholar.sun.ac.za

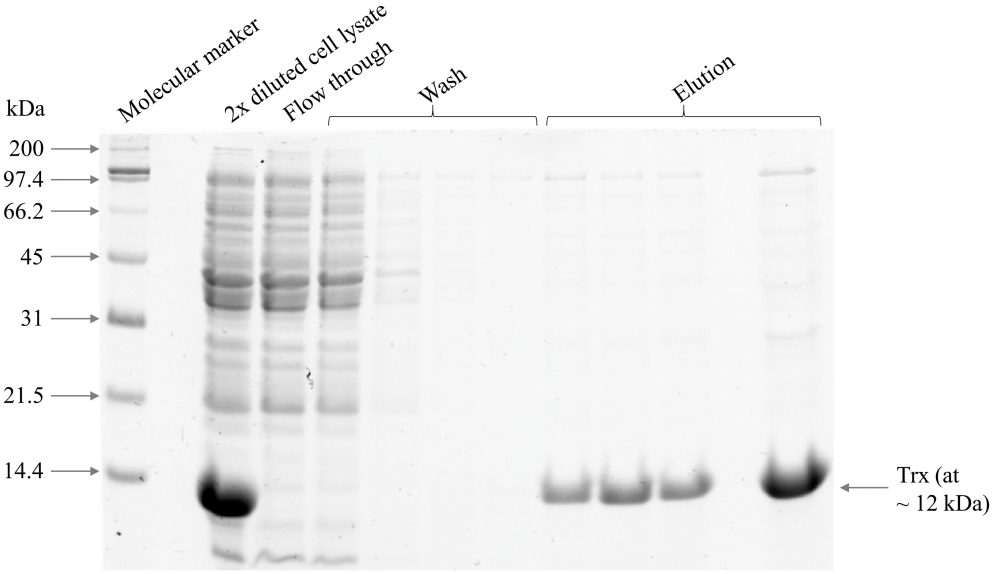

Figure 4.2: SDS-PAGE of Trx purification by IMAC. *E. coli* BL21 (DE3) cells cloned with *S. cerevisiae* Trx were induced for protein overexpression with IPTG. An equal volume of protein sample was loaded into each lane. Samples were prepared in denaturing SDS-PAGE sample buffer. The molecular weight marker (7 µL) was loaded in the first lane. The lane with crude cell lysate shows the overexpressed protein and is visible as a dark band at approximately 12 kDa. The IMAC flow through and wash fractions contained no Trx. The last lane shows the IMAC elution fraction with a dark band for Trx at the expected size of approximately 12 kDa.

4.1.3 Thiol-specific antioxidant protein (peroxiredoxin)

TSA was successfully expressed by IPTG induction indicated by the intense dark band in the lanes loaded with cell lysate (Figure 4.3). The protein was purified to a high degree of homogeneity indicated by dark bands in the lanes loaded with elution samples, and has minimal contamination. Since TSA in the reduced state forms dimers, both a non-denaturing and denaturing SDS-PAGE gel were run with these IMAC fractions. The non-denaturing gel indeed shows that majority of TSA in the elution fraction is reduced as can be seen on the gel at the expected size of 46 kDa for a TSA dimer. The denaturing gel, on the other hand, shows the TSA elution fraction at the expected size of 23 kDa for a TSA monomer.

Stellenbosch University https://scholar.sun.ac.za

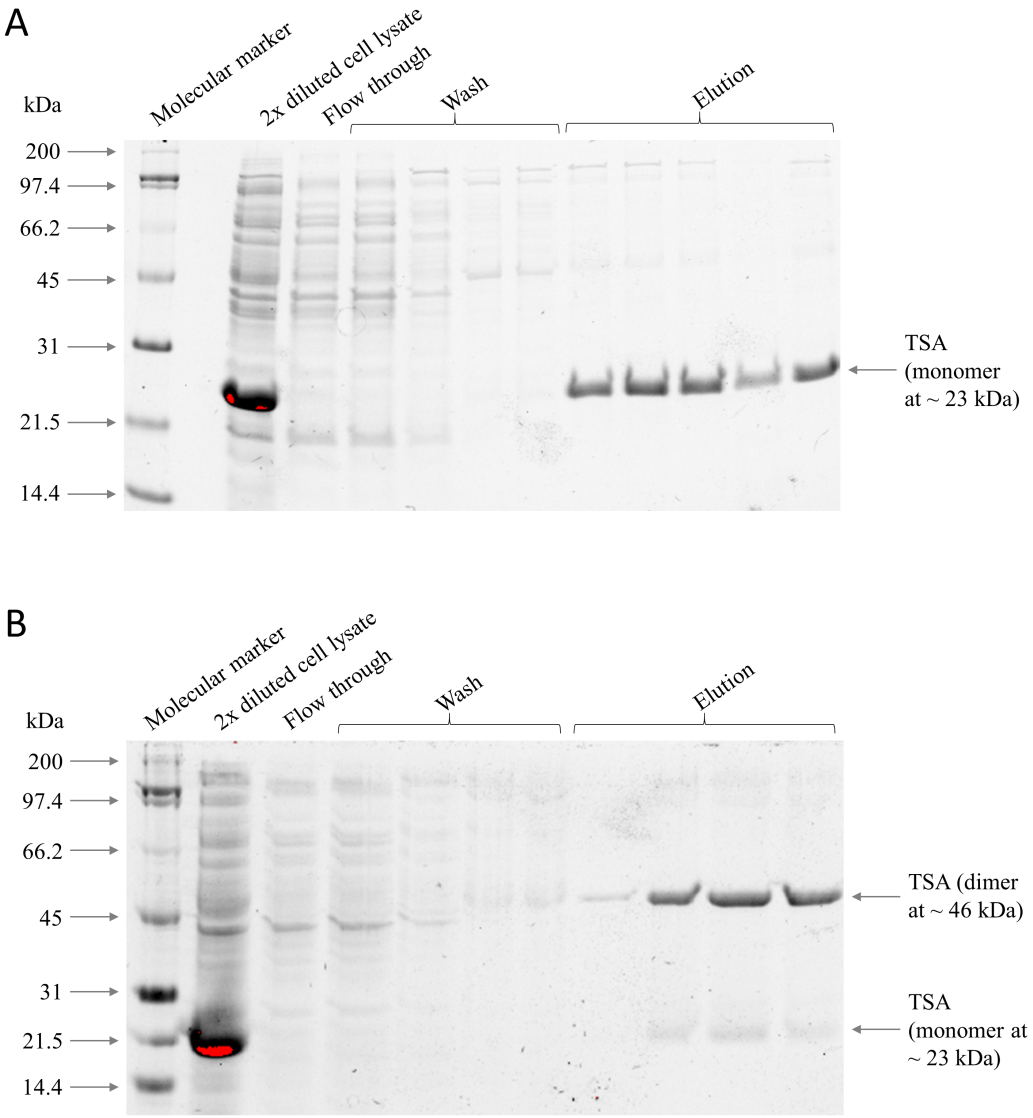

Figure 4.3: SDS-PAGE of TSA purification by IMAC. *E. coli* BL21 (DE3) cells cloned with *S. cerevisiae* TSA were induced for protein overexpression with IPTG. **A** and **B**: An equal volume of of protein sample was loaded into each lane. The molecular weight marker (7 µL) was loaded in the first lane of each gel. The lane with crude cell lysate shows the overexpressed protein and is visible as an intense dark band. **A**: Samples were prepared in denaturing SDS-PAGE sample buffer to observe monomeric TSA and the elution fractions show dark bands at approximately 23 kDa. **B**: Samples were prepared in non-denaturing SDS-PAGE sample buffer to confirm that majority of TSA was in the reduced state (dimeric) and the elution fractions show dark bands at approximately 46 kDa.

Stellenbosch University https://scholar.sun.ac.za

4.1.4 Protein yield

Table 4.1 below gives information about all the purifications performed. The volume and protein concentration (in mg/mL) of lysate obtained from a specific weight of *E. coli* cells harvested are given. The volume and concentration (in mg/mL and µM) of the final elution sample after dialysis are also shown. From this the total amount of protein (in mg) was calculated for both the lysate and elution. The yield column indicates the amount of purified protein (mg) out of the total amount of protein that was present in the lysate as a percentage. Protein concentration of lysates were determined with the BCA assay. The concentrations of purified proteins were determined spectrophotometrically using the A_{280} method as described in Section 3.3.5 above.

The purified proteins from the batches indicated in Table 4.1 were used in all kinetic assays of this study.

Stellenbosch University https://scholar.sun.ac.za

Table 4.1: Protein yield from IMAC purification.

Protein	Batch	*E. coli* dry weight (g)	Lysate (mL)	Lysate (mg/mL)	Lysate (mg)	Elution (mL)	Elution (mg/mL)	Elution (mg)	Elution (µM)	Yield (%)
TrxR	1	9.37	9.9	2.65	26.2	2.95	3.09	9.10	88.0	34.7
Trx	1	8.58	9.4	2.04	19.2	1.85	2.52	4.66	208.7	24.2
Trx	2	3.92	8.5	4.90	41.7	0.48	17.16	8.24	1423.3	19.8
TSA	1	6.89	6.8	4.54	30.8	2.98	2.06	6.14	91.9	19.9
TSA	2	8.52	14	2.30	32.2	2.95	1.59	4.68	70.8	14.5

Stellenbosch University https://scholar.sun.ac.za

4.2 Determination of model parameters for the peroxiredoxin system of *S. cerevisiae*

This section will report the results from the kinetic assays performed to experimentally determine parameters for the construction of a kinetic model. The model (Figure 4.4) consists of three reactions: *reaction 1*, the enzymatic reaction between NADPH and oxidized Trx (Trx_{SS}) modeled with Michaelis-Menten kinetics with the assumption of independent and rapid equilibrium binding of both substrates to separate binding sites on TrxR; *reaction 2*, the reaction between reduced Trx (Trx_{SH}) and oxidized TSA (TSA_{SS}); and *reaction 3*, the reaction between reduced TSA (TSA_{SH}) and H_2O_2. Both *reactions 2* and *3* were modeled with mass action kinetics.

Stellenbosch University https://scholar.sun.ac.za

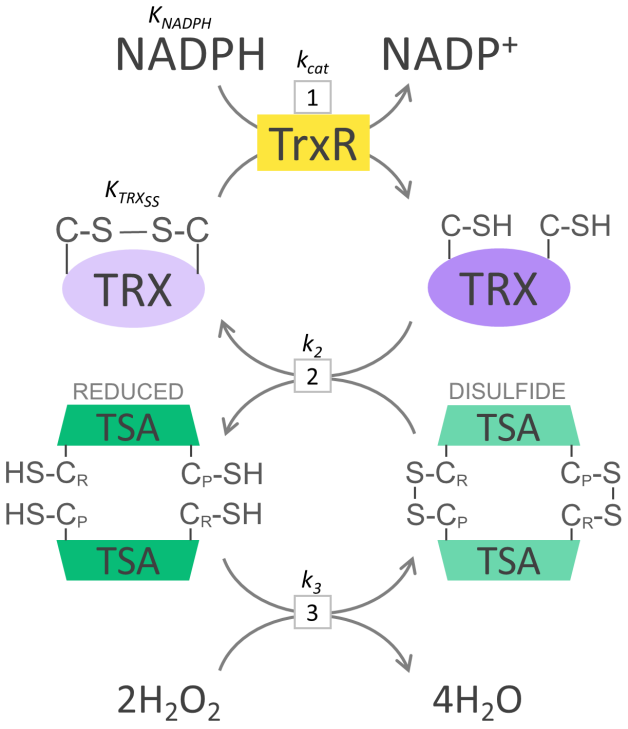

Figure 4.4: Simple model of the peroxiredoxin system of *S. cerevisiae*. This figure is also a schematic representation of the complete system assay discussed below. Reaction 1 is an enzymatic reaction between NADPH and Trx_{SS} catalyzed by TrxR. *Reaction 2* is a mass action reaction between Trx_{SH} and TSA_{SS} with second order rate constant, k_2. *Reaction 3* is a mass action reaction between TSA_{SH} and H_2O_2 with second order rate constant, k_3. C_P = peroxidatic cysteine, C_R = resolving cysteine.

The model required five kinetic parameters. For *reaction 1*: k_{cat}, a catalytic constant; $K_{Trx_{SS}}$, a binding constant for Trx_{SS} to TrxR; and K_{NADPH}, a binding constant for NADPH to TrxR. For mass action *reactions 2* and *3* the required parameters were second order kinetic rate constants k_2 and k_3, respectively.

4.2.1 DTNB reduction assay

This assay was used to determine K_{NADPH} experimentally. A diagram representative of the assay is shown in Figure 4.5. The additional kinetic parameters that could be obtained were K_{DTNB} and k_{cat} with DTNB as second substrate.

Stellenbosch University https://scholar.sun.ac.za

Initial rates were determined over concentration ranges of TrxR, NADPH and DTNB as described in Section 3.4.1.1.

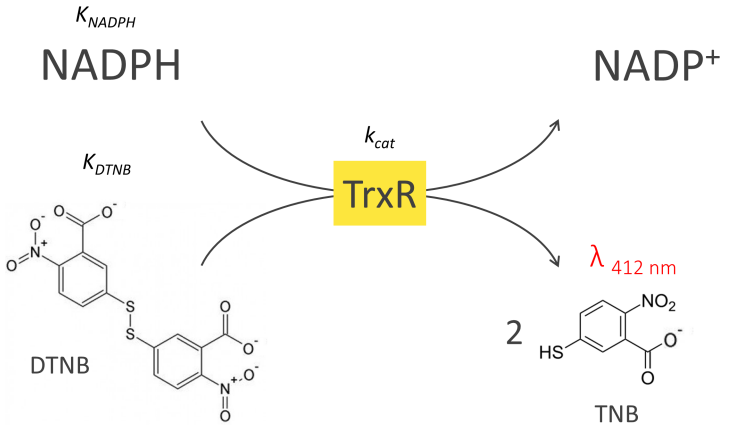

Figure 4.5: DTNB reduction assay. DTNB is reduced by NADPH in an enzymatic reaction catalyzed by TrxR to produce $NADP^+$ and 2 molecules of TNB. The latter can be measured spectrophotometrically at 412 nm (ε_{412} = 13 600 M^{-1} cm^{-1}).

The reaction was modeled with Michaelis-Menten kinetics with the assumption of independent and rapid equilibrium binding of both substrates to separate binding sites on TrxR. The following rate equation describes the reaction:

$$v = \frac{k_{cat} \cdot [TrxR] \cdot \left(\frac{[NADPH]}{K_{NADPH}}\right)\left(\frac{[DTNB]}{K_{DTNB}}\right)}{\left(\frac{1+[NADPH]}{K_{NADPH}}\right) \cdot \left(\frac{1+[DTNB]}{K_{DTNB}}\right)} \tag{4.2.1}$$

The concentration of TrxR was varied from 0 to 5 µM (Figure 4.6). A linear regression was performed on this data set to observe the linear relationship between reaction rate and enzyme concentration (see Appendix B.1). This experiment was performed in triplicate from the same batch of enzyme. The value of **n**, where indicated, thus represents three technical repeats.

Stellenbosch University https://scholar.sun.ac.za

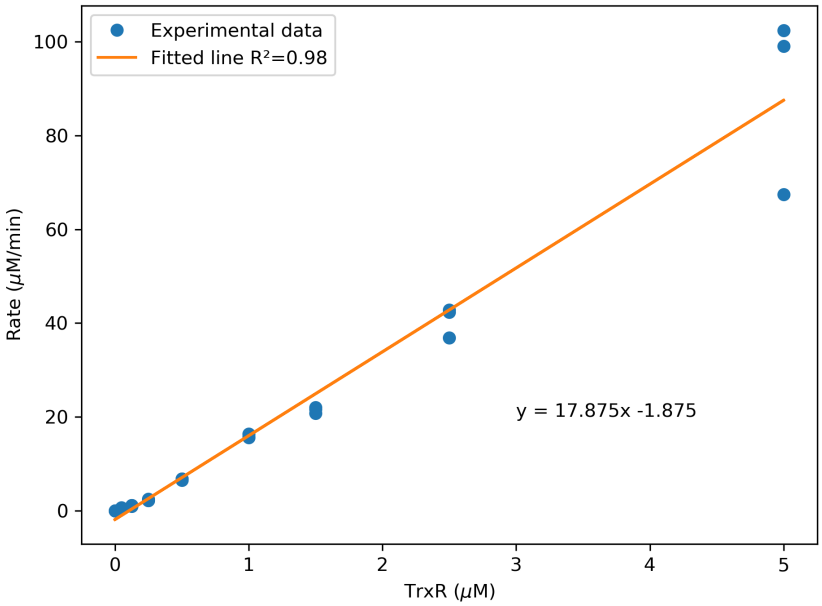

Figure 4.6: DTNB reduction assay with varying TrxR. The relationship between reaction rate and enzyme concentration was linear. Increase in product (TNB) was monitored spectrophotometrically over time at 412 nm at 25°C. Initial slopes of time-courses, i.e. reaction rates, are plotted against TrxR concentration. Blue data points represent experimental data. The solid line (orange) represents the result of the linear regression performed on the data set ($R^2 = 0.98$). Assay conditions: TrxR, 0 to 5 µM; NADPH, 250 µM; DTNB, 2.5 mM; potassium phosphate (pH 7), 0.5 M; EDTA, 10 mM; NaCl, 0.5 M; KCl, 50 mM; BSA, 0.2 mg/mL (n = 3).

The concentrations of both substrates for the DTNB reduction assay were varied (Figure 4.7). DTNB was varied from 0 to 7 mM while NADPH was kept constant at 250 µM. NADPH was varied from 0 to 500 µM while DTNB was kept constant at 2.5 mM. The two data sets were used to perform a global fit for K_{DTNB}, K_{NADPH} and k_{cat} using Eq. 4.2.1 as a model for this reaction (see Appendix B.2). Model parameter values from the fitting result are shown in Table 4.2. These experiments were performed in triplicate from the same batch of enzyme. The value of **n**, where indicated, thus represents three technical repeats.

Stellenbosch University https://scholar.sun.ac.za

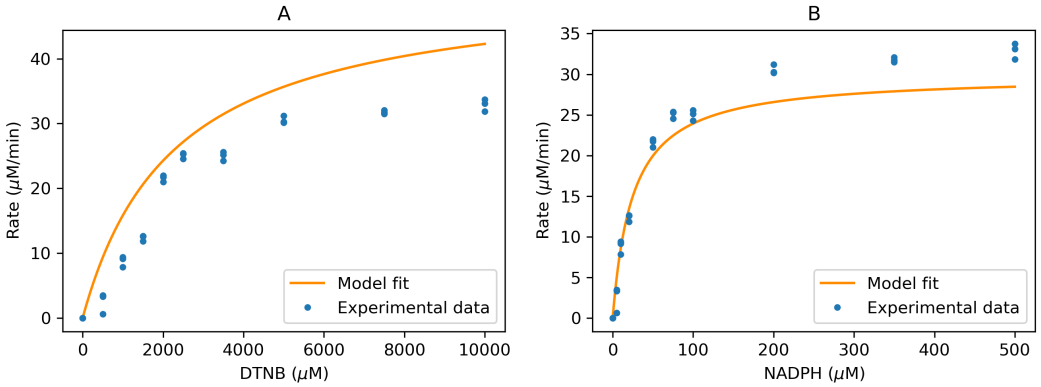

Figure 4.7: Global fitting of TrxR kinetics. Increase in product (TNB) was monitored spectrophotometrically over time at 412 nm at 25°C. Initial slopes of time-courses, i.e. reaction rates, are plotted against DTNB and NADPH concentrations in **A** and **B** respectively. Blue data points represent experimental data. The orange solid line represents the global fitting result. The non-linear least-squares minimization and curve-fitting Python package, LmFit, was used for fitting. Assay conditions: TrxR, 1.5 µM; potassium phosphate (pH 7), 0.5 M; EDTA, 10 mM; NaCl, 0.5 M; KCl, 50 mM; BSA, 0.2 mg/mL. (**A**): DTNB, 0 to 10 mM; NADPH, 250 µM. (**B**): NADPH, 0 to 500 µM; DTNB, 2.5 mM (n = 3).

Fitted parameters are shown in Table 4.2 below.

Table 4.2: Model parameters obtained from the DTNB reduction assay (n=3).

Parameter	Value ± standard error	Unit	Relative error (%)
K_{DTNB}	2277 ± 230	µM	10.1
K_{NADPH}	24.9 ± 3.5	µM	14.2
k_{cat}	38.1 ± 1.6	min^{-1}	4.2

4.2.2 Insulin reduction assay

The insulin reduction assay is based on an increase in solution turbidity as the concentration of reduced insulin ($insulin_{SH}$) increases. This can be measured spectrophotometrically at 650 nm. Diagrams representative of the two types

Stellenbosch University https://scholar.sun.ac.za

of insulin reduction assays are shown in Figure 4.8. A calibration curve was constructed using the DTT-coupled insulin reduction assay (Figure 4.8a). The insulin reduction assay coupled to the complete Trx system (Figure 4.8b) was used to determine the necessary kinetic parameters for model construction. The TrxR enzymatic reaction was modeled with Michaelis-Menten kinetics with the assumption of independent and rapid equilibrium binding of both substrates to separate binding sites on TrxR. The reaction between Trx_{SH} and oxidized insulin (insulin_{SS}) was modeled with mass action kinetics with a second order rate constant, $k_{insulin}$.

The kinetic parameters that could be obtained from these experiments were $K_{Trx_{SS}}$, $k_{insulin}$ and the k_{cat} with Trx_{SS} as second substrate for TrxR (Figure 4.8b). Initial rates were determined over concentration ranges of Trx and insulin as described in Section 3.4.2.2.

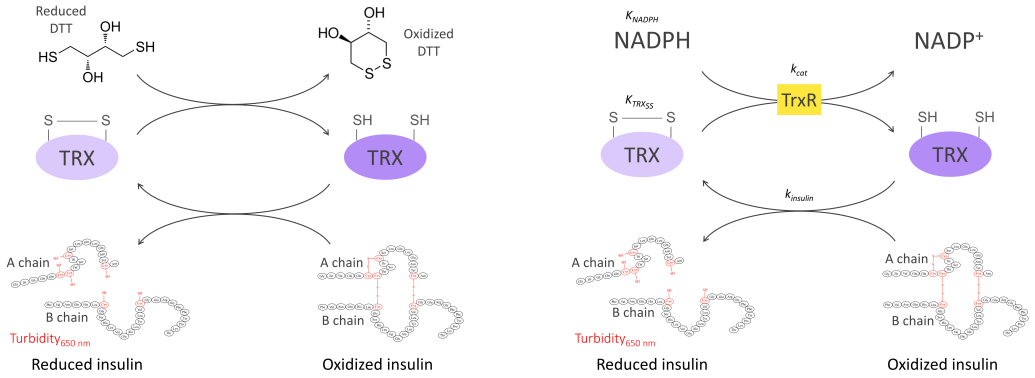

(a) DTT-coupled insulin reduction assay

(b) Trx system-coupled insulin reduction assay

Figure 4.8: Insulin reduction assay. In these assays insulin gets reduced by Trx_{SH}. Increase in turbidity caused by the free B-chain of oxidized insulin can be measured spectrophotometrically at 650 nm. (**a**): Trx_{SH} gets reduced by DTT. (**b**): Trx_{SH} gets reduced by NADPH in an enzymatic reaction catalyzed by TrxR.

4.2.2.1 Calibration curve for insulin_{SH}

The insulin calibration curve was constructed by performing a DTT-coupled insulin reduction assay with four different concentrations of insulin as described in Section 3.4.2.1. The time-course results are shown in Figure 4.9 below (see Appendix B.3). This experiment was performed in triplicate from the same

Stellenbosch University https://scholar.sun.ac.za

batch of Trx protein. The value of **n**, where indicated, thus represents three technical repeats.

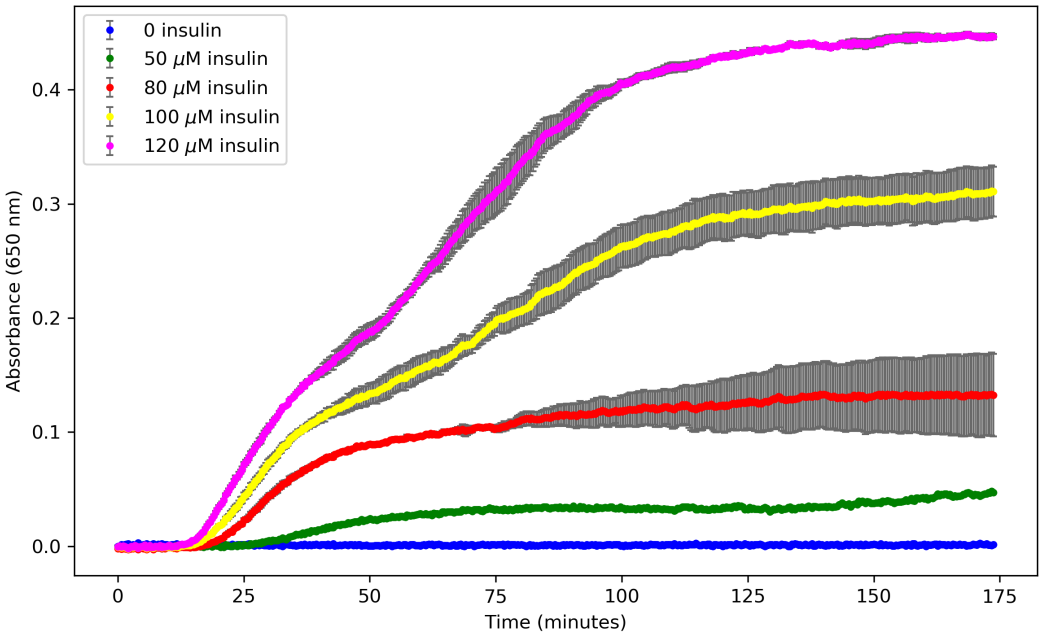

Figure 4.9: Absorbance time-courses for insulin$_{SH}$ calibration curve. The DTT-coupled insulin reduction assay was performed over a time period of 2.9 hours. Increase in turbidity was monitored spectrophotometrically over time at 650 nm, at 25°C, until a plateau was reached indicating the end of the reaction. Afterwards, 0.5 µL of 0.01 HCl was added to each well, the plate was shaken in the microtiter plate reader for 30 seconds and an endpoint absorbance measurement was then taken for each sample. Four insulin concentrations were used: 50, 80, 100 and 120 µM indicated by green, red, yellow and violet data points, respectively. Results are shown as average absorbance values with error bars over time in minutes (n=3). Assay conditions: potassium phosphate, 100 mM (pH 6); EDTA, 2 mM; DTT, 1 mM; Trx, 2 µM.

The calibration curve (Figure 4.10) was used in all subsequent insulin reduction assay experiments to determine the rate of insulin$_{SH}$ reduction by Trx$_{SH}$ in µM/min. See Section 5.2.2 for an explanation regarding the negative y-intercept of the calibration curve. See Appendix B.3.

Stellenbosch University https://scholar.sun.ac.za

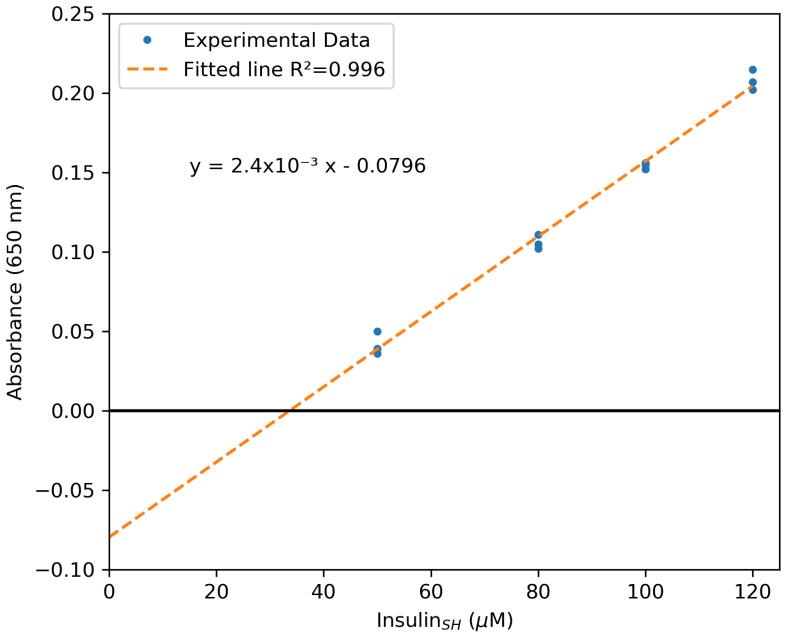

Figure 4.10: Insulin$_{SH}$ calibration curve. An endpoint absorbance measurement was taken for each sample after 2.9 hours of the DTT-coupled insulin reduction assay. These absorbance values were then used to plot a calibration curve against the total insulin added. Four insulin concentrations were used: 50, 80, 100 and 120 µM. Data points (blue) indicate the experimental data and the dotted line (orange) is the result of a linear regression performed on the data set ($R^2 = 0.996$) (n = 3).

4.2.2.2 The insulin reduction assay coupled to the Trx system

The reactions for the insulin reduction assay using the Trx system as reductant for Trx$_{SS}$ were modeled with the following rate equations:

$$v_1 = \frac{k_{cat} \cdot [TrxR] \cdot \left(\frac{[NADPH]}{K_{NADPH}}\right)\left(\frac{[Trx_{SS}]}{K_{Trx_{SS}}}\right)}{\left(\frac{1+[NADPH]}{K_{NADPH}}\right) \cdot \left(\frac{1+[Trx_{SS}]}{K_{Trx_{SS}}}\right)} \tag{4.2.2}$$

$$v_{insulin} = k_{insulin} \cdot [Trx_{SH}] \cdot [insulin_{SS}] \tag{4.2.3}$$

The concentration of one of the two substrates for the insulin reduction reaction (Eq. 4.2.3) was varied while keeping the concentration of the other constant.

Stellenbosch University https://scholar.sun.ac.za

In both experiments the concentrations of the Trx system components were also kept constant. The resulting rate *vs.* substrate concentration plots were then analyzed to determine the initial linear relationship (Figure 4.11). These experiments were performed in triplicate from the same batch of Trx protein. The value of **n**, where indicated, thus represents three technical repeats. At low substrate concentrations the initial reaction rate increased linearly and the assumption was made that under these conditions the amount of product formed was negligible. The slope of the linear section of the curve represents the second order reaction rate constant for Eq. 4.2.3.

Insulin was varied from 0 to 250 µM while Trx was kept constant at 0.4 µM (Figure 4.11a and Appendix B.4). Trx was varied from 0 to 5 µM while insulin was kept constant at 130 µM (Figure 4.12 and Appendix B.5). The initial linear section of the curve from the same data set in Figure 4.12 was used for linear regression to obtain the second order rate constant for the insulin reduction reaction, $k_{insulin}$, (Figure 4.11b). According to the mass action rate equation for the insulin reduction reaction (Eq. 4.2.3), $k_{insulin}$ equals the reaction rate divided by the product of each substrate concentration. The initial rate *vs.* substrate plots obtained from the two experiments had to be normalized by dividing the rate with the concentration of the substrate that was held constant in the assay. This ensured that the slope from these plots was truly representative of the second order rate constant, $k_{insulin}$.

Stellenbosch University https://scholar.sun.ac.za

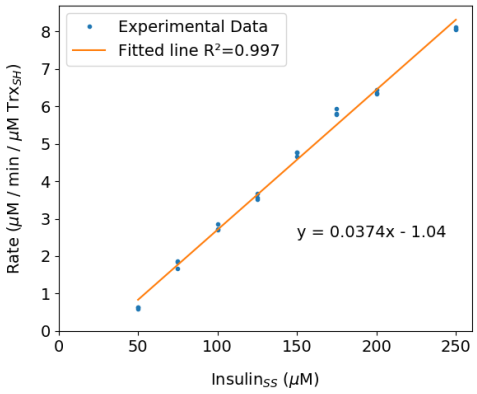

(a) Reaction rate *vs.* insulin$_{SS}$.

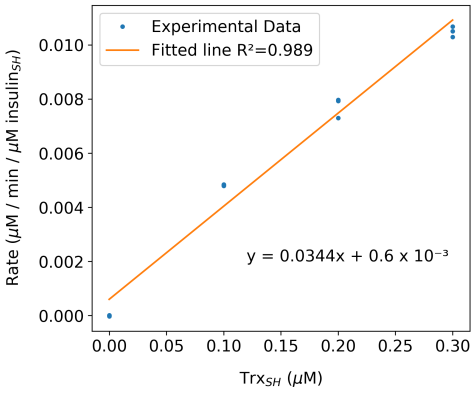

(b) Reaction rate *vs.* Trx$_{SH}$.

Figure 4.11: Insulin reduction assay coupled to the Trx system. Increase in turbidity due to the reduction of insulin by Trx was monitored spectrophotometrically at 650 nm at 25°C. Initial slopes of time-courses, i.e. reaction rates, are plotted against insulin (**a**) and Trx (**b**), respectively. Blue data points represent experimental data. The orange solid line represents the result of the linear regression performed on the data set (**a**: $R^2 = 0.997$ and **b**: $R^2 = 0.987$). Assay conditions: TrxR, 2 µM; NADPH, 250 µM; potassium phosphate, 100 mM (pH 6.5); EDTA, 2 mM. (**a**): insulin, 50 to 250 µM; Trx, 0.4 µM. (**b**): Trx, 0 to 0.3 µM; insulin, 130 µM. (n=3)

The complete data set in which Trx was varied from 0 to 5 µM was used to fit the parameters k_{cat} and $K_{Trx_{SS}}$ (Figure 4.12). A simple PySCeS model was constructed that contained the two reactions defined by Eqs. 4.2.2 and 4.2.3 (see Appendix A.1). This model required three parameters: $k_{insulin}$, k_{cat} and $K_{Trx_{SS}}$. The value of 0.0359 for $k_{insulin}$ (as calculated from the results shown above) was set in the model. The initial rates from this experiment were then fitted to the model to estimate the values for the two remaining parameters, k_{cat} and $K_{Trx_{SS}}$. The steady state flux was calculated using the model for the same range of Trx concentrations that were used in the experiment (0 to 5 µM Trx). The experimental data were then fitted to the steady flux using a non-linear least-squares minimization and curve-fitting method based on the Levenberg-Marquardt algorithm. See Appendix B.6.

Stellenbosch University https://scholar.sun.ac.za

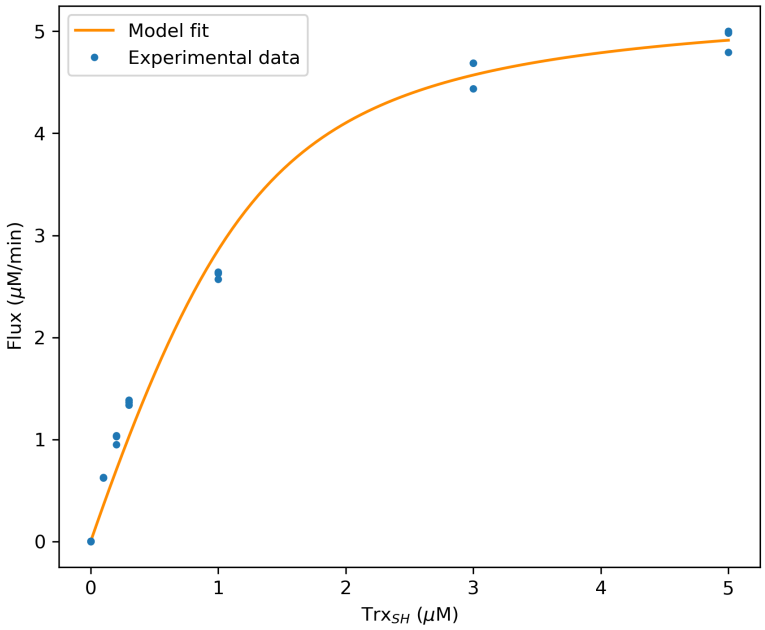

Figure 4.12: Fitting k_{cat} and $K_{Trx_{SS}}$ with varying Trx data set. The non-linear least-squares minimization and curve-fitting Python package, Lm-Fit, was used to fit the parameters k_{cat} and $K_{Trx_{SS}}$ using an experimental data set, i.e. the initial rates obtained for the range of 0 to 5 µM of Trx from the insulin reduction assay coupled to the Trx system. Blue data points represent experimental data (n=3). The orange solid line represents the fit result.

Fitted parameters are shown in Table 4.3 below.

Table 4.3: Model parameters obtained from the insulin reduction assay (n=3).

Parameter	Value ± standard error	Unit	Relative error (%)
$k_{insulin}$	0.0359 ± 0.002	µM^{-1} min^{-1}	4.2
k_{cat}	2.97 ± 0.1	min^{-1}	3.5
$K_{Trx_{SS}}$	0.335 ± 0.07	µM	21

Stellenbosch University https://scholar.sun.ac.za

4.2.3 DTT oxidation assay

The following result was obtained from the DTT oxidation assay in an attempt to determine the second order rate constant for the reaction between TSA and H_2O_2. In the assay, the concentration of TSA was varied from 0 to 35 µM with a constant H_2O_2 of 1 mM. TSA was pre-incubated with 10 mM DTT in the assay cocktail which ensured that all TSA was present in the reduced form, TSA_{SH}, at the start of the reaction. See Appendix B.7. This experiment was performed in triplicate from the same batch of TSA protein. The value of **n**, where indicated, thus represents three technical repeats.

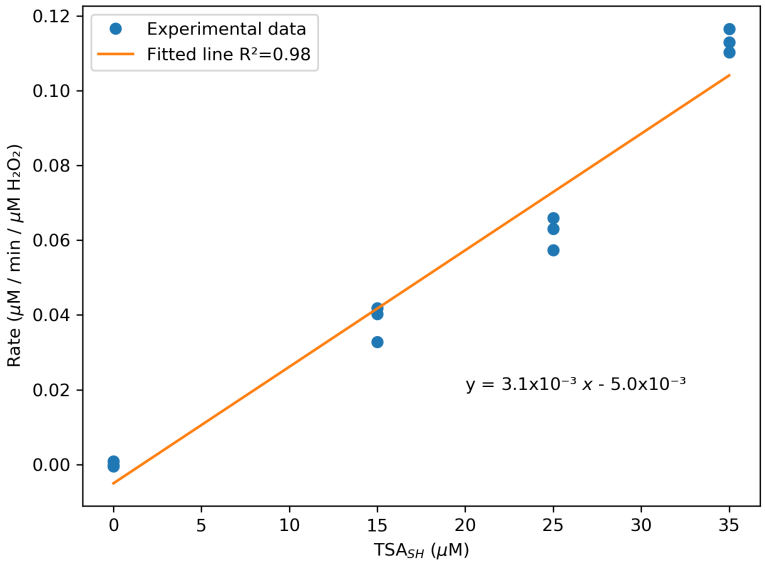

Figure 4.13: DTT oxidation assay. Increase in product (oxidized DTT) was monitored spectrophotometrically at 310 nm at 25°C. Initial slopes of time-courses, i.e. reaction rates, are plotted against TSA_{SH} concentration. Blue data points represent experimental data. The orange solid line represents the result of the linear regression performed on the data set ($R^2 = 0.98$). Assay conditions: TSA, 0 to 35 µM; H_2O_2, 1 mM; DTT, 10 mM; ammonium sulfate, 100 mM; EDTA, 1 mM; potassium phosphate, 25 mM (pH 7) (n = 3).

4.2.4 Complete system assay

The complete system assay included all reactions of the peroxiredoxin system (see Figure 4.4 for a schematic representation of the assay). Therefore, the

Stellenbosch University https://scholar.sun.ac.za

assay also represents the kinetic model constructed. In this assay, NADPH oxidation was measured spectrophotometrically at 340 nm (see Section 3.4.4).

The reactions in both the assay and the model, were modeled with the following rate equations:

$$v_1 = \frac{k_{cat} \cdot [TrxR] \cdot \left(\frac{[NADPH]}{K_{NADPH}}\right)\left(\frac{[Trx_{SS}]}{K_{Trx_{SS}}}\right)}{\left(\frac{1+[NADPH]}{K_{NADPH}}\right) \cdot \left(\frac{1+[Trx_{SS}]}{K_{Trx_{SS}}}\right)} \tag{4.2.4}$$

$$v_2 = k_2 \cdot [Trx_{SH}] \cdot [TSA_{SS}] \tag{4.2.5}$$

$$v_3 = k_3 \cdot [TSA_{SH}] \cdot [H_2O_2] \tag{4.2.6}$$

The parameters obtained from the DTNB assay (K_{NADPH}) and insulin reduction assay ($kcat$ and $K_{Trx_{SS}}$) were used in Eq. 4.2.4. The remaining parameters, k_2 and k_3, were determined with the complete system assay described in Section 3.4.4.

The concentration of one of the two substrates for *reaction 3* was varied while keeping the concentration of the other constant. In both experiments the concentrations of the Trx system components were also kept constant. The resulting rate *vs.* substrate concentration plots were then analyzed to determine the initial linear relationship (Figure 4.14 and Appendices B.8 and B.9). These experiments were performed in duplicate. The value of **n**, where indicated, thus represents two technical repeats. Similar to the mass action reaction between insulin and Trx, the amount of TSA_{SS} formed would be negligible when determining the initial reaction rate at low substrate concentrations. At these conditions, the reaction rate would increase linearly and the resulting slope would represent the second order reaction rate constant. However, this was not the case for these experiments as model simulations showed that the assumption of total TSA being equal to TSA_{SH} at the start of the reaction could not be made. This will be discussed further in Section 5.2.5.3 below.

Stellenbosch University https://scholar.sun.ac.za

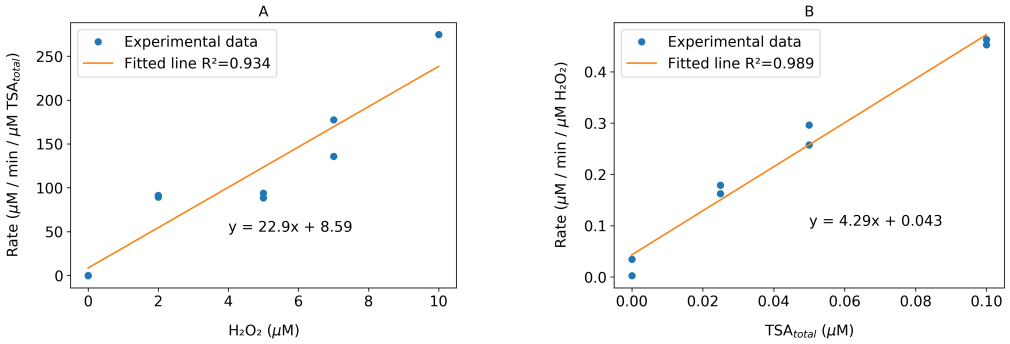

Figure 4.14: Complete system assay. Once the reaction was initiated by the addition of H_2O_2 to the assay mixture, the decrease in NADPH was monitored spectrophotometrically at 340 nm, at 25°C ($\varepsilon_{340} = 6\ 220\ M^{-1}\ cm^{-1}$). Initial slopes of time-courses, i.e. reaction rates, are plotted against H_2O_2 (**A**) and TSA (**B**), respectively. Blue data points represent experimental data. The orange solid line represents the result of the linear regression performed on the data set (**A**: $R^2 = 0.856$ and **B**: $R^2 = 0.989$). Assay conditions: NADPH, 150 µM; TrxR, 0.5 µM; Trx, 10 µM; ammonium sulfate, 100 mM; EDTA, 1 mM; potassium phosphate, 25 mM (pH 7). (**A**): H_2O_2, 0 to 10 µM; TSA, 0.05 µM. (**B**): TSA, 0 to 0.1 µM; H_2O_2, 20 µM (n = 2).

The complete data set in which TSA was varied from 0 to 2 µM was used to fit the parameter k_2 (Figure 4.15). A PySCeS model for an *in vitro* peroxiredoxin system for *S. cerevisiae* was constructed that contained the three reactions defined by Eqs. 4.2.4 to 4.2.6. This model required five parameters: K_{NADPH}, $K_{Trx_{SS}}$, k_{cat}, k_2 and k_3 (see Figure 4.4). Values obtained for K_{NADPH}, $K_{Trx_{SS}}$ and k_{cat} as determined by the DTNB reduction and insulin reduction assays were set in the model. The value of 22.9 was chosen for k_3 (Figure 4.14 A). The steady state flux was calculated using the model for the same range of TSA concentrations that were used in the experiment (0 to 2 µM). The experimental data were then fitted to the steady state flux using a non-linear least-squares minimization and curve-fitting method based on the Levenberg-Marquardt algorithm to estimate the value for k_2. See Appendix B.10.

Stellenbosch University https://scholar.sun.ac.za

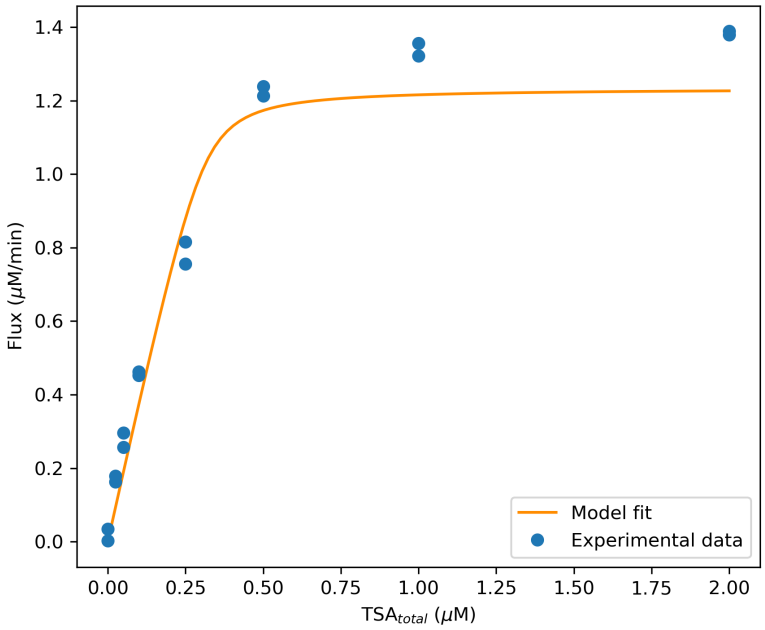

Figure 4.15: Fitting k_2 with varying TSA data set. The non-linear least-squares minimization and curve-fitting Python package, LmFit, was used to fit the parameter k_2 using an experimental data set, i.e. the initial rates obtained from the complete system assay in which TSA was varied from 0 to 2 µM. Blue data points represent experimental data (n=2). The orange solid line represents the fit result.

Fitted parameters are shown in Table 4.4 below.

Table 4.4: Model parameters obtained from the complete system assay (n=2).

Parameter	Value ± standard error	Unit	Relative error (%)
k_3	22.9 ± 3	µM^{-1} min^{-1}	14.4
k_2	0.383 ± 0.03	µM^{-1} min^{-1}	8.6

Stellenbosch University https://scholar.sun.ac.za

4.3 Model simulation with an *in vitro* kinetic model for the peroxiredoxin system of *S. cerevisiae*

A PySCeS model for the peroxiredoxin system of *S. cerevisiae* was constructed and populated with the final experimental parameters obtained (Table 4.5). See Appendix A.2 for the model file. The next section reports model simulation results using the populated model. The simulation experiments were designed to focus on the reaction of H_2O_2 reduction by TSA, i.e., *reaction 3*.

Table 4.5: Summary of model parameters for the simple computational model for an *in vitro* peroxiredoxin system of *S. cerevisiae*.

Parameter	Value ± standard error	Unit	Relative error (%)
K_{NADPH}	24.9 ± 3.5	µM	14.2
$K_{Trx_{SS}}$	0.335 ± 0.07	µM	21
k_{cat}	2.97 ± 0.1	min^{-1}	3.5
k_2	0.383 ± 0.03	μM^{-1} min^{-1}	8.6
k_3	22.9 ± 3	μM^{-1} min^{-1}	14.4

4.3.1 Model evaluation: H_2O_2 reduction by TSA

Figures 4.16 and 4.17 show the results for model independent experiments that plot the steady state flux against the concentration of H_2O_2. The experimental data was obtained from a complete system assay experiment in which H_2O_2 was varied from 0 to 10 µM with a TSA concentration of 0.05 µM (Figure 4.16). In the second experiment, the H_2O_2 concentration was varied from 0 to 50 µM with a TSA concentration of 0.5 µM (Figure 4.17). See Appendix C.1.

Stellenbosch University https://scholar.sun.ac.za

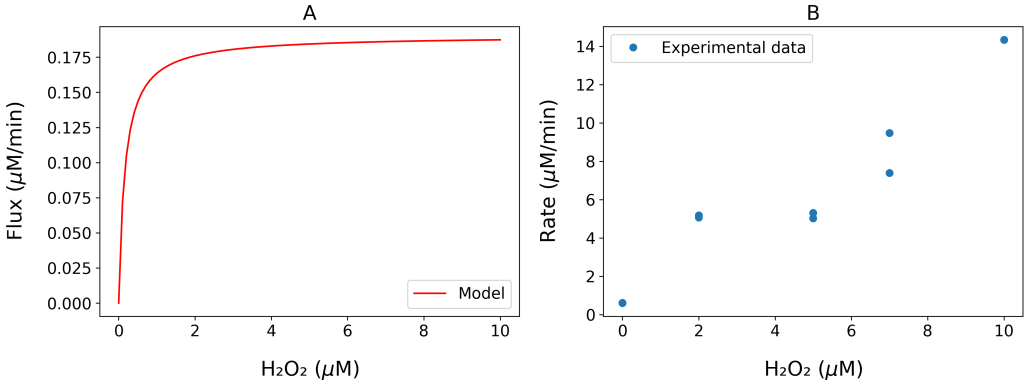

Figure 4.16: Model simulation with a data set for varying H_2O_2 from 0 to 10 µM. A model simulation was performed that mimicked the experimental assay conditions for the complete system assay in which H_2O_2 was varied from 0 to 10 µM. The steady state flux was calculated for the same range of varying H_2O_2 concentrations. **(A):** The red solid line represents the model simulation. **(B):** Blue data points represent the experimental data (n=3). Experimental data and model simulation are plotted separately due to the difference in y-axis values. Metabolite concentrations: H_2O_2, 0 to 10 µM; TSA_{SH}, 0.05 µM; NADPH, 150 µM; TrxR, 0.5 µM; Trx_{SH}, 10 µM.

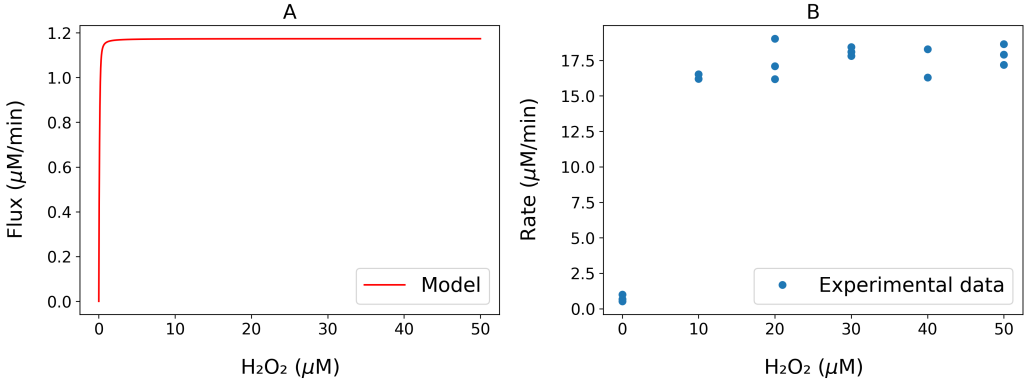

Figure 4.17: Model simulation with a model independent data set for varying H_2O_2 from 0 to 50 µM. A model simulation was performed that mimicked the experimental assay conditions for the complete system assay in which H_2O_2 was varied from 0 to 50 µM. The steady state flux was calculated for the same range of varying H_2O_2 concentrations. **(A):** The red solid line represents the model simulation. **(B):** Blue data points represent the experimental data (n=3). Experimental data and model simulation are plotted separately due to the difference in y-axis values. Metabolite concentrations: H_2O_2, 0 to 50 µM; TSA_{SH}, 0.5 µM; NADPH, 150 µM; TrxR, 0.5 µM; Trx_{SH}, 10 µM.

Stellenbosch University https://scholar.sun.ac.za

A parameter scan was performed that showed the concentration of TSA_{SS} and TSA_{SH} for the same range of H_2O_2 concentrations used in the complete system assay experiment varying H_2O_2 (Figure 4.18 A and Appendix C.1). The model conditions were identical to the assay conditions of the experiment. This scan shows at which H_2O_2 concentration the TSA moiety switches to the mostly oxidized form (approximately 0.2 µM H_2O_2). The TSA redox charge is also plotted for a range of H_2O_2 concentrations (Figure 4.18 B). The redox charge is defined as a fraction of the reduced form out of the total moiety of TSA[146].

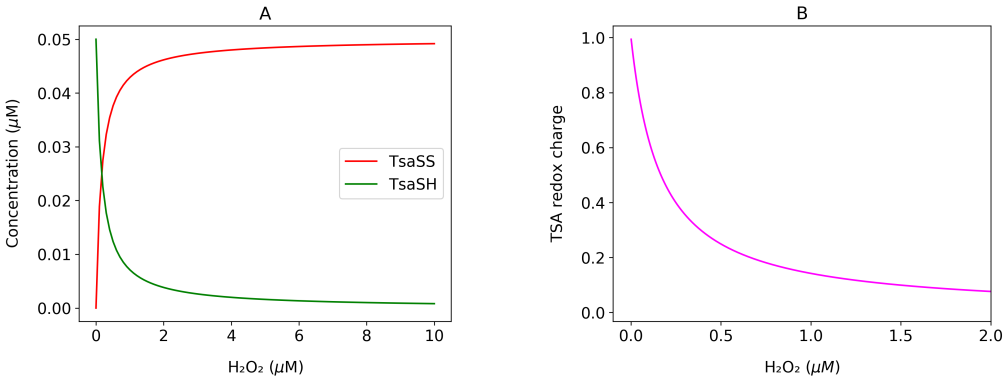

Figure 4.18: H_2O_2 scan result and TSA redox charge. A: A PySCeS parameter scan plotting the TSA moiety against H_2O_2 is shown here. The metabolite concentrations that were used in the complete system assay in which the concentration of H_2O_2 was varied, were set to the same values in the model. This scan result clearly shows that TSA rapidly switches from the reduced form to the oxidized form at a H_2O_2 concentration as low as approximately 0.2 µM. **B:** The redox charge for a H_2O_2 concentration range between 0 and 2 µM. The redox charge is defined as a fraction of the reduced form of TSA out of the total TSA moiety.

4.3.2 H_2O_2-pulse simulation

The *in vitro* model was subjected to a pulse-like H_2O_2 input (Figure 4.19 and Appendices C.2 and C.3). The conditions were identical to those used in the complete system assay save for the initial concentration of H_2O_2 which was set to 1 µM. A time-simulation of 40 minutes was performed and the system subjected to five H_2O_2 pulses with varying concencentrations. The resistance of the system towards the H_2O_2-pulses was then examined by monitoring the

Stellenbosch University https://scholar.sun.ac.za

change in concentration of the system moieties, TSA and Trx. When a certain H_2O_2-pulse threshold concentration was reached, the system switched to a more oxidized steady state over time. At low H_2O_2-pulse concentrations (Figure 4.19 A-D) Trx_{SH} and TSA_{SH} returned to their original concentrations after each pulse and the system was able to neutralize H_2O_2 efficiently. When the H_2O_2-pulse reached a concentration of 2.5 µM (Figure 4.19 E-F), the two moieties started to switch from reduced to oxidized although H_2O_2 could still be brought back to its original concentration. At higher H_2O_2-pulse concentrations, the capacity of the system to decrease H_2O_2 became limited and this can be seen as a H_2O_2 build-up over time (Figure 4.19 G-J). Under these conditions the moiety switch from reduced to oxidized also occurred more rapidly.

Stellenbosch University https://scholar.sun.ac.za

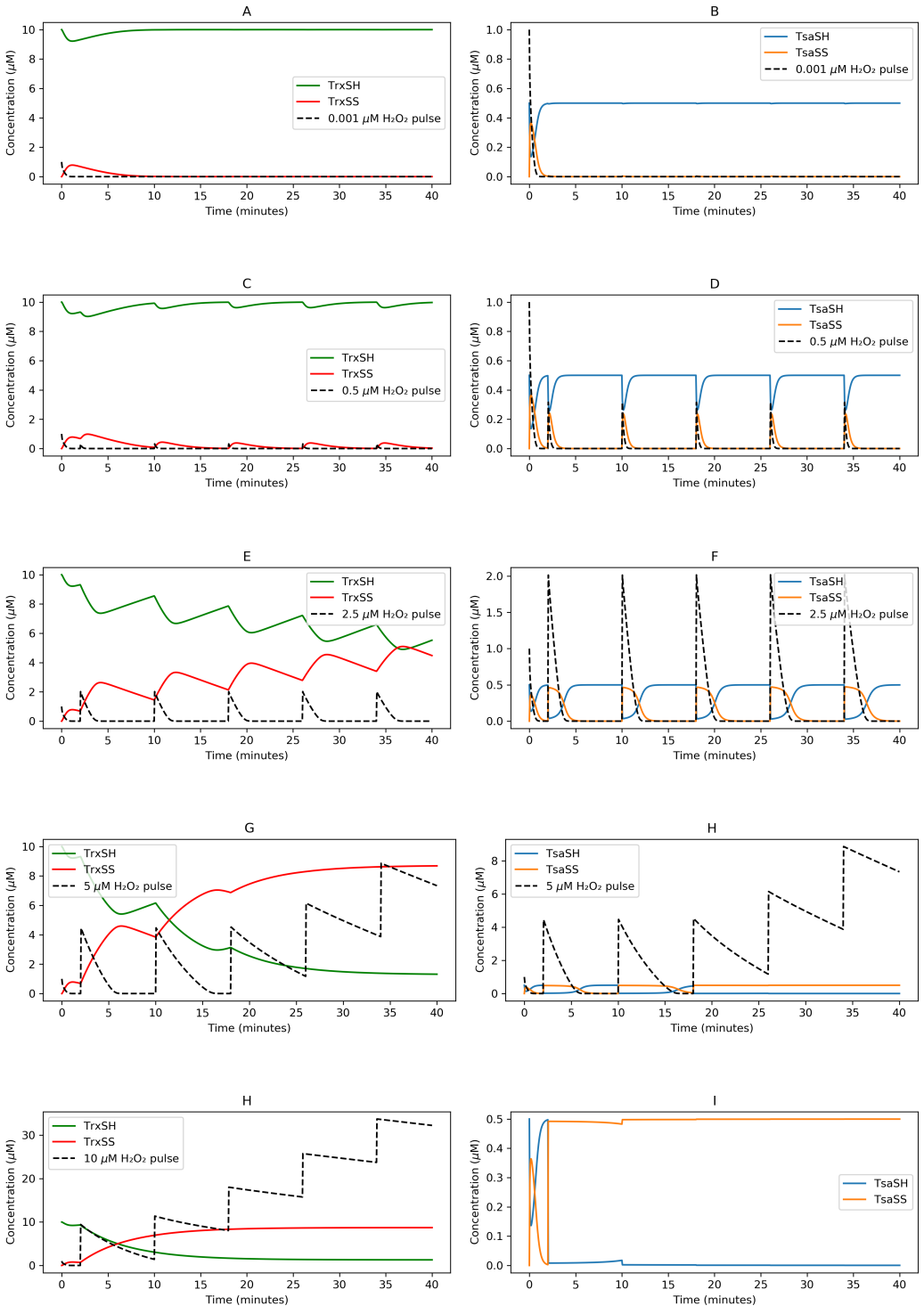

Figure 4.19: H_2O_2-pulse simulation. Five H_2O_2-pulses of different concentrations (**A-J**) were subjected to the *in vitro* system model for a time period of 40 minutes. The change in concentration over time of the Trx moiety (plots on the left-hand side) and the TSA moiety (plots on the right-hand side) are plotted together with the concentration of H_2O_2 (dotted line). The H_2O_2-pulse concentration varied as follows: **A-B**, 0.001 µM; **C-D**, 0.5 µM; **E-F**, 2.5 µM; **G-H**, 5 µM; and **I-J**, 10 µM. H_2O_2 was not plotted on **J** due to differences in y-axis values but is identical to H_2O_2 plotted in **I**.

Stellenbosch University https://scholar.sun.ac.za

4.4 Conclusion

The results shown here will be discussed in more detail in the next chapter. These results were sufficient for achieving the aims set out for this project. A simple kinetic model could be constructed using the estimated parameters obtained from all the experiments conducted. Simulation experiments using the constructed model aided in explaining the discrepancies seen in some of the data. A critical evaluation of the results and their significance in regard to the research questions are also provided in the next chapter.

Stellenbosch University https://scholar.sun.ac.za

Chapter 5

Discussion

S. cerevisiae is an ideal model organism to study peroxiredoxin systems because it represents the simplest eukaryotic system. Additionally, the proteins from *S. cerevisiae* are easy to isolate in order to perform *in vitro* experiments. However, the primary reason for using the *S. cerevisiae* system is the fact that a kinetic model for the peroxiredoxin system of this organism is not yet available. It is evident that the peroxiredoxin system forms part of an intricate redox network that is not yet fully understood. Moreover, the peroxiredoxin network in higher evolved organisms is significantly more complex than that in prokaryotes. Computational systems biology is an ideal tool when embarking on an investigation into this complex network as many of its aspects cannot simply be investigated using standard biochemical techniques in the laboratory only. Being able to describe the full complexity of these systems from the get-go is a very ambitious task. It is more practical to start with a simple description of the system and to build, refine and improve from there.

This chapter is dedicated to provide a thorough discussion of the relevant information that could be extracted from the results of this study and how it contributed to the original research question. The main goal of this research, and specifically this study, is to develop a realistic kinetic computational model for the peroxiredoxin system of *S. cerevisiae* as such a model for this organism does not yet exist. The results from this study created a platform for further improvement of such a model. This study was designed with three major aims in mind. Firstly, three proteins that form part of the peroxiredoxin system of *S. cerevisiae* had to be expressed and purified. Secondly, model

Stellenbosch University https://scholar.sun.ac.za

parameters had to be obtained in order to construct a simple kinetic model for the system. This was done experimentally by assaying the purified proteins. And lastly, the model had to be evaluated for predictability and accuracy by simulation of certain conditions. The model was also subjected to a stress input to demonstrate the inherent kinetic behaviour of the system.

A detailed discussion and explanation of the results shown will be given first. This will be followed by a summary of the findings of this study. The limitations of the study will then be discussed in addition to recommendations for future studies. The final section will be a short conclusion.

5.1 *S. cerevisiae* peroxiredoxin system proteins were successfully expressed and purified

The three peroxiredoxin system proteins, TrxR, Trx and TSA, were purified to a high degree of homogeneity using IMAC. Induction by IPTG was introduced during bacterial culturing of *E. coli* BL21 (DE3) host organisms cloned with the His-tagged proteins. Successful induction was confirmed by loading a diluted sample of the crude cell lysate on a tricine-SDS-PAGE gel. The overexpressed protein in the crude lysate can be observed as a single intense dark band for all three proteins (Figures 4.1 to 4.3). The purification was considered successful if bands for all cytosolic proteins, except for the His-tagged protein, could be seen in the flow through and wash steps. This was indeed the case for all three protein purifications shown. The elution sample was considered as homogeneous if there were only minimal contamination. There were, however, some contaminating bands present on all gels but their intensity was much less relative to the band for the recombinant protein.

An interesting finding was that the step of adding an extra amount of DTT to the TSA crude lysate was absolutely essential to ensure that TSA would be purified in the reduced form (section 3.3.2). Figure 4.3 B shows an SDS-PAGE gel with the crude lysate and IMAC fraction samples loaded with non-denaturing SDS-PAGE sample buffer. It was expected that proteins would electrophorese in their fully folded state. An aliquot of the crude lysate sample was taken

Stellenbosch University https://scholar.sun.ac.za

before the extra amount of DTT was added for incubation on the IMAC resin. The overexpressed protein band in the crude lysate was at the position for a TSA monomer (at 23 kDa) despite the non-denaturing conditions. The elution bands, however, show that most of the TSA was purified in the fully reduced form (at 46 kDa for a TSA dimer). This could indicate that the DTT present in the extraction buffer was not enough to keep all cytosolic proteins in the reduced form during the extraction process.

The concentration in mg/mL of purified TrxR, Trx and TSA, were calculated from an A_{280} measurement using each protein's molecular weight and theoretical extinction coefficient (ε_{280}) for a purified protein (obtained using the ProtParam tool from ExPASy: https://web.expasy.org/protparam/). This method avoided the loss of precious sample as the amount of protein that could be purified per culture batch was relatively small (Table 4.1). Further optimization of culturing conditions would be necessary to ensure higher protein yields. The protein yield (purified protein in mg) ranged from 14.5 to 34.7% out of the total protein (in mg) present in the crude lysate.

5.2 Determination and estimation of model parameters using spectrophotometric assays

This section will discuss the results relevant to obtaining the required model parameters: K_{NADPH}, $K_{Trx_{SS}}$, k_{cat}, k_2 and k_3. All of these parameters were obtained with kinetic assays using a standard desktop spectrophotometer or microtiter plate reader. Most of the assay methods, as will become clear, are adequate for the determination of the kinetic parameters of the peroxiredoxin system components. However, these methods become limited for reactions with fast initial reaction rates as is the case for reduction of H_2O_2 by TSA. Determination of a second order reaction rate constant for a reaction with fast kinetics is challenging when the time between the reaction initiation and start of absorbance readings is controlled by hand.

Stellenbosch University https://scholar.sun.ac.za

5.2.1 DTNB reduction assay and K_{NADPH}

This spectrophotometric assay, previously described by Holmgren *et al.*[128], was used in this study to obtain the value for K_{NADPH} required for the computational model. The enzymatic reaction was modeled with Michaelis-Menten kinetics with the assumption of independent binding of two substrates, NADPH and DTNB, to separate binding sites on TrxR. The substrate binding constants, obtained after two independent data sets were used to perform a global fit using Eq. 4.2.1 were 2.28 ± 0.23 mM and 24.9 ± 3.5 µM for DTNB and NADPH, respectively (Figure 4.7). The value for k_{cat} from the same fitting analysis was 38.1 ± 2 min^{-1}. The apparent K_m value for NADPH as a substrate for a yeast TrxR has been previously been reported as 1.2 µM[147]. The result obtained for K_{NADPH} in this study indicates a lower affinity of TrxR for NADPH in comparison.

5.2.2 Insulin$_{SH}$ calibration curve

When constructing a computational model, it is essential that the units for reaction rates and metabolite concentrations are consistent. In the case of constructing a PySCeS model, the required unit for a reaction rate is concentration per time. For all PySCeS models constructed in this study, the concentration unit was chosen as µM and the time unit was chosen as minutes. Thus, all reaction rates are defined with unit µM min^{-1} and metabolite concentrations are defined with unit µM. These units were used consistently throughout all analyses in the study. Also, these reactions were modelled with mass action kinetics and not as enzymes. Thus, moles are reacting instead of grams of protein.

Spectrophotometric assays typically take advantage of at least one chromophore that forms part of a reaction in order to convert the rate in absorbance per minute to concentration (in molar) per minute using the Beer-Lambert law[148]. Since reduced insulin (insulin$_{SH}$) is not a chromophore, an extinction coefficient could not be used to calculate the concentration of product formed from absorbance readings. Thus, a calibration curve for insulin$_{SH}$ had to be set up first (Figure 4.10). The insulin calibration curve was constructed by assaying four different insulin concentrations (50, 80, 100 and 120 µM) using the DTT-coupled insulin reduction assay (Figure 4.8a). As can be seen in the absorbance

Stellenbosch University https://scholar.sun.ac.za

time-course result (Figure 4.9) a measurable solution turbidity could only be achieved approximately 15 minutes after the start of the reaction. Additionally, the calibration curve shown in Figure 4.10 has a negative y-intercept and the implication of this is that concentrations of insulin$_{SH}$ below approximately 33 µM (x-intercept of the calibration curve) could not be extrapolated with accuracy using the calibration curve. A possible explanation for this observation is that insulin$_{SH}$, as mentioned before, is not a true chromophore. Reduction of the disulfide bridges in an oxidized molecule of insulin by Trx causes the separation of the insulin A chain from the B chain[125]. Insulin B chains precipitate in solution and cause an increase in solution turbidity which can be measured at 650 nm[125]. It is thus the result of a precipitated molecule that results in an absorbance reading and not a chromophore. It is likely that an absorbance measurement could only be made once precipitated insulin$_{SH}$ had reached a certain threshold concentration (approx. 33 µM).

An additional complication of this assay was that insulin has a low solubility at pH values above 7[126]. For this reason, the assay mixture was buffered at pH 6[126]. This is also the reason for adding 0.5 µM of 0.01 M HCl to all samples at the end of the insulin calibration assay. This ensured that the precipitation present in the solution at that time point was as a result of insulin$_{SH}$ B chains only. The mixing step was also essential as precipitated products settled to the bottom of the wells of a 96-well microtiter plate. These two steps both solubilized and homogenized the solution before the end-point absorbance reading was taken. It is important to consider the difference between turbidity of the solution and the precipitation that occurs as a result of particles settling to the bottom of a microtiter plate well. The latter will lead to a higher absorbance measurement that is not representative of its turbidity.

The absorbance time-course result (Figure 4.9) illustrates the necessity of these two steps. For example, considering the 100 µM insulin sample in Figure 4.9, the reaction rate increased linearly and then approached a plateau after approximately 70 minutes. At this point, however, the absorbance started to increase linearly again and reached a higher second plateau. It is likely that at the point where the absorbance increased for the second time, the reaction had actually ceased and that precipitated product had settled to the bottom of the plate. The end-point absorbance reading taken after the solubilization

Stellenbosch University https://scholar.sun.ac.za

and homogenization steps was plotted against the total initial insulin concentration in Figure 4.10. The absorbance reading for the 100 µM insulin sample was just above 0.15, which was also the absorbance value of the first plateau observed in the absorbance time-course. Once the insulin$_{SH}$ calibration curve was set up, initial reaction rates could then be converted to the correct unit of µM min^{-1}.

5.2.3 The insulin reduction assay coupled to the Trx system

The model parameters that had to be determined next were the substrate binding constant, $K_{Trx_{SS}}$, and k_{cat} with Trx as a second substrate for TrxR. Since Trx forms part of a redox couple that can be either in the reduced form or the oxidized form, it was important to consider that it is the oxidized form, Trx$_{SS}$, that is the true substrate for the reaction. It is experimentally challenging to transform the total Trx moiety into the oxidized form to directly follow the enzymatic reaction by measuring NADPH oxidation. Thus, using the insulin reduction assay coupled to the Trx system it was possible to obtain data sets which could be used to fit both $K_{Trx_{SS}}$ and k_{cat} using the PySCeS model for the reduction of insulin coupled to the Trx system (Figure 4.8b). This two-reaction model took four parameters, one of which was determined by the DTNB assay (K_{NADPH}). $K_{Trx_{SS}}$ and k_{cat} were the two parameters that were to be fitted. The remaining parameter was the second order reaction rate constant of the mass action reaction between Trx$_{SH}$ and insulin$_{SS}$, $k_{insulin}$.

5.2.3.1 $k_{insulin}$

Two independent insulin reduction assays performed resulted in a nearly indistinguishable value for $k_{insulin}$ (Figure 4.11). The reaction rate increased linearly at low substrate concentrations. For varying insulin, the relationship was linear across the entire range of 0 to 250 µM. For Trx, the relationship was linear from 0 to 0.3 µM. It was assumed that during the initial part of the reaction the total Trx was equal to Trx$_{SH}$ and that the amount of Trx$_{SS}$ formed at this stage was negligible. In the first experiment, insulin was varied while keeping Trx constant and the result plotted shows reaction rate against insulin concentration (Figure 4.11a). Note the reaction rate is normalized by dividing

Stellenbosch University https://scholar.sun.ac.za

with the constant concentration of the other substrate (Trx) used in the assay. The slope of this plot represents the second order rate constant for the reaction and was calculated as 0.0374 μM^{-1} min^{-1} by linear regression (R^2 = 0.997). The same procedure was followed for the second experiment in which Trx was varied. The initial linear portion of the plot of reaction rate *vs.* substrate concentration was used for calculating the second order rate constant (Figure 4.11b). The slope of this plot was calculated as 0.0344 μ M^{-1} min^{-1} (R^2 = 0.989). This value correlates relatively well with a previously reported second order rate constant of 0.18 μM^{-1} min^{-1} for insulin reduction by Trx, with only a five-fold difference[149]. The validity of the value for $k_{insulin}$ obtained in this study, however, is supported by a standard error of less than 5% between the results of two independent experiments (Table 4.3).

5.2.3.2 $K_{Trx_{SS}}$ and k_{cat}

The complete data set obtained for the insulin reduction assay in which Trx was varied from 0 to 5 µM while insulin was kept constant (Figure 4.12) shows a hyperbolic relationship between the rate of the reaction and substrate concentration. Michaelis-Menten kinetics have formerly been assigned to redoxins, including Trx[106]. However, it has been demonstrated by computational modeling using *in vitro* data sets that the substrate saturation profile observed for Trx can be attributed to the redoxin moiety being redistributed to the oxidized form[102]. Trx_{SS} is inactive and can only be regenerated by another reduction reaction catalyzed by TrxR, which explains the apparent saturation observed at higher Trx concentrations. It was further shown that redoxin reactions could be described adequately with mass action kinetics[102].

Mass action kinetics were successfully fitted to the data set of varying Trx in this study (Figure 4.12). $K_{Trx_{SS}}$ and k_{cat} were fitted by calculating the steady state flux through the system in the PySCeS model for the same range of Trx concentrations used in the experiment (see Appendix A.1 for the PySCeS model). The fitted values were 0.335 $\pm$ 0.07 µM and 2.97 $\pm$ 0.1 min^{-1} for $K_{Trx_{SS}}$ and k_{cat}, respectively (Table 4.3). Previous studies have reported varying apparent K_m values for Trx of 4.4 and 1.3 µM for TrxR from *S. cerevisiae*[150;151]. The latter correlates relatively well with the $K_{Trx_{SS}}$ obtained in this study with only a four-fold difference. A study conducted by Lacey *et al.*

Stellenbosch University https://scholar.sun.ac.za

obtained an apparent K_m value of 0.4 µM and k_{cat} of 14.3 min^{-1} for human Trx and TrxR, which also correlates well with the values obtained in this study[152].

5.2.4 DTT oxidation assay

Determination of the second order rate constant for *reaction 3* was attempted using the DTT oxidation assay[119]. In this assay, TSA gets reduced by DTT while TSA in turn gets oxidized by H_2O_2. At steady state, the rate of oxidation of DTT will be equal to the rate of TSA oxidation by H_2O_2. Oxidized DTT can be monitored spectrophotometrically at 310 nm ($\varepsilon_{310} = 110\ M^{-1}\ cm^{-1}$)[142]. After many attempts at this assay, however, the results obtained were not reproducible. An unexpected and inexplicable initial spike in absorbance occurred for some replicates of individual test samples. This made it challenging to choose the correct section of the absorbance time-course that represented the true initial rate of the reaction. Figure 4.13 shows a plot of rate *vs.* TSA concentration of an experiment that resulted in what seemed to be a usable slope representative of the second order rate constant for *reaction 3*. The complete system assay, described in Section 3.4.4, was conducted with even lower substrate concentrations for *reaction 3* to test whether a similar value could be obtained. The second order rate constant of 3.12×10^{-3} µ M^{-1} min^{-1} calculated from the result of the DTT assay was more than a 1000-fold less when compared to the second order rate constant of 4.29 μM^{-1} min^{-1} calculated from the complete system assay with an experiment that also varied the concentration of TSA (Figure 4.14 B). It was therefore decided to use the complete system assay to determine k_3 as this assay led to more reproducible results.

5.2.5 Complete system assay

The complete system assay includes all the components of the peroxiredoxin system and is representative of the system *in vivo*. The rate of *reaction 3* was measured by monitoring the steady state oxidation of NADPH in the enzymatic reaction catalyzed by TrxR spectrophotometrically. Since the reduction of Trx is also coupled in this assay and can directly react with NADPH, it was important to keep the concentration of Trx at least five times higher than the concentration of TSA in order to prevent the rate becoming limited by

Stellenbosch University https://scholar.sun.ac.za

Trx. The second order reaction rate constants, k_2 and k_3, were determined by taking a similar approach as for the determination of $k_{insulin}$ and $K_{Trx_{SS}}$ above using a combination of experimental determination and computational fitting of parameters.

5.2.5.1 k_3

Two independent complete system assay experiments were conducted with the aim of obtaining a similar value for k_3. In one of the experiments TSA was varied while keeping H_2O_2 constant. The linear portion of the complete data set is shown in Figure 4.14 B. Note the reaction rate here was also normalized by dividing with the constant concentration of the other substrate (H_2O_2) used in the assay. The slope of this plot was calculated as 4.29 ± 0.3 μM^{-1} min^{-1} by linear regression ($R^2 = 0.989$). The same procedure was followed for the other experiment. Figure 4.14 A shows the result for the experiment in which H_2O_2 was varied while the concentration of TSA was kept constant at 0.05 µM. This concentration of TSA was chosen since it fell within the linear range of the previous experiment. The value for k_3 calculated by linear regression from this result was 22.9 ± 3 μM^{-1} min^{-1}. Unlike with the results obtained from the two independent insulin reduction assay experiments to determine the value for $k_{insulin}$ (discussed in Section 5.2.3.1), quite a large deviation exists between the two values obtained from these two experiments. Simply taking the average of these two values would not be a true representation of the second order rate constant. A five-fold difference in this case indicated that something was lacking in the experimental setup which reduced the confidence in the values obtained. The discrepancies found here are discussed further in Section 5.2.5.3 below.

Despite the fact that the two values obtained differ from each other, they are also slightly lower than what was reported by a study which also determined the rate kinetics of H_2O_2 reduction by TSA from *S. cerevisiae* [112]. This study reported a second order rate constant for this reaction in the range of 10^7 M^{-1} s^{-1}. Second order rate constants for the reduction of H_2O_2 by peroxiredoxins have, however, previously been reported by other studies to be in the range of 10^4 to 10^7 M s^{-1} which correlates well with the value obtained in this study [97;113;114].

Stellenbosch University https://scholar.sun.ac.za

5.2.5.2 k_2

The data set obtained with the complete system assay in which TSA was varied from 0 to 2 µM while H_2O_2 was kept constant (Figure 4.15) also shows a hyperbolic relationship between the rate of the reaction and substrate concentration. As described above, the apparent substrate saturation profile seen in this result is also due to the redistribution of the redoxin to its oxidized form at higher TSA concentrations rather than enzymatic substrate saturation (Figure 4.15). Mass action kinetics were also fitted to this data set of varying TSA. At this stage, a PySCeS model for the complete system was constructed and populated with the experimentally determined and fitted parameters K_{NADPH}, K_{TrxSS}, k_{cat} and k_3 (see Appendix A.2 for the PySCeS model). The only remaining model parameter was k_2. This parameter was fitted by calculating the steady state flux through the system in the PySCeS model for the same range of TSA concentrations used in the experiment. The fitted value for k_2 was 0.383 ± 0.03 µM^{-1} min^{-1} (Table 4.4).

The same experimental data set was also used in an attempt to simultaneously fit both k_3 and k_2 parameters. However, this fit resulted in a relative error of above 1000%, while the relative error for fitting k_2 only was 8.82%. The result for the simultaneous fitting was therefore disregarded.

5.2.5.3 Understanding data discrepancies using model simulation

Once values for all the model parameters were determined, some model simulations were performed to evaluate the model and try to resolve any discrepancies in the experimental data obtained. The conditions in the computational PySCeS model were set to reflect the experimental conditions in the complete system assay (see Appendix A.2 for the PySCeS model).

Figures 4.16 and 4.17 show the results of two complete system assay experiments in which the concentration of H_2O_2 was varied while TSA was kept constant at 0.05 and 0.5 µM, respectively. The PySCeS model, constructed with the parameter values shown in Table 4.5, was simulated with the same experimental conditions. More specifically, the steady state flux of the system was calculated for the same range of H_2O_2 concentrations as in both experiments (0 to 10 µM for Figure 4.16 and 0 to 50 µM for Figure 4.17). The model simulation and experimental data for both experiments are plotted se-

Stellenbosch University https://scholar.sun.ac.za

parately due to the large difference in y-axis values. The model simulation in Figure 4.16 A shows the flux against 0 to 10 µM of H_2O_2 as a hyperbolic relationship. This does not correspond to the linear relationship obtained in the experimental data set (Figure 4.16 B) with the same range of H_2O_2 concentrations. Furthermore, the data in Figure 4.17 follow the same trend as the simulation, however, the model clearly underestimates the experimental results. The maximum flux value between the model and the experimental data differs by a factor of 10. Further model simulations were performed in an attempt to explain these discrepancies.

Figure 4.18 A shows the result of a PySCeS model parameter scan. The TSA moiety was scanned over a range of H_2O_2 concentrations and the output plotted the concentration of TSA_{SS} and TSA_{SH} over this range. What can be concluded from this result is that the TSA moiety is mostly in the oxidized form at approximately 0.2 µM of H_2O_2 already. Thus, the assumption that total TSA was equal to TSA_{SH} and that the amount of TSA_{SS} present at the start of the reaction was negligible in the complete system assays performed, was in fact not true. This is because the H_2O_2 concentration ranges of the experiments in which H_2O_2 was varied were far beyond 0.2 µM. Moreover, the constant H_2O_2 concentration used in the experiment in which TSA was varied was 20 µM. The parameter scan confirms that at both these conditions, the majority of TSA was most probably already in the oxidized form. The redox charge of the TSA moiety was also plotted for a range of H_2O_2 concentrations (Figure 4.18 B). This result clearly shows that almost 90% of TSA is already in the oxidized form at a H_2O_2 of 2 µM. This further substantiates the incorrect assumption of no TSA_{SS} present at the start of the reaction for the experiments performed. These results could possibly explain the differences seen in the experimental data *vs.* the model. However, a definite conclusion could not be made and further experimentation is required to investigate these discrepancies in greater detail.

Stellenbosch University https://scholar.sun.ac.za

5.3 Model simulation with a pulse-like H_2O_2 input

Despite the discrepancies found in some of the results obtained in this study, the *in vitro* model constructed could nonetheless still be simulated to demonstrate inherent system properties. A version of the *in vitro* computational model was modified to add a pulse-like behaviour for the concentration of H_2O_2 during time simulations (see Appendix A.3). More specifically, a number of pulses of H_2O_2 at a specified concentration was subjected to the model and the capacity of the system to cope with this type of stress input was evaluated. The response was investigated in terms of the oxidation state of the system moieties, Trx and TSA.

Figure 4.19 shows the result of such a model simulation performed. Five different H_2O_2-pulse concentrations were tested: 0.001, 0.5, 2.5, 5 and 10 µM H_2O_2. The system was then subjected to five subsequent H_2O_2-pulses over a simulated time period of 40 minutes. The left-hand plots of Figure 4.19 show the Trx moiety with the reduced form of Trx in green and the oxidized form in red. The right-hand plots show the TSA moiety with the reduced form of TSA in blue and the oxidized form in orange. The H_2O_2-pulse concentration is also plotted on each plot as a dotted black line except for plot **I** due to the large difference in concentration values for H_2O_2 and TSA in that simulation.

At low H_2O_2-pulse concentrations (0.001 and 0.5 µM) the system is still cabable of neutralizing H_2O_2 efficiently (Figure 4.19 A-D). Although the concentration of the reduced species of each moiety decreases initially, a steady state follows soon after in which the majority of Trx and TSA are both in the reduced form. At these conditions, H_2O_2 can still be decreased back by the system to its original concentration. At a H_2O_2-pulse concentration of 2.5 µM it can be seen that the overall redox state of the two moieties approaches a switch to the oxidized form (Figure 4.19 E-F). At H_2O_2-pulse concentrations higher than 2.5 µM, the system switches to the oxidized form more rapidly and the majority of Trx and TSA are in the oxidized form over time. At this stage, the system fails to neutralize H_2O_2 efficiently as H_2O_2 never reaches its original concentration again after each pulse and simply builds up over time (Figure 4.19 G-J). This type of model simulation is valuable in the sense that a certain H_2O_2 threshold

Stellenbosch University https://scholar.sun.ac.za

concentration could be determined at which the system fails to remove H_2O_2.

5.4 Summary of findings

The peroxiredoxin system is a key role player in H_2O_2 metabolism in all organisms. It has become evident that the use of computational models are specifically advantageous when it comes to investigating metabolic networks. This study contributed to building a platform for developing a computational model for the peroxiredoxin system of *S. cerevisiae* and addressed the research questions of this study in the following ways:

- The proteins of the peroxiredoxin system of *S. cerevisiae*, TrxR, Trx and TSA, were successfully expressed in a bacterial host organism and purified to a high degree of homogeneity.
- A spectrophotometric assay to determine the activity of TrxR, the DTNB reduction assay, was used to determine the model parameter, K_{NADPH}.
- An insulin calibration curve was set up to determine the concentration of product, insulin$_{SH}$, in all insulin reduction assays.
- A two-reaction PySCeS model for the reduction of insulin by the Trx system was parameterized with a combination of experimental techniques and parameter fitting. A second order rate constant, $k_{insulin}$ for the reduction of insulin by Trx was determined directly from two independent experiments. The remaining two parameters for this model, $K_{Trx_{SS}}$ and k_{cat}, were fitted using experimental data sets.
- Determination of the second order rate constants for both H_2O_2 reduction by TSA and TSA reduction by Trx was attempted. The constructed *in vitro* PySCeS model parameterized with the rate constants obtained underestimated the experimental data of model independent data sets. Modeling simulation with conditions similar to the experimental assay were, however, able to resolve the discrepancies seen in the experimental data.
- The constructed *in vitro* PySCeS model for the peroxiredoxin system constructed could nonetheless be used to investigate H_2O_2 metabolism

Stellenbosch University https://scholar.sun.ac.za

in the system. Time simulations with a pulse-like H_2O_2 input demonstrated that at a certain threshold H_2O_2-pulse concentration, the system becomes limiting in its capacity to efficiently neutralize H_2O_2. Above this threshold the system moieties, Trx and TSA, become mostly oxidized leading to a H_2O_2 build-up.

5.5 Limitations, recommendations and future studies

5.5.1 Protein purification

A limitation that affected many aspects in this study was the relatively small amount of protein that could be purified from a single growth batch and purification. The number of assays that were performed in this study required larger amounts of purified protein samples at higher concentrations. A way to overcome this limitation is to upscale the bacterial culturing and purification steps of a single protein as to limit the number of purifications necessary to complete a specific project. Further optimization of culturing conditions would also be necessary to ensure the highest possible protein yields. The purity of the isolated proteins could be further quantified using image analysis software. This method entails determining the density of both the purified protein band as well as the total density of the entire lane. These values can then be used to calculate a percentage that indicates the purity of the sample.

The activity of the proteins purified in this study was slightly less compared to previous studies. Compare, for example, the higher K_{NADPH} and very low catalytic turnover number for TrxR (Table 4.5). Although a number of potential factors exist that would lead to decreased activity or protein stability, it is possible that the dialysis step in this study was inadequate for removal of contaminants, such as imidazole, that were present in IMAC buffers. A recommendation for minimizing possible contaminants in future purifications procedures would be to add an additional purification step, for example buffer exchange by size-exclusion chromotography, in addition to dialysis.

Stellenbosch University https://scholar.sun.ac.za

5.5.2 Determination of more accurate model parameters

One limitation of the insulin reduction assay was that low $insulin_{SH}$ concentrations could not be determined using the constructed calibration curve. The concentration of $insulin_{SH}$ below 33 µM could perhaps be determined by a different assay. DTNB reacts with free thiols to produce a bright yellow product that can be measured spectrophotometrically at 412 nm[153]. Arnér *et al.* describe this protocol in which the free thiols formed in $insulin_{SH}$ can be determined after the addition of DTNB to the assay mixture[126]. This might be a more sensitive assay for the accurate determination of $insulin_{SH}$.

More experiments using the complete system assay could be performed with lower H_2O_2 concentrations in order to clear up the discrepancies in the results obtained in this study. Moreover, reactions with second order rate constants in the range of 10^7 M^{-1} sec^{-1} could potentially be determined more accurately using a stopped flow spectrophotometer which can directly measure very rapid reaction and allows for mixing of reaction contents in the millisecond range[112]. Furthermore, the activity of peroxiredoxins has been measured with success by competition kinetics in order to determine the second order reaction rate constant of H_2O_2 reduction[112;154;155]. Nelson *et al.* describe protocols for measuring the fast kinetics of H_2O_2 reduction with both a horseradish peroxidase competition assay and with stopped flow spectrophotometry[156].

5.5.3 Modeling the peroxiredoxin system of *S. cerevisiae*

A recommendation for further model development is to add the reaction for TSA hyperoxidation which occurs exclusively in eukaryotic peroxiredoxin systems[66]. This would require the addition of the ATP-dependent reaction catalyzed by sulfiredoxin which regenerates hyperoxidized TSA into the sulfenic acid form (see Figure 2.3)[68]. Determination of the model parameters for these reactions would require the purification of another protein, sulfiredoxin, as well as the design and optimization of assays to obtain reaction rates for both these reactions.

In this study, the H_2O_2-pulse simulation could successfully demonstrate the behaviour of a peroxiredoxin system subjected to a stress input. A precise

Stellenbosch University https://scholar.sun.ac.za

H_2O_2-pulse threshold concentration is, of course, dependent on an accurately described computational model. This simulation experiment could be validated further in combination with wet laboratory experiments. Experiments could be designed in which H_2O_2 is added to the reaction mixture at regular intervals. A sample from the assay mixture could then be taken before, at, and after each addition of H_2O_2. The redox state and concentration of each form could then be determined using maleimide-polyethylene glycol (m-PEG) tagging[157]. In this technique, m-PEG reacts with free thiols of cysteine residues and a mobility shift can be observed on an immunoblot with anti-Trx or anti-TSA antibodies[157].

5.6 Conclusion

H_2O_2 plays an important role in oxidative stress and signaling. The model constructed in this study is a step towards improving our understanding of how the peroxiredoxin system metabolizes H_2O_2. Model simulation, such as the H_2O_2-pulse simulation described in this study, enabled us to demonstrate the kinetic dynamics of this system in a way that is challenging with standard biochemical techniques alone. The experiment could illustrate what happens to different components that form part of the system over time when subjected to an input that simulated oxidative stress conditions.

Purification of the peroxiredoxin system proteins in this study proved to be an efficient and more cost-effective alternative to purchasing the proteins from a supplier of biological products. The spectrophotometric assays used in this study were efficient and mostly reliable for determination of the parameters required for model construction. Experiments conducted in this study led to results that could be used to construct a simple kinetic model for the peroxiredoxin system of *S. cerevisiae* sufficiently. However, the accuracy of the model was limited by the discrepancies found in the results for determining the second order reaction rate constant for H_2O_2 reduction. Nonetheless, the model constructed is a simplified representation of a eukaryotic peroxiredoxin system and could lay the foundation for developing a more complex model.

The use of experimental wet laboratory techniques in combination with computational modeling was demonstrated as a powerful tool to embark on the

Stellenbosch University https://scholar.sun.ac.za

investigation of complex cellular networks such as the peroxiredoxin system. An accurate kinetic model for a eukaryotic peroxiredoxin system could enable us to make predictions in both physiological and pathophysiological conditions as well as identify potential drug targets in diseased states.

Stellenbosch University https://scholar.sun.ac.za

Appendices

Stellenbosch University https://scholar.sun.ac.za

Appendix A

PySCeS Models

A.1 Insulin reduction coupled to the Trx system

Refer to attached file *TRR_NADPH_Trx_Insulin.psc*.

A.2 *In vitro* peroxiredoxin system for *S. cerevisiae*

Refer to attached file *Melinda_cerevisiae.psc*.

A.3 *In vitro* peroxiredoxin system for *S. cerevisiae* with H_2O_2-pulse input

Refer to attached file *PulseModel.psc*.

Stellenbosch University https://scholar.sun.ac.za

Appendix B

Data Analysis and Parameter Fitting

All the necessary files for each result figure shown in this thesis can be located in a folder in the Supplementary Material with a title referring to that specific figure. This folder also contains the Jupyter Notebook containing all the code that will output the specific result figure. All the required Excel spreadsheets and text files for running a particular notebook can also be found in these folders.

B.1 DTNB reduction assay with varying TrxR

Refer to attached file *Fig_4_6_DTNB_Assay_Vary_TrxR_LinRegress.ipynb* for Figure 4.6.

B.2 Global fitting of TrxR kinetics

Refer to attached file *Fig_4_7_DTNB_Assay_Global_Fit.ipynb* for Figure 4.7.

B.3 Insulin calibration curve

Refer to attached file *Fig_4_9_and_4_10_Insulin_Calibration_Curve.ipynb* for Figures 4.9 and 4.10.

Stellenbosch University https://scholar.sun.ac.za

B.4 Insulin reduction assay: vary insulin

Refer to attached file *Fig_4_11_a_Insulin_Reduction_Assay_Vary_Insulin.ipynb* for Figure 4.11a.

B.5 Insulin reduction assay: vary Trx

Refer to attached file *Fig_4_11_b_Insulin_Reduction_Assay_Vary_Trx* for Figure 4.11b.

B.6 Fitting k_{cat} and $K_{Trx_{SS}}$ with varying Trx data set

Refer to attached file *Fig_4_12_Fitting_Result_kcat_and_Ktrxss.ipynb* for Figure 4.12.

B.7 DTT oxidation assay

Refer to attached file *Fig_4_13_DTT_Oxidation_Assay_Vary_TSA.ipynb* for Figure 4.13.

B.8 Complete system assay: vary H_2O_2

Refer to attached file *Fig_4_14_A_CSA_Vary_H2O2_10.ipynb* for Figure 4.14 A.

B.9 Complete system assay: vary TSA

Refer to attached file *Fig_4_14_B_CSA_Vary_TSA.ipynb* for Figure 4.14 B.

B.10 Fitting k_2 with varying TSA data set

Refer to attached file *Fig_4_15_Fitting_Result_for_k2.ipynb* for Figure 4.15.

Stellenbosch University https://scholar.sun.ac.za

Appendix C

Model Simulation

All the necessary files for each result figure shown in this thesis can be located in a folder in the Supplementary Material with a title referring to that specific figure. This folder also contains the Jupyter Notebook containing all the code that will output the specific result figure. All the required Excel spreadsheets and text files for running a particular notebook can also be found in these folders.

C.1 Model evaluation

Refer to attached file *Figs_4_16_to_4_18_Model_Evaluation.ipynb* for Figures 4.16 to 4.18.

C.2 H_2O_2-pulse simulation (with PySUNDIALS)

Refer to attached file *Fig_4_19_Pulse_Sim_Python_2_with_PySUNDIALS.ipynb* for Figure 4.19.

Stellenbosch University https://scholar.sun.ac.za

C.3 H_2O_2-pulse simulation (without PySUNDIALS)

Refer to attached file *Fig_4_19_Pulse_Sim_Python_3_No_PySUNDIALS.ipynb* for Figure 4.19.

Stellenbosch University https://scholar.sun.ac.za

Bibliography

[1] Dickinson, B.C. and Chang, C.J.: Chemistry and biology of reactive oxygen species in signaling or stress responses. *Nature Chemical Biology*, vol. 7, no. 8, pp. 504–511, 2012.

[2] Betteridge, D.J.: What is oxidative stress? *Metabolism*, vol. 49, no. 2, pp. 3–8, 2000.

[3] Perkins, A., Nelson, K.J., Parsonage, D., Poole, L.B. and Karplus, P.A.: Peroxiredoxins: Guardians against oxidative stress and modulators of peroxide signaling. *Trends in Biochemical Sciences*, vol. 40, no. 8, pp. 435–445, 2015. ISSN 0968-0004.

[4] Martinez-Outschoorn, U.E., Lin, Z., Trimmer, C., Flomenberg, N., Wang, C., Pavlides, S., Pestell, R.G., Howell, A., Sotgia, F. and Lisanti, M.P.: Cancer cells metabolically "fertilize" the tumor microenvironment with hydrogen peroxide, driving the Warburg effect. *Cell Cycle*, vol. 10, no. 15, pp. 2504–2520, 2011.

[5] Lisanti, M.P., Martinez-Outschoorn, U.E., Lin, Z., Pavlides, S., Whitaker-Menezes, D., Pestell, R.G., Howell, A. and Sotgia, F.: Hydrogen peroxide fuels aging, inflammation, cancer metabolism and metastasis: The seed and soil also needs "fertilizer". *Cell Cycle*, vol. 10, no. 15, pp. 2440–2449, 2011. ISSN 15514005.

[6] Wang, X., Takeda, S., Mochizuki, S., Jindal, R. and Dhalla, N.S.: Mechanisms of hydrogen peroxide-induced increase in intracellular calcium in cardiomyocytes. *Journal of Cardiovascular Pharmacology and Therapeutics*, vol. 4, no. 1, pp. 41–48, 2007. ISSN 1074-2484.

[7] Sandstrom, P.A., Roberts, B., Folks, T.M. and Buttke, T.M.: HIV gene expression enhances T cell susceptibility to hydrogen peroxide-induced apoptosis.

Stellenbosch University https://scholar.sun.ac.za

AIDS Research and Human Retroviruses, vol. 9, no. 11, pp. 1107–1113, 1993. ISSN 0889-2229.

[8] Veal, E. and Day, A.: Hydrogen peroxide as a signaling molecule. *Antioxidants & Redox Signaling*, vol. 15, no. 1, pp. 147–151, 2011. ISSN 1523-0864.

[9] Fridovich, I.: Fundamental aspects of reactive oxygen species, or what's the matter with oxygen? *Annals of the New York Academy of Sciences*, vol. 893, pp. 13–18, 1999. ISSN 00778923.

[10] Nordberg, J. and Arnér, E.S.: Reactive oxygen species, antioxidants, and the mammalian thioredoxin system. *Free Radical Biology and Medicine*, vol. 31, no. 11, pp. 1287–1312, 2001. ISSN 08915849.

[11] Jena, N.R.: DNA damage by reactive species: Mechanisms, mutation and repair. *Journal of biosciences*, vol. 37, no. 3, pp. 503–17, 2012. ISSN 0973-7138.

[12] Stadtman, E.R. and Levine, R.L.: Protein oxidation. *Annals of the New York Academy of Sciences*, vol. 663, no. 1, pp. 110–119, 1992. ISSN 17496632.

[13] El-Beltagi, H.S. and Mohamed, H.I.: Reactive oxygen species, lipid peroxidation and antioxidative defense mechanism. *Notulae Botanicae Horti Agrobotanici Cluj-Napoca*, vol. 41, no. 1, pp. 44–57, 2013. ISSN 0255965X.

[14] Winterbourn, C.C.: *The biological chemistry of hydrogen peroxide*, vol. 528. 1st edn. Elsevier Inc., 2013. ISBN 9780124058811.

[15] Birben, E., Sahiner, U.M., Sackesen, C., Erzurum, S. and Kalayci, O.: Oxidative stress and antioxidant defense in malarial parasites. *World Allergy Organization*, pp. 9–19, 2012.

[16] De Jager, T.L., Cockrell, A.E. and Du Plessis, S.S.: Ultraviolet light induced generation of reactive oxygen species. In: Ahmad, S. (ed.), *Ultraviolet Light in Human Health, Diseases and Environment*, chap. 2, pp. 15–23. Springer, Tygerberg, 2017. ISBN 9783319560175.

[17] Azzam, E.I., Jay-Gerin, J.-P. and Pain, D.: Ionizing radiation-induced metabolic oxidative stress and prolonged cell injury. *Cancer Letters*, vol. 327, 2012.

Stellenbosch University https://scholar.sun.ac.za

[18] Hildebrandt, A.G. and Roots, I.: Reduced nicotinamide adenine dinucleotide phosphate (NADPH)-dependent formation and breakdown of hydrogen peroxide during mixed function oxidation reactions in liver microsomes. *Archives of Biochemistry and Biophysics*, vol. 171, no. 2, pp. 385–397, 1975. ISSN 10960384.

[19] Imlay, J.A.: Pathways of oxidative damage. *Annual Review of Microbiology*, vol. 57, no. 1, pp. 395–418, 2004. ISSN 0066-4227.

[20] Lambeth, J.D.: NOX enzymes and the biology of reactive oxygen. *Nature Reviews Immunology*, vol. 4, no. March, pp. 1–9, 2004.

[21] Le Bras, M., Clément, M.-V., Pervaiz, S. and Brenner, C.: Reactive oxygen species and the mitochondrial signaling pathway of cell death. *Histology and histopathology*, vol. 20, no. 1, pp. 205–219, 2005. ISSN 0213-3911.

[22] Halliwell, B.: Reactive species and antioxidants. Redox biology is a fundamental theme of aerobic life. *Plant Physiology*, vol. 141, no. 2, pp. 312–322, 2006. ISSN 0032-0889.

[23] Waris, G. and Ahsan, H.: Reactive oxygen species: Role in the development of cancer and various chronic conditions. *Journal of Carcinogenesis*, vol. 5, no. 14, pp. 1–8, 2006. ISSN 14773163.

[24] Jones, B.P. and Suggett, A.: The catalase-hydrogen peroxide system. *Biochemical Journal*, vol. 110, pp. 621–629, 1968.

[25] Schafer, F.Q. and Buettner, G.R.: Redox environment of the cell as viewed through the redox state of the glutathione disulfide/glutathione couple. *Free Radical Biology & Medicine*, vol. 30, no. 11, pp. 1191–1212, 2001. ISSN 0891-5849.

[26] Flohé, L. and Harris, J.R. (eds.): *Peroxiredoxin Systems*, vol. 44. 1st edn. Springer, 2007. ISBN 9781402060502.

[27] Sies, H.: Hydrogen peroxide as a central redox signaling molecule in physiological oxidative stress: Oxidative eustress. *Redox Biology*, vol. 11, pp. 613–619, 2017. ISSN 22132317.

[28] Schieber, M. and Chandel, N.S.: ROS function in redox signaling and oxidative stress. *Current Biology*, vol. 24, no. 10, pp. R453–R462, 2014. ISSN 09609822.

Stellenbosch University https://scholar.sun.ac.za

[29] Winterbourn, C.C. and Hampton, M.B.: Thiol chemistry and specificity in redox signaling. *Free Radical Biology and Medicine*, vol. 45, no. 5, pp. 549–561, 2008. ISSN 08915849.

[30] Liguori, I., Russo, G., Curcio, F., Bulli, G., Aran, L., Della-Morte, D., Gargiulo, G., Testa, G., Cacciatore, F., Bonaduce, D. and Abete, P.: Oxidative stress, aging, and diseases. *Clinical Interventions in Aging*, vol. 13, pp. 757–772, 2018. ISSN 1178-1998.

[31] Storz, P.: Oxidative stress in cancer. In: Jakob, U. and Reichmann, D. (eds.), *Oxidative Stress and Redox Regulation*, chap. 15, pp. 427–447. Springer, Dordrecht, Dordrecht, 2013. ISBN 9789400757875.

[32] Dhalla, N.S., Temsah, R.M. and Netticadan, T.: Role of oxidative stress in cardiovascular diseases. *Journal of hypertension*, vol. 18, no. 6, pp. 655–673, 2000. ISSN 0263-6352.

[33] Milton, N.G.N.: Role of hydrogen peroxide in the aetiology of Alzheimer's disease implications for treatment. *Drugs Aging*, vol. 21, no. 2, pp. 81–100, 2004.

[34] Jimenez Del Rio, M. and Velez-Pardo, C.: The hydrogen peroxide and its importance in Alzheimer's and Parkinson's disease. *Current Medicinal Chemistry - Central Nervous System Agents*, vol. 4, no. 4, pp. 279–285, 2004. ISSN 15680150.

[35] Paul, B.D. and Snyder, S.H.: Impaired redox signaling in Huntington's disease: Therapeutic implications. *Frontiers in Molecular Neuroscience*, vol. 12, no. March, pp. 1–13, 2019. ISSN 16625099.

[36] Lin, M. and Beal, M.F.: Mitochondrial dysfunction and oxidative stress in neurodegenerative diseases. *Nature*, vol. 443, pp. 787–795, 2006. ISSN 0028-0836.

[37] Winterbourn, C.C. and Metodiewa, D.: Reactivity of biologically important thiol compounds with superoxide and hydrogen peroxide. *Free Radical Biology and Medicine*, vol. 27, no. 3-4, pp. 322–328, 1999. ISSN 08915849.

[38] Nguyen, T.H., Burnier, J. and Meng, W.: The kinetics of relaxin oxidation by hydrogen peroxide. *Pharmaceutical Research*, vol. 10, no. 11, pp. 1563–1571, 1993.

Stellenbosch University https://scholar.sun.ac.za

[39] Winterbourn, C.C. and Hampton, M.B.: Thiol chemistry and specificity in redox signaling. *Free Radical Biology and Medicine*, vol. 45, no. 5, pp. 549–561, 2008. ISSN 08915849.

[40] Barton, J.P., Packer, J.E. and Sims, R.J.: Kinetics of the reaction of hydrogen peroxide with cysteine and cysteamine. *Journal of the Chemical Society, Perkin Transactions 2*, vol. 20, no. 11, pp. 1547–1549, 1973.

[41] Rhee, S.G.: H2O2, a necessary evil for cell signaling. *Science*, vol. 312, no. June, pp. 1882–1884, 2006.

[42] Stone, J.R. and Yang, S.: Hydrogen peroxide: A signaling messenger. *Antioxidants & Redox Signaling*, vol. 8, pp. 243–270, 2006.

[43] Rhee, S.G., Kang, S.W., Jeong, W., Chang, T.S., Yang, K.S. and Woo, H.A.: Intracellular messenger function of hydrogen peroxide and its regulation by peroxiredoxins. *Current Opinion in Cell Biology*, vol. 17, no. 2, pp. 183–189, 2005. ISSN 09550674.

[44] Hancock, J., Desikan, R. and Neil, S.: Role of reactive oxygen species in cell signalling pathways. *Biochemical Society Transactions*, vol. 29, pp. 345–350, 2001.

[45] Winterbourn, C.C.: Radical scavenging by thiols and the fate of thiyl radicals. In: Jakob, U. and Reichmann, D. (eds.), *Oxidative Stress and Redox Regulation*, chap. 2, pp. 43–58. Springer, Dordrecht, Dordrecht, 2013. ISBN 9789400757875.

[46] Bae, Y.S., Kang, S.W., Seo, M.S., Baines, I.C., Tekle, E., Chock, P.B. and Rhee, S.G.: Epidermal growth factor (EGF)-induced generation of hydrogen peroxide. *Journal of Biological Chemistry*, vol. 272, no. 1, pp. 217–221, 1997. ISSN 0021-9258.

[47] Runchel, C., Matsuzawa, A. and Ichijo, H.: Mitogen-activated protein kinases in mammalian oxidative stress responses. *Antioxidants & Redox Signaling*, vol. 15, no. 1, pp. 205–218, 2010. ISSN 1523-0864.

[48] Guyton, K.Z., Liu, Y., Gorospe, M., Xu, Q. and Holbrook, N.J.: Activation of mitogen-activated protein kinase by H_2O_2. *The Journal of Biological Chemistry*, vol. 271, no. 8, pp. 4138–4142, 1996.

Stellenbosch University https://scholar.sun.ac.za

[49] Ichijo, H., Saitoh, M., Miyazono, K., Nishida, E., Moriguchi, T., Gotoh, Y., Irie, K., Matsumoto, K., Ten Dijke, P. and Takagi, M.: Induction of apoptosis by ASK1, a mammalian MAPKKK that activates SAPK/JNK and p38 signaling pathways. *Science*, vol. 275, no. 5296, pp. 90–94, 1997. ISSN 0036-8075.

[50] Knoops, B., Loumaye, E. and Van der Eecken, V.: Evolution of the peroxiredoxins. In: Flohé, L. and Harris, J.R. (eds.), *Peroxiredoxin Systems*, chap. 2, pp. 27–40. Springer, 2007.

[51] Lu, J. and Holmgren, A.: The thioredoxin antioxidant system. *Free Radical Biology and Medicine*, vol. 66, pp. 75–87, 2014. ISSN 18734596.

[52] Flohé, L. and Harris, J.R.: Introduction. History of the peroxiredoxins and topical perspectives. In: Flohé, L. and Harris, J.R. (eds.), *Peroxiredoxin Systems*, vol. 44, chap. 1, pp. 1–25. Springer, 2007. ISBN 978-1-4020-6050-2.

[53] Kim, K., Kim, I.H., Lee, K.Y., Rhee, S.G. and Stadtman, E.R.: The isolation and purification of a specific 'protector' protein which inhibits enzyme inactivation by a Thiol/Fe(III)/O_2 mixed-function oxidation system. *Journal of Biological Chemistry*, vol. 263, no. 10, pp. 4704–4711, 1988. ISSN 00219258.

[54] Rhee, S.G. and Chae, H.Z.: Thioredoxin Peroxidase and Peroxiredoxin Family. *Molecules and Cells*, vol. 4, no. 2, pp. 137–142, 1994.

[55] Jacobson, F.S., Morgan, R.W., Christman, M.F. and Ames, B.N.: An alkyl hydroperoxide reductase from *Salmonella typhimurium* involved in the defense of DNA against oxidative damage. *Journal of Biological Chemistry*, vol. 264, no. 3, pp. 1488–1496, 1989. ISSN 00219258.

[56] Chae, H.Z., Robison, K., Poole, L.B., Church, G., Storz, G. and Rhee, S.G.: Cloning and sequencing of thiol-specific antioxidant from mammalian brain: alkyl hydroperoxide reductase and thiol-specific antioxidant define a large family of antioxidant enzymes. *Proceedings of the National Academy of Sciences*, vol. 91, no. 15, pp. 7017–7021, 1994. ISSN 0027-8424.

[57] Hofmann, B., Hecht, H.-J. and Flohé, L.: Peroxiredoxins. *The Journal of Biological Chemistry*, vol. 383, no. April, pp. 347 – 364, 2002.

[58] Karplus, P.A. and Hall, A.: Structural Survey of the Peroxiredoxins. In: Flohé, L. and Harris, J.R. (eds.), *Peroxiredoxin Systems*, chap. 3, pp. 41–60. Springer, 2007.

Stellenbosch University https://scholar.sun.ac.za

[59] Wood, Z.A., Schröder, E., Harris, J.R. and Poole, L.B.: Structure, mechanism and regulation of peroxiredoxins. *Trends in Biochemical Sciences*, vol. 28, no. 1, pp. 32–40, 2003. ISSN 09680004.

[60] Rhee, S.G., Kang, S.W., Chang, T., Jeong, W. and Kim, K.: Peroxiredoxin, a novel family of peroxidases. *Life*, vol. 52, pp. 35–41, 2001.

[61] Leyens, G., Donnay, I. and Knoops, B.: Cloning of bovine peroxiredoxins - gene expression in bovine tissues and amino acid sequence comparison with rat, mouse and primate peroxiredoxins. *Comparitive Biochemistry and Physiology Part B*, vol. 136, pp. 943–955, 2003.

[62] Dubbs, J.M. and Mongkolsuk, S.: Peroxiredoxins in bacterial antioxidant defense. In: Flohé, L. and Harris, J.R. (eds.), *Peroxiredoxin Systems*, chap. 7, pp. 143–193. Springer, 2007.

[63] Poole, L.B.: The catalytic mechanism of peroxiredoxins. In: Flohé, L. and Harris, J.R. (eds.), *Peroxiredoxin Systems*, chap. 4, pp. 61–81. Springer, 2007.

[64] Hall, A., Karplus, P.A. and Poole, L.B.: Typical 2-Cys peroxiredoxins - Structures, mechanisms and functions. *FEBS Journal*, vol. 276, no. 9, pp. 2469–2477, 2009. ISSN 1742464X.

[65] Manevich, Y., Feinstein, S.I. and Fisher, A.B.: Activation of the antioxidant enzyme 1-CYS peroxiredoxin requires glutathionylation mediated by heterodimerization with πGST. *Proceedings of the National Academy of Sciences*, vol. 101, no. 11, pp. 3780–3785, 2004. ISSN 0027-8424.

[66] Yang, K.S., Kang, S.W., Woo, H.A., Hwang, S.C., Chae, H.Z., Kim, K. and Rhee, S.G.: Inactivation of human peroxiredoxin I during catalysis as the result of the oxidation of the catalytic site cysteine to cysteine-sulfinic acid. *Journal of Biological Chemistry*, vol. 277, no. 41, pp. 38029–38036, 2002. ISSN 00219258.

[67] Biteau, B., Labarre, J. and Toledano, M.B.: ATP-dependent reduction of cysteine - sulphinic acid by *S. cerevisiae* sulphiredoxin. *Nature*, vol. 425, no. October 2003, pp. 980–984, 2003.

[68] Chang, T., Jeong, W., Woo, H.A., Lee, S.M., Park, S. and Rhee, S.G.: Characterization of mammalian sulfiredoxin and its reactivation of hyperoxidized peroxiredoxin through reduction of cysteine sulfinic acid in the active site to

Stellenbosch University https://scholar.sun.ac.za

cysteine. *The Journal of Biological Chemistry*, vol. 279, no. 49, pp. 50994–51001, 2004.

[69] Wood, Z.A., Poole, L.B. and Karplus, P.A.: Peroxiredoxin evolution and the regulation of hydrogen peroxide signaling. *Science*, vol. 300, no. April, pp. 650–653, 2003. ISSN 00368075.

[70] Rhee, G.S., Chae, H.Z. and Kim, K.: Peroxiredoxins: A historical overview and speculative preview of novel mechanisms and emerging concepts in cell signaling. *Free Radical Biology and Medicine*, vol. 38, no. 12, pp. 1543–1552, 2005. ISSN 08915849.

[71] Holmgren, A., Johansson, C., Berndt, C., Lönn, M., Hudemann, C. and Lillig, C.: Thiol redox control via thioredoxin and glutaredoxin systems. *Biochemical Society Transactions*, vol. 33, no. 6, p. 1375, 2005. ISSN 03005127.

[72] Matsuzawa, A.: Thioredoxin and redox signaling: Roles of the thioredoxin system in control of cell fate. *Archives of Biochemistry and Biophysics*, vol. 617, pp. 101–105, 2017.

[73] Arnér, E.S.J. and Holmgren, A.: Physiological functions of thioredoxin and thioredoxin reductase. *European Journal of Biochemistry J. Biochem*, vol. 267, pp. 6102–6109, 2000.

[74] Russel, M. and Model, P.: The role of thioredoxin in filamentous phage assembly. Construction, isolation, and characterization of mutant thioredoxins. *Journal of Biological Chemistry*, vol. 261, no. 32, pp. 14997–15005, 1986. ISSN 00219258.

[75] Brot, N. and Weissbach, H.: The biochemistry of methionine sulfoxide residues in proteins. *Trends in Biochemical Sciences*, vol. 7, no. 4, pp. 137–139, 1982. ISSN 09680004.

[76] Lillig, C.H., Prior, A., Schwenn, J.D., Åslund, F., Ritz, D., Vlamis-Gardikas, A. and Holmgren, A.: New thioredoxins and glutaredoxins as electron donors of 3'-phosphoadenylylsulfate reductase. *Journal of Biological Chemistry*, vol. 274, no. 12, pp. 7695–7698, 1999. ISSN 00219258.

[77] Holmgren, A.: Thioredoxin and glutaredoxin systems. *The Journal of Biochemistry*, vol. 264, no. 24, pp. 13963–13966, 1989. ISSN 00766879.

Stellenbosch University https://scholar.sun.ac.za

[78] Holmgren, A. and Lu, J.: Thioredoxin and thioredoxin reductase: Current research with special reference to human disease. *Biochemical and Biophysical Research Communications*, vol. 396, pp. 120–124, 2010.

[79] Masutani, H. and Ueda, S.: The thioredoxin system in retroviral infection and apoptosis. *Cell Death and Differentiation*, vol. 12, no. May 2014, pp. 991–998, 2005. ISSN 14765403.

[80] Masutani, H., Naito, M., Takahashi, K., Hattori, T., Koito, A., Takatsuki, K., Go, T., Nakamura, H., Fujii, S., Yoshida, Y., Okuma, M. and Yodoi, J.: Dysregulation of adult T-cell leukemia-derived factor (ADF)/thioredoxin in HIV infection: Loss of ADF high-producer cells in lymphoid tissues of AIDS patients. *AIDS Research and Human Retroviruses*, vol. 8, no. 9, pp. 1707–1715, 1992. ISSN 19318405.

[81] Hampton, M.B. and Orrenius, S.: Dual regulation of caspase activity by hydrogen peroxide: Implications for apoptosis. *FEBS Letters*, vol. 414, no. 3, pp. 552–556, 1997. ISSN 00145793.

[82] Day, A.M., Brown, J.D., Taylor, S.R., Rand, J.D., Morgan, B.A. and Veal, E.A.: Inactivation of a peroxiredoxin by hydrogen peroxide is critical for thioredoxin-mediated repair of oxidized proteins and cell survival. *Molecular Cell*, vol. 45, no. 3, pp. 398–408, 2012. ISSN 10972765.

[83] Jaeger, T., Budde, H., Flohé, L., Menge, U., Singh, M., Trujillo, M. and Radi, R.: Multiple thioredoxin-mediated routes to detoxify hydroperoxides in *Mycobacterium tuberculosis*. *Archives of Biochemistry and Biophysics*, vol. 423, no. 1, pp. 182–191, 2004. ISSN 00039861.

[84] Bruggeman, F.J. and Westerhoff, H.V.: The nature of systems biology. *Trends in Microbiology*, vol. 15, no. 1, pp. 45–50, 2007. ISSN 0966842X.

[85] Barabási, A.L. and Oltvai, Z.N.: Network biology: Understanding the cell's functional organization. *Nature Reviews Genetics*, vol. 5, no. 2, pp. 101–113, 2004. ISSN 14710056.

[86] Snoep, J.L. and Westerhoff, H.V.: From isolation to integration, a systems biology approach for building the Silicon Cell. *Systems Biology*, vol. 13, no. January, pp. 13–30, 2005.

[87] Jiang, F.: The expanding list of redox-sensing transcription factors in mammalian cells. *Journal of Cell Signaling*, vol. 01, no. 01, pp. 1–2, 2016.

Stellenbosch University https://scholar.sun.ac.za

[88] Zhang, Y., Lee, J.H., Paull, T.T., Gehrke, S., D'Alessandro, A., Dou, Q., Gladyshev, V.N., Schroeder, E.A., Steyl, S.K., Christian, B.E. and Shadel, G.S.: Mitochondrial redox sensing by the kinase ATM maintains cellular antioxidant capacity. *Science Signaling*, vol. 11, no. 538, 2018. ISSN 19379145.

[89] Voth, W., Schick, M., Gates, S., Li, S., Vilardi, F., Gostimskaya, I., Southworth, D.R., Schwappach, B. and Jakob, U.: The protein targeting factor Get3 functions as ATP-independent chaperone under oxidative stress conditions. *Molecular Cell*, vol. 56, no. 1, pp. 116–127, 2014. ISSN 10974164.

[90] Foyer, C.H. and Noctor, G.: Redox homeostasis and antioxidant signaling: A metabolic interface between stress perception and physiological responses. *Plant Cell*, vol. 17, no. 7, pp. 1866–1875, 2005. ISSN 10404651.

[91] Rohwer, J.M.: Kinetic modelling of plant metabolic pathways. *Journal of Experimental Botany*, vol. 63, no. 6, pp. 2275–2292, 2012. ISSN 00220957.

[92] Kitano, H.: Computational systems biology. *Nature*, vol. 420, no. November, pp. 206–2010, 2002.

[93] Curien, G., Bastien, O., Robert-Genthon, M., Cornish-Bowden, A., Cárdenas, M.L. and Dumas, R.: Understanding the regulation of aspartate metabolism using a model based on measured kinetic parameters. *Molecular Systems Biology*, vol. 5, no. 271, 2009. ISSN 17444292.

[94] Teusink, B., Passarge, J., Reijenga, C.A., Esgalhado, E., Van Der Weijden, C.C., Schepper, M., Walsh, M.C., Bakker, B.M., Van Dam, K., Westerhoff, H.V. and Snoep, J.L.: Can yeast glycolysis be understood terms of *in vitro* kinetics of the constituent enzymes? Testing biochemistry. *European Journal of Biochemistry*, vol. 267, no. 17, pp. 5313–5329, 2000. ISSN 00142956.

[95] Taylor, C.F., Paton, N.W., Garwood, K.L., Kirby, P.D., Stead, D.A., Yin, Z., Deutsch, E.W., Selway, L., Walker, J., Riba-Garcia, I., Mohammed, S., Deery, M.J., Howard, J.A., Dunkley, T., Aebersold, R., Kell, D.B., Lilley, K.S., Roepstorff, P., Yates, J.R., Brass, A., Brown, A.J., Cash, P., Gaskell, S.J., Hubbard, S.J. and Oliver, S.G.: A systematic approach to modeling, capturing, and disseminating proteomics experimental data. *Nature Biotechnology*, vol. 21, no. 3, pp. 247–254, 2003. ISSN 10870156.

[96] Tomalin, L.E., Day, A.M., Underwood, Z.E., Smith, G.R., Dalle Pezze, P., Rallis, C., Patel, W., Dickinson, B.C., Bähler, J., Brewer, T.F., Chang, C.J.L.,

Stellenbosch University https://scholar.sun.ac.za

Shanley, D.P. and Veal, E.A.: Increasing extracellular H_2O_2 produces a biphasic response in intracellular H_2O_2, with peroxiredoxin hyperoxidation only triggered once the cellular H_2O_2-buffering capacity is overwhelmed. *Free Radical Biology and Medicine*, vol. 95, pp. 333–348, 2016. ISSN 18734596.

[97] Adimora, N.J., Jones, D.P. and Kemp, M.L.: A model of redox kinetics implicates the thiol proteome in cellular hydrogen peroxide responses. *Antioxidants & Redox Signaling*, vol. 13, no. 6, pp. 731–743, 2010.

[98] Von Mering, C., Krause, R., Snel, B., Cornell, M., Oliver, S.G., Fields, S. and Bork, P.: Comparative assessment of large-scale data sets of protein-protein interactions. *Nature*, vol. 417, pp. 399–403, 2002.

[99] Pillay, S., Hofmeyr, J.-h., Mashamaite, L.N. and Rohwer, J.M.: From top-down to bottom-up: Computational modeling approaches for cellular redoxin networks. *Antioxidants & redox signaling*, vol. 18, no. 16, 2013.

[100] Schomburg, I.: BRENDA, the enzyme database: updates and major new developments. *Nucleic Acids Research*, vol. 32, no. 90001, pp. 431D–433, 2004. ISSN 0305-1048.

[101] Ashyraliyev, M., Fomekong-Nanfack, Y., Kaandorp, J.A. and Blom, J.G.: Systems biology: Parameter estimation for biochemical models. *FEBS Journal*, vol. 276, no. 4, pp. 886–902, 2009. ISSN 1742464X.

[102] Pillay, C.S., Hofmeyr, J.-H.S., Olivier, B.G., Snoep, J.L. and Rohwer, J.M.: Enzymes or redox couples? The kinetics of thioredoxin and glutaredoxin reactions in a systems biology context. *Biochemical Journal*, vol. 417, no. 1, pp. 269–277, 2009. ISSN 0264-6021.

[103] Snoep, J.L., Bruggeman, F., Olivier, B.G. and Westerhoff, H.V.: Towards building the silicon cell: A modular approach. *BioSystems*, vol. 83, no. 2-3 SPEC. ISS., pp. 207–216, 2006. ISSN 03032647.

[104] Trotter, E.W. and Grant, C.M.: Non-reciprocal regulation of the redox state of the glutathione-glutaredoxin and thioredoxin systems. *EMBO Reports*, vol. 4, no. 2, pp. 184–188, 2003. ISSN 1469221X.

[105] Åslund, F., Berndt, K.D. and Holmgren, A.: Redox potentials of glutaredoxins and other thiol-disulfide oxidoreductases of the thioredoxin superfamily determined by direct protein-protein redox equilibria. *The Journal of Biological Chemistry*, vol. 272, no. 49, pp. 30780–30786, 1997.

Stellenbosch University https://scholar.sun.ac.za

[106] Holmgren, A.: Reduction of disulfides by thioredoxin. *The Journal of Biological Chemistry*, vol. 254, no. 18, pp. 9113–9119, 1979.

[107] Sayed, A.A. and Williams, D.L.: Biochemical characterization of 2-Cys peroxiredoxins from *Schistosoma mansoni*. *The Journal of Biochemistry*, vol. 279, no. 25, pp. 26159–26166, 2004.

[108] Akerman, S.E. and Müller, S.: 2-Cys peroxiredoxin Pf Trx-Px1 is involved in the antioxidant defence of *Plasmodium falciparum*. *Molecular & Biochemical Parasitology*, vol. 130, pp. 75–81, 2003.

[109] Pillay, C.S., Hofmeyr, J.H.S. and Rohwer, J.M.: The logic of kinetic regulation in the thioredoxin system. *BMC Systems Biology*, vol. 5, no. 1, p. 15, 2011. ISSN 17520509.

[110] Rohwer, J.M., Viljoen, C. and Christensen, C.D.: Identifying the conditions necessary for the thioredoxin ultrasensitive response. *Perspectives in Science*, vol. 9, pp. 53–59, 2016.

[111] Benfeitas, R., Selvaggio, G., Antunes, F., Coelho, P.M. and Salvador, A.: Hydrogen peroxide metabolism and sensing in human erythrocytes: A validated kinetic model and reappraisal of the role of peroxiredoxin II. *Free Radical Biology and Medicine*, vol. 74, pp. 35–49, 2014. ISSN 18734596.

[112] Ogusucu, R., Rettori, D., Munhoz, D.C., Soares Netto, L.E. and Augusto, O.: Reactions of yeast thioredoxin peroxidases I and II with hydrogen peroxide and peroxynitrite: Rate constants by competitive kinetics. *Free Radical Biology and Medicine*, vol. 42, no. 3, pp. 326–334, 2007. ISSN 08915849.

[113] Peskin, A.V., Low, F.M., Paton, L.N., Maghzal, G.J., Hampton, M.B. and Winterbourn, C.C.: The high reactivity of peroxiredoxin 2 with H_2O_2 is not reflected in its reaction with other oxidants and thiol reagents. *Journal of Biological Chemistry*, vol. 282, no. 16, pp. 11885–11892, 2007. ISSN 00219258.

[114] Manta, B., Hugo, M., Ortiz, C., Ferrer-Sueta, G., Trujillo, M. and Denicola, A.: The peroxidase and peroxynitrite reductase activity of human erythrocyte peroxiredoxin 2. *Archives of Biochemistry and Biophysics*, vol. 484, no. 2, pp. 146–154, 2009. ISSN 10960384.

[115] Kanzok, S.M., Schirmer, R.H., Türbachova, I., Iozef, R. and Becker, K.: The thioredoxin system of the malaria parasite *Plasmodium falciparum*. *Journal of Biological Chemistry*, vol. 275, no. 51, pp. 40180–40186, 2000. ISSN 0021-9258.

Stellenbosch University https://scholar.sun.ac.za

[116] Akif, M., Khare, G., Tyagi, A.K., Mande, S.C. and Sardesai, A.A.: Functional studies of multiple thioredoxins from *Mycobacterium tuberculosis*. *Journal of Bacteriology*, vol. 190, no. 21, pp. 7087–7095, 2008.

[117] Hugo, M., Turell, L., Manta, B., Botti, H., Monteiro, G., Netto, L.E., Alvarez, B., Radi, R. and Trujillo, M.: Thiol and sulfenic acid oxidation of AhpE, the one-cysteine peroxiredoxin from *Mycobacterium tuberculosis*: Kinetics, acidity constants, and conformational dynamics. *Biochemistry*, vol. 48, no. 40, pp. 9416–9426, 2009. ISSN 00062960.

[118] Jaeger, T.: Peroxiredoxin systems in mycobacteria. In: Flohé, L. and Harris, J.R. (eds.), *Peroxiredoxin Systems*, chap. 9, pp. 207–217. Springer, 2007.

[119] Tairum, C.A., Oliveira, M.A.D., Horta, B.B., Zara, F.J. and Netto, L.E.S.: Disulfide biochemistry in 2-Cys peroxiredoxin: Requirement of Glu50 and Arg146 for the reduction of yeast Tsa1 by thioredoxin. *Journal of Molecular Biology*, vol. 424, no. 1-2, pp. 28–41, 2012. ISSN 0022-2836.

[120] Loberg, M.A., Hurtig, J.E., Graff, A.H., Allan, K.M., Buchan, J.A., Spencer, M.K., Kelly, J.E., Clodfelter, J.E., Morano, K.A., Lowther, W.T. and West, J.D.: Aromatic residues at the dimer-dimer interface in the peroxiredoxin Tsa1 facilitate decamer formation and biological function. *Chemical Research in Toxicology*, vol. 32, no. 3, pp. 474–483, 2019. ISSN 15205010.

[121] Morgan, B.A. and Veal, E.A.: Functions of typical 2-Cys peroxiredoxins in yeast. In: *Peroxiredoxin Systems*, 1st edn, chap. 12, pp. 253–265. Springer Netherlands, 2007.

[122] Faye, G., Kolodner, R.D., Huang, M.-E., Baldacci, G., Soeur, J., Kienda, G. and Iraqui, I.: Peroxiredoxin Tsa1 is the key peroxidase suppressing genome instability and protecting against cell death in *Saccharomyces cerevisiae*. *PLoS Genetics*, vol. 5, no. 6, pp. 1–14, 2009.

[123] Karathia, H., Vilaprinyo, E., Sorribas, A. and Alves, R.: *Saccharomyces cerevisiae* as a model organism: A comparative study. *PLoS ONE*, vol. 6, no. 2, 2011. ISSN 19326203.

[124] Rosano, G.L. and Ceccarelli, E.A.: Recombinant protein expression in *Escherichia coli*: Advances and challenges. *Frontiers in Microbiology*, vol. 5, no. APR, pp. 1–17, 2014. ISSN 1664302X.

Stellenbosch University https://scholar.sun.ac.za

[125] Holmgren, A.: Thioredoxin catalyzes the reduction of insulin disulfides by dithiothreitol and dihydrolipoamide. *The Journal of Biological Chemistry*, vol. 254, no. 19, pp. 9627–9632, 1979.

[126] Arner, E.S. and Holmgren, A.: Measurement of thioredoxin and thioredoxin reductase. *Current Protocols in Toxicology*, , no. 2000, pp. 1–14, 2005.

[127] Nelson, K.J. and Parsonage, D.: Measurement of peroxiredoxin activity. *Current Protocols in Toxicology*, pp. 1–33, 2013.

[128] Holmgren, B.A. and Bjornstedt, M.: Thioredoxin and thioredoxin reductase. *Methods in Enzymology*, vol. 252, pp. 199–208, 1995.

[129] Fell, D.A.: Metabolic control analysis: A survey of its theoretical and experimental development. *Biochemical Journal*, vol. 286, pp. 313–330, 1992.

[130] Ingalls, B.: *Mathematical modelling in systems biology: An introduction*. MIT Press, Cambridge, Massachusetts, 2012.

[131] O'Neill, J.S., Ooijen, G.V., Dixon, L.E., Troein, C., Corellou, F., Bouget, F.-y., Reddy, A.B. and Millar, A.J.: Circadian rhythms persist without transcription in a eukaryote. *Nature*, vol. 469, no. 7331, pp. 554–558, 2011. ISSN 0028-0836.

[132] Edgar, R.S., Green, E.W., Zhao, Y., Van Ooijen, G., Olmedo, M., Qin, X., Xu, Y., Pan, M., Valekunja, U.K., Feeney, K.A., Maywood, E.S., Hastings, M.H., Baliga, N.S., Merrow, M., Millar, A.J., Johnson, C.H., Kyriacou, C.P., O'Neill, J.S. and Reddy, A.B.: Peroxiredoxins are conserved markers of circadian rhythms. *Nature*, vol. 485, no. 7399, pp. 459–464, 2012. ISSN 00280836.

[133] Stangherlin, A. and Reddy, A.B.: Regulation of circadian clocks by redox homeostasis. *Journal of Biological Chemistry*, vol. 288, no. 37, pp. 26505–26511, 2013. ISSN 00219258.

[134] O-Neill, J.S. and Reddy, A.B.: Circadian clocks in human red blood cells. *Nature*, vol. 469, no. 7331, pp. 498–504, 2011. ISSN 00280836.

[135] Noble, R.W. and Gibson, Q.H.: The reaction of ferrous horseradish peroxidase with hydrogen peroxide. *Journal of Biological Chemistry*, vol. 245, no. 9, pp. 2409–2413, 1970. ISSN 00219258.

[136] Haider, S.R., Reid, H.J. and Sharp, B.L.: Tricine-SDS-PAGE. In: Kurien, B.T. and Scofield, R.H. (eds.), *Protein Electrophoresis*, vol. 869, chap. 8, pp. 81–91. Humana Press, 2012. ISBN 978-1-61779-821-4.

Stellenbosch University https://scholar.sun.ac.za

[137] Smith, P.K., Krohn, R.I., Hermanson, G.T., Mallia, A.K., Gartner, F.H., Provenzano, M.D., Fujimoto, E.K., Goeke, N.M., Olson, B.J. and Klenk, D.C.: Measurement of protein using bicinchoninic acid. *Analytical Biochemistry*, vol. 150, no. 1, pp. 76–85, 1985. ISSN 10960309.

[138] Simonian, M.H.: Spectrophotometric determination of protein concentration. *Current Protocols in Cell Biology*, vol. 15, no. 1, pp. B1.3.1–B1.3.7, 2002. ISSN 03673014.

[139] Laemmli, U.: Cleavage of structural proteins during the assembly of the head of bacteriophage T4. *Nature*, vol. 227, no. August, pp. 680–685, 1970.

[140] Okajima, T., Tanabe, T. and Yasuda, T.: Nonurea sodium dodecyl sulfate-polyacrylamide gel electrophoresis with high-molarity buffers for the separation of proteins and peptides. *Analytical Biochemistry*, vol. 211, no. 2, pp. 293–300, 1993. ISSN 00032697.

[141] Schägger, H. and von Jagow, G.: Tricine-sodium dodecyl sulfate-polyacrylamide gel electrophoresis for the separation of proteins in the range from 1 to 100 kDa. *Analytical Biochemistry*, vol. 166, no. 2, pp. 368–379, 1987. ISSN 10960309.

[142] Subramonia Iyer, K. and Klee, W.A.: Spectrophotometric of reduction measurement of disulfide the rate of reduction of disulfide bonds. *The Journal of Biological Chemistry*, vol. 248, no. 2, pp. 707–710, 1973.

[143] Nelson, K.J. and Parsonage, D.: Measurement of peroxiredoxin activity. *Current Protocols in Toxicology*, , no. SUPPL. 49, pp. 1–28, 2011. ISSN 19349262.

[144] Badenhorst, M., Barry, C.J., Swanepoel, C.J., van Staden, C.T., Wissing, J. and Rohwer, J.M.: Workflow for data analysis in experimental and ocmputational systems biology: Using Python. *Processes*, vol. 7, no. 460, pp. 1–17, 2019.

[145] Olivier, B.G., Rohwer, J.M. and Hofmeyr, J.H.S.: Modelling cellular systems with PySCeS. *Bioinformatics*, vol. 21, no. 4, pp. 560–561, 2005. ISSN 13674803.

[146] Padayachee, L., Rohwer, J.M. and Pillay, C.S.: The thioredoxin redox potential and redox charge are surrogate measures for flux in the thioredoxin system. *Archives of Biochemistry and Biophysics*, dec 2019. ISSN 0003-9861.

[147] Williams, C.: Flavin-containing dehydrogenases. In: *The Enzymes*, chap. 3, pp. 89–173. Elsevier B.V., 1976.

Stellenbosch University https://scholar.sun.ac.za

[148] John, R.A.: Photometric assays. In: Eisenthal, R. and Danson, M.J. (eds.), *Enzyme Assays A Practical Approach*, 2nd edn, chap. 2, pp. 49–78. Oxford University Press, Bath, 2002.

[149] Padayachee, L. and Pillay, C.S.: The thioredoxin system and not the Michaelis-Menten equation should be fitted to substrate saturation datasets from the thioredoxin insulin assay. *Redox Report*, vol. 21, no. 4, pp. 170–179, 2016. ISSN 17432928.

[150] Speranza, M.L., Ronchi, S. and Minchiotti, L.: Purification and characterization of yeast thioredoxin reductase. *BBA - Enzymology*, vol. 327, no. 2, pp. 274–281, 1973. ISSN 00052744.

[151] Oliveira, M.A., Discola, K.F., Alves, S.V., Medrano, F.J., Guimar, B.G. and Netto, L.E.S.: Insights into the specificity of thioredoxin reductase - thioredoxin interactions. A structural and functional investigation of the yeast thioredoxin system. *Biochemistry*, vol. 49, pp. 3317–3326, 2010.

[152] Lacey, B.M., Eckenroth, B.E., Flemer, S. and Hondal, R.J.: Selenium in thioredoxin reductase: A mechanistic perspective. *Biochemistry*, vol. 47, no. 48, pp. 12810–12821, 2008. ISSN 00062960.

[153] Ellman, G.L.: Tissue sulfhydryl groups. *Archives of Biochemistry and Biophysics*, vol. 82, pp. 70–77, 1959.

[154] Nagy, P., Karton, A., Betz, A., Peskin, A.V., Pace, P., O'Reilly, R.J., Hampton, M.B., Radom, L. and Winterbourn, C.C.: Model for the exceptional reactivity of peroxiredoxins 2 and 3 with hydrogen peroxide: A kinetic and computational study. *Journal of Biological Chemistry*, vol. 286, no. 20, pp. 18048–18055, 2011. ISSN 00219258.

[155] Winterbourn, C.C. and Peskin, A.V.: Kinetic approaches to measuring peroxiredoxin reactivity. *Molecules and Cells*, vol. 39, no. 1, pp. 26–30, 2016.

[156] Nelson, K.J. and Parsonage, D.: Measurement of peroxiredoxin activity. *Current Protocols in Toxicology*, , no. SUPPL. 49, pp. 1–28, 2011. ISSN 19349262.

[157] Lee, Y.J. and Chang, G.D.: Quantitative display of the redox status of proteins with maleimide-polyethylene glycol tagging. *Electrophoresis*, vol. 40, no. 4, pp. 491–498, 2018. ISSN 15222683.